AD-A166 386 GAS FILTER CORRELATION IMAGERY FOR HCI MONITORING(U) 1/2
OPTIMETRICS INC ANN ARBOR MI B K MATISE ET AL. JAN 86
OMI-133 AFESC/ESL-RR-85-36 F08635-84-C-0318

UNCLASSIFIED F/G 22/2 NL

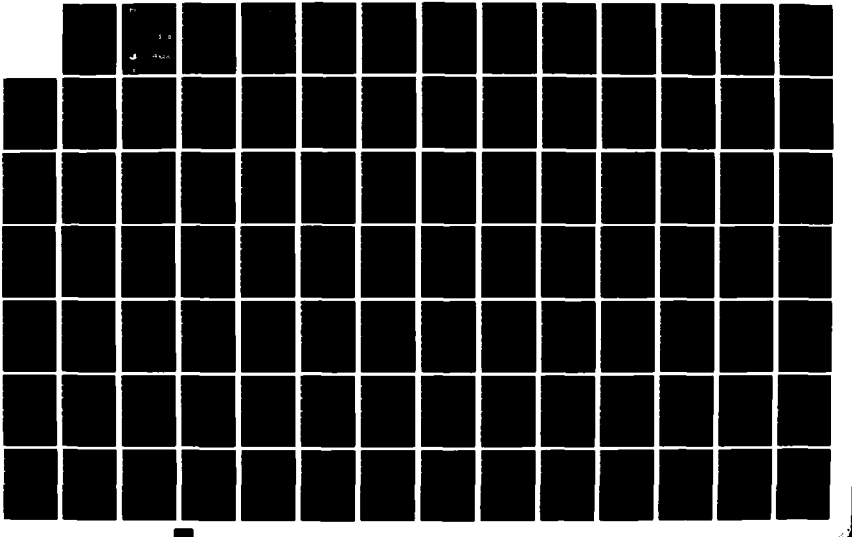

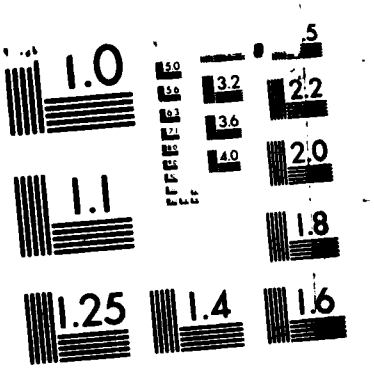

MICROCOPY RESOLUTION TEST CHART
NATIONAL BUREAU OF STANDARDS 1963-A

AD-A166 386

OTIC FILE COPY

ESL-TR-85-36

Gas Filter Correlation Imagery for HCl Monitoring

BRIAN K. MATISE
LUCIAN W. CHANEY
TIMOTHY J. ROGNE
FREDERICK G. SMITH

OPTIMETRICS, INC.
2000 HOGBACK ROAD, SUITE 3
ANN ARBOR, MICHIGAN 48105

DTIC
ELECTE
APR 0 8 1986
S D
D

JANUARY 1986

FINAL REPORT

SEPTEMBER 1984 - APRIL 1985

APPROVED FOR PUBLIC RELEASE: DISTRIBUTION UNLIMITED

AFESC

ENGINEERING & SERVICES LABORATORY
AIR FORCE ENGINEERING & SERVICES CENTER
TYNDALL AIR FORCE BASE, FLORIDA 32403

86 4 7 01

NOTICE

PLEASE DO NOT REQUEST COPIES OF THIS REPORT FROM HQ AFESC/RD (ENGINEERING AND SERVICES LABORATORY). ADDITIONAL COPIES MAY BE PURCHASED FROM:

NATIONAL TECHNICAL INFORMATION SERVICE
5285 PORT ROYAL ROAD
SPRINGFIELD, VIRGINIA 22161

FEDERAL GOVERNMENT AGENCIES AND THEIR CONTRACTORS REGISTERED WITH DEFENSE TECHNICAL INFORMATION CENTER SHOULD DIRECT REQUESTS FOR COPIES OF THIS REPORT TO:

DEFENSE TECHNICAL INFORMATION CENTER
CAMERON STATION
ALEXANDRIA, VIRGINIA 22314

UNCLASSIFIED

SECURITY CLASSIFICATION OF THIS PAGE (When Data Entered)

REPORT DOCUMENTATION PAGE		READ INSTRUCTIONS BEFORE COMPLETING FORM
1. REPORT NUMBER ESL-TR-85-36	2. GOVT ACCESSION NO. AD-A166386	3. RECIPIENT'S CATALOG NUMBER
4. TITLE (and Subtitle) GAS FILTER CORRELATION IMAGERY FOR HCl MONITORING		5. TYPE OF REPORT & PERIOD COVERED Final Report 26 Sep 84 - 26 Apr 85
		6. PERFORMING ORG. REPORT NUMBER OMI-133
7. AUTHOR(s) Brian K. Matise Timothy J. Rogne Lucian W. Chaney Frederick G. Smith		8. CONTRACT OR GRANT NUMBER(s) F08653-84-C-0318
9. PERFORMING ORGANIZATION NAME AND ADDRESS OptiMetrics, Inc. 2000 Hogback Road, Suite 3 Ann Arbor, Michigan 48105		10. PROGRAM ELEMENT, PROJECT, TASK AREA & WORK UNIT NUMBERS Program Element 65502F Project 3005 0004
11. CONTROLLING OFFICE NAME AND ADDRESS Department of the Air Force HQ AF Engineering & Services Center/RDVS Tyndall AFB FL 32403-6001		12. REPORT DATE January 1986
		13. NUMBER OF PAGES 118
14. MONITORING AGENCY NAME & ADDRESS(if different from Controlling Office)		15. SECURITY CLASS. (of this report) Unclassified
		15a. DECLASSIFICATION/DOWNGRADING SCHEDULE

16. DISTRIBUTION STATEMENT (of this Report)

Approved for public release. Distribution unlimited.

17. DISTRIBUTION STATEMENT (of the abstract entered in Block 20, if different from Report)

18. SUPPLEMENTARY NOTES

Availability of this report is specified on reverse of front cover.

19. KEY WORDS (Continue on reverse side if necessary and identify by block number)

- Gas Filter Correlation
- HCl
- Space Transportation System (STS)
- Pollutant Monitoring
- Environmental Protection Technology

20. ABSTRACT (Continue on reverse side if necessary and identify by block number)

See reverse.

DD FORM 1 JAN 73 1473 EDITION OF 1 NOV 65 IS OBSOLETE

UNCLASSIFIED

SECURITY CLASSIFICATION OF THIS PAGE (When Data Entered)

The feasibility of applying gas filter correlation techniques and infrared imaging technology to the problem of quantifying gaseous HCl produced in the exhaust of the Space Transportation System (STS) is explored. Modeling of HCl absorption and emission for various spectral bandpasses, atmospheric conditions, and concentrations is performed to obtain estimates of modulated detected power as a function of HCl concentration. Several optical system designs are examined. Results of a laboratory demonstration of the gas filter correlation technique for quantifying HCl while rejecting broadband absorbers are presented. The findings of the study are:

1. Commercial infrared imagers do not have sufficient sensitivity to detect HCl emissions;

2. Gas filter correlation systems detecting HCl absorption of solar radiation or a high-intensity source can quantify HCl to better than 30 parts per million-meters (ppm-m); and

3. Specially designed high-sensitivity instruments can be built to detect HCl emissions while operating in a staring mode or slow line scanning mode.

Several designs for HCl detection systems are presented with estimates of technical feasibility. Potential applications of this work include inexpensive remote monitoring of industrial gaseous pollutants discharged into the atmosphere.

Keywords: Pollutant monitoring; Environmental Protection Technology

PREFACE

This report was prepared by Optimetrics, Incorporated, 2000 Hogback Road, Suite 3, Ann Arbor, Michigan 48105, under Contract Number F08635-84-C-0318. The work was technically monitored by the Air Force Engineering and Services Center, Engineering and Sevices Laboratory (AFESC/RDVS), Tyndall Air Force Base, Florida, 32403-6001 and funded by the West Coast Office, Air Force Space Technology Center, Box 92960, WPC, Los Angeles, CA 90009-2960.

This report summarizes work accomplished between 19 September 1984 and 26 April 1985. HQ AFESC/RDVS Project Officer was Capt Robert C. Beggs.

This report has been reviewed by the Public Affairs Office (PA) and is releasable to the National Technical Information Service (NTIS). At NTIS it will be available to the general public, including foreign nationals.

This technical report has been reviewed and is approved for publication.

ROBERT C. BEGGS, Capt, USAF
Project Officer

ROBERT E. BOYER, Colonel, USAF
Director, Engineering and
Services Laboratory

ROBERT F. OLFENBUTTEL, Lt Col, USAF, BSC
Chief, Environics Division

(The reverse of this page is blank.)

TABLE OF CONTENTS

Section	Title	Page
I	INTRODUCTION	1
	A. OBJECTIVE	1
	B. BACKGROUND	1
	C. SCOPE	2
II	THEORETICAL DEVELOPMENT	3
	A. DESCRIPTION OF EMISSION AND ABSORPTION MODE OPERATION	3
	B. EMISSION MODE OPERATION	3
	C. ABSORPTION MODE OPERATION	6
III	MODELING GAS FILTER CORRELATION MODULATION	9
	A. SELECTION OF SPECTRAL BANDPASS	9
	B. MODULATION FROM EMISSION MODE OPERATION	11
	C. MODULATION FROM ABSORPTION MODE OPERATION	15
	1. Correlation Cell HCl Concentrations	17
	2. Interference Calculations	23
	3. Air Temperature Effects	35
IV	PRELIMINARY INSTRUMENT FEASIBILITY STUDIES	43
	A. USE OF INFRAMETRICS IMAGER DETECTING HCl EMISSIONS	43
	B. SCATTERING OF SOLAR RADIATION	44
V	LABORATORY DEMONSTRATION OF GFCS IN ABSORPTION MODE	51
	A. SYSTEM DESIGN	51
	B. SYSTEM PERFORMANCE	51
VI	FIELD SYSTEM DESIGN	65
	A. HIGH-SENSITIVITY IMAGER OPERATING IN EMISSION MODE	65
	B. GFCS DETECTING SCATTERED SOLAR RADIATION	70
	C. GFCS OPERATING IN ABSORPTION MODE ALONG SEVERAL LINES OF SIGHT	72
	D. SUMMARY	75

Dist | Avail and/or Special
A-1

TABLE OF CONTENTS

Section	Title	Page
VII	CONCLUSIONS AND RECOMMENDATIONS.....	79
	REFERENCES.....	83
APPENDIX		
A	PLOTS.....	85

LIST OF FIGURES

Figure	Title	Page
1	Radiation Sources in a Generalized Gas Filter Correlation Spectrometer Configuration	4
2	Absorption Mode Modulation for an Ideal Gas Filter	7
3	Comparison of HCl Absorption Lines with Measured Long-Path Transmittance	12
4	Spectral Response of Interference Filter Including HCl Lines P(3)-R(2)	13
5	Spectral Response of Interference Filter Including HCl Lines P(1)-P(5)	14
6	Modulation as a Function of HCl Column Density for Various Amounts of HCl in Correlation Cell	18
7	Modulation as a Function of HCl Column Density for Various Amounts of HCl in Correlation Cell	19
8	Modulation Versus HCl Column Density for Three Different Temperatures of HCl in Correlation Cell	20
9	Modulation Versus HCl Column Density for Three Different Temperatures of HCl in Correlation Cell	21
10	Modulation Versus HCl Column Density for Three Different Temperatures of HCl in Correlation Cell	22
11	Modulation Versus HCl Column Density for Three Different Partial Pressures of Water Vapor in the Atmospheric Path	24
12	Modulation Versus HCl Column Density for Three Different Partial Pressures of Water Vapor in the Atmospheric Path	25
13	Modulation Versus HCl Column Density for Three Different Partial Pressures of Water Vapor in the Atmospheric Path	26
14	Modulation Versus HCl Column Density for Three Different Partial Pressures of Water Vapor in the Atmospheric Path	27
15	Modulation Versus HCl Column Density for Three Different Partial Pressures of Water Vapor in the Atmospheric Path	28
16	Calibration and Interference Estimates, GFCS in Absorption Mode	29
17	Calibration and Interference Estimates, GFCS in Absorption Mode	30
18	Calibration and Interference Estimates, GFCS in Absorption Mode	31
19	Calibration and Interference Estimates, GFCS in Absorption Mode	32
20	Calibration and Interference Estimates, GFCS in Absorption Mode	33
21	Calibration and Interference Estimates, GFCS in Absorption Mode	34

22 Modulation Resulting from HCl Present in a 1 km Midlatitude Summer (294 K), Tropical (300 K), and Sub-Arctic Winter (257 K) Atmosphere.....37
23 Modulation from HCl Present in a 1 km Midlatitude Summer (294 K), Tropical (300 K), and Sub-Arctic Winter (257 K) Atmosphere.....38
24 Modulation from HCl Present in a 1 km Midlatitude Summer (294 K), Tropical (300 K), and Sub-Arctic Winter (257 K) Atmosphere.....39
25 Modulation from HCl Present in a 1 km Midlatitude Summer (294 K), Tropical (300 K), and Sub-Arctic Winter (257 K) Atmosphere.....40
26 Modulation from HCl Present in a 1 km Midlatitude Summer (294 K), Tropical (300 K), and Sub-Arctic Winter (257 K) Atmosphere.....41
27 Modulation from HCl Present in a 1 km Midlatitude Summer (294 K), Tropical (300 K), and Sub-Arctic Winter (257 K) Atmosphere.....42
28 Particle Size Distribution Used to Represent STS Launch Cloud.....46
29 Particle Size Distribution Used to Represent Cumulus Cloud.....47
30 Scattered Solar Radiance tor a Cumulus Cloud Background.....48
31 Solar Radiance Scattered by STS Launch Cloud.....49
32 Optical System Design for GFCS Operating in Absorption Mode.....52
33 Transmitted Signal (upper curve) and Modulation (lower curve) for Clean Air and Four Cells with 0 kp, 11 kp, 13 kp, and 26 kp HCl.....54
34 Transmittal Signal (upper curve) and Modulation Signal (lower curve) for Clean Air and Three Neutral Attenuators.....56
35 Theoretical Versus Measured Modulation, Bandpass 2770-2870 cm^{-1}, 0.37 atm-cm HCl in Correlation Cell.....59
36 Theoretical Versus Measured Modulation, Bandpass 2806-2948 cm^{-1}, 0.75 atm-cm HCl in Correlation Cell.....60
37 Scattering of Source Radiation Directly into Detector Field of View by Beam Splitter.....61
38 Design for a GFCS Which Maps a Cloud by Successive Linear Scans Perpendicular to Wind Vector.....67
39 Geometry Required for Detection of HCl Absorption of Scattered Solar Radiation by a GFCS.....71
40 Geometry for GFCS System Which Scans Over Several Lines of Sight.....73
41 Multiple-GFCS Approach to Map HCl Cloud.....74

LIST OF TABLES

Table	Title	Page
1	HCl Absorption Line Parameters as Compiled by the Air Force Geophysics Laboratory	10
2	Calculation of Modulated Radiance in Emission Mode Calculation	16
3	Equivalent HCL Column Density Due to Interfering Gases	36
4	Specifications for Inframetrics Model 525	43
5	Performance Estimates of GFCS in Laboratory Tests	64
6	Specifications for GFCS Operating in Emission Mode for HCl Detection	66
7	Design Specifications for High-Sensitivity Line Scanner for HCL Detection	68
8	Advantages and Disadvantages of the Various Gas Filters Correlation Approaches to HCl Detection	76
9	Maximum Theoretical Sensitivity of Various Proposed Field Instruments	77

(The reverse of this page is blank.)

SECTION I
INTRODUCTION

A. OBJECTIVE

The Air Force has a need to measure the levels of HCl gas produced by NASA's Space Transportation System (STS) over long atmospheric paths. Current point sampling techniques have several disadvantages, such as requiring deployment, collection, and analysis of a large number of samples. Novel techniques for real-time HCl monitoring devices are sought.

B. BACKGROUND

The STS is launched by two solid rocket boosters and three liquid propellant main engines. These solid rocket motors have been observed to produce large quantities of hydrogen chloride vapor (References 1-3) which can be hazardous to animals and plants when present in sufficient quantities. With the expected launch of the STS from Vandenberg Air Force Base (VAFB), California, the problem is magnified by the site meteorology and the presence of civilian population centers downwind of the launch site. The need, therefore, exists to measure the concentration and distribution of HCl in the exhaust cloud.

C. SCOPE

The present effort is a study of the feasibility of combining a technique known as Gas Filter Correlation Spectroscopy (GFCS) with infrared imaging technology to monitor HCl vapor. This report describes the results of the study as well as providing potential designs for a fieldable system.

(The reverse of this page is blank.)

SECTION II
THEORETICAL DEVELOPMENT

A. DESCRIPTION OF EMISSION AND ABSORPTION MODE OPERATION

Gas filter correlation approaches to the problem of HCl detection may involve operation in either emission mode or absorption mode. Figure 1 illustrates the general configuration of a gas filter correlation spectrometer (GFCS) system, with the major sources of radiance. The principal difference between these two modes of operation is whether the radiance passing through the HCl cloud from a background source is sufficiently large so that contributions due to path radiance may be neglected. If this is true, then HCl absorption is detected by the system and calibration of the system is greatly simplified. Otherwise, HCl emissions are the principal source of modulation detected by the system.

B. EMISSION MODE OPERATION

For detection of HCl in emission mode operation, no source of radiation other than the HCl cloud and the ambient atmospheric background is present. The radiance detected with the reference cell in place is given by

$$L_{ref} = L_r + \tau_r(L_i + \tau_i(L_p + \tau_p L_b)) \qquad (1)$$

where

L_r, L_i, L_p, L_b = radiance from reference cell, intervening atmosphere, plume and background, respectively

τ_r, τ_i, τ_p = transmittance due to reference cell, intervening atmosphere and plume, respectively.

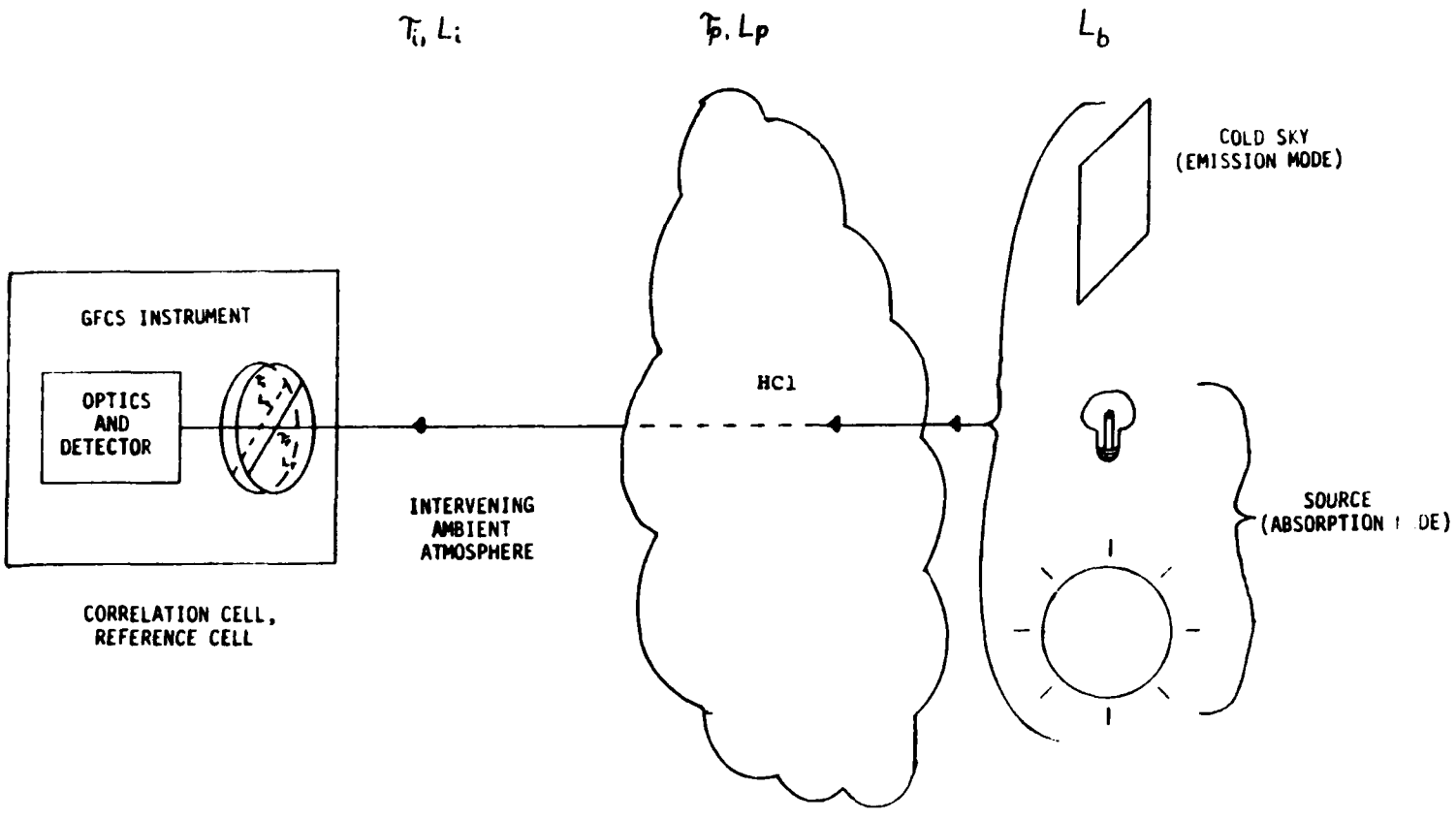

Figure 1. Radiation Sources in a Generalized Gas Filter Correlation Spectrometer Configuration.

The corresponding radiance detected with the correlation cell in place is

$$L_{cor} = L_c + \tau_c(L_i + \tau_i(L_p + \tau_p L_b)) \qquad (2)$$

where

L_c, τ_c = radiance and transmittance due to the correlation cell.

All quantities in the above two equations are implicitly spectrally dependent. The modulated radiance in emission mode is computed from the band-average correlation cell and reference cell radiances:

$$\bar{L}_{mod} = \bar{L}_{cor} - \bar{L}_{ref} \qquad (3)$$

$$= \bar{L}_c - \bar{L}_r + \int (\tau_c - \tau_r)(L_i + \tau_i (L_p + \tau_p L_b))d\nu$$

where the notation $\bar{L}$ denotes band-average radiance

Since the first two terms are not dependent on the quantity of HCl in the plume, they may be combined into a constant offset term which is a function of the correlation cell and reference cell properties (temperature, HCl partial pressure, cell length). The path radiance introduced by atmospheric constituents present in the reference cell will normally be insignificant.

The instrument is balanced by adjusting the amplifiers so that the signals are equal when there is no HCl present in the path. If HCl is present in the path, the radiance detected through the reference cell will be increased while the radiance detected through the correlation cell will be relatively unchanged.

C. ABSORPTION MODE OPERATION

In absorption mode operation, only the background, or source term, is significant. The modulation signal detected by a GFCS operating in absorption mode is calculated from

$$M = \frac{\bar{\tau}_{ac} - \bar{\tau}_a \bar{\tau}_c}{\bar{\tau}_{ac} + \bar{\tau}_a \bar{\tau}_c} \tag{4}$$

where

$\bar{\tau}_{ac}$ = band-average transmittance through the atmospheric path and correlation cell.

$\bar{\tau}_a$ = band-average transmittance through the atmosphere

$\bar{\tau}_c$ = band-average transmittance through the correlation cell

The band-average transmittance through the correlation cell is measured by adjusting the gain applied to the detected signal when the reference cell is in place and there is no HCl in the path so that the amplified signal is equal to the signal when the correlation cell is in place. If there is HCl in the path, the band-average transmittance through the atmospheric path and correlation cell becomes greater than the product of the band-average transmittances through the correlation cell and atmosphere. Figure 2 illustrates an idealized case. Note that if absorption in the atmospheric path is not correlated to the absorption of HCl in the gas cell, no modulation results.

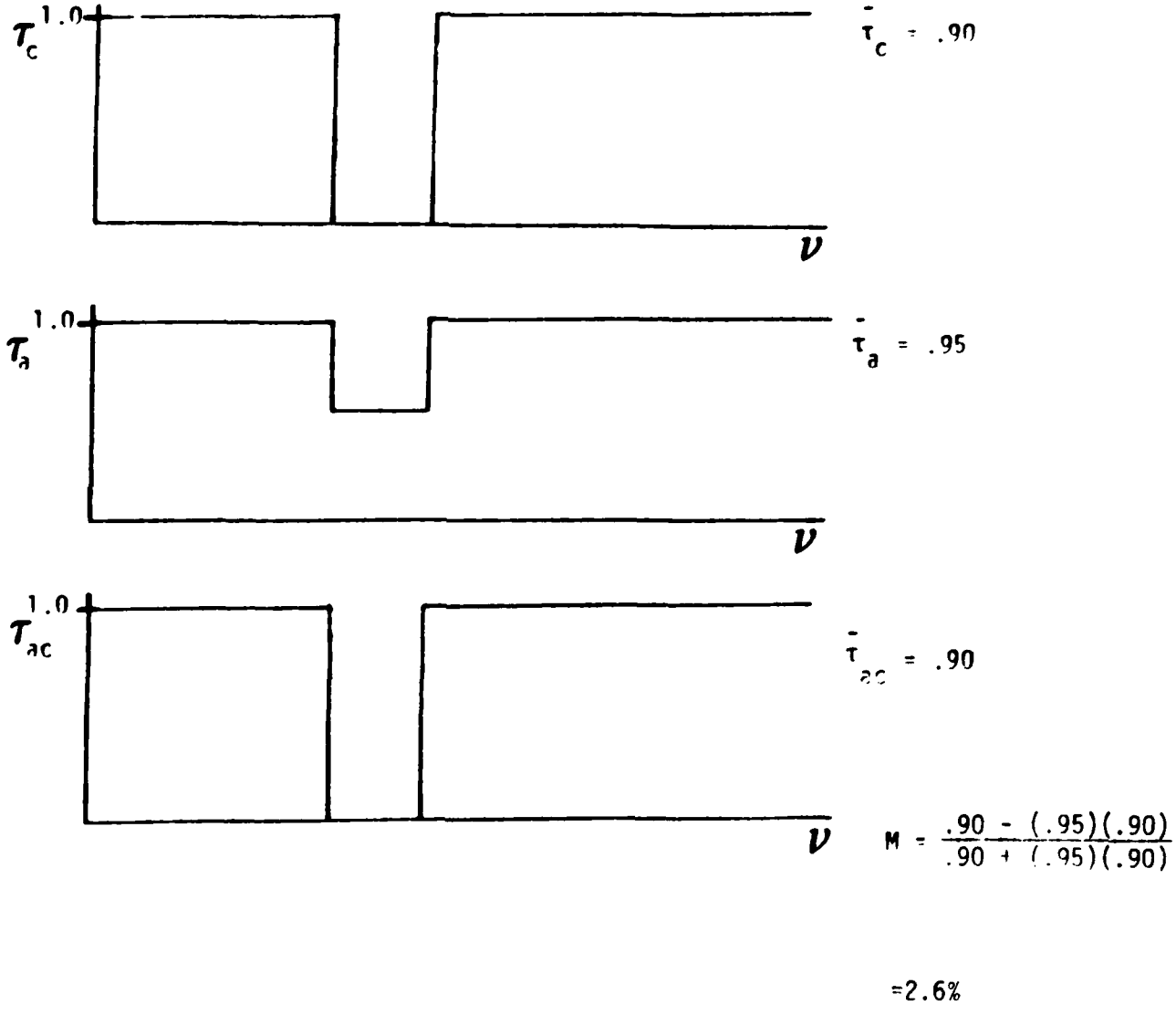

Figure 2. Absorption Mode Modulation for an Ideal Gas Filter.

(The reverse of this page is blank.)

SECTION III
MODELING GAS FILTER CORRELATION MODULATION

A. SELECTION OF SPECTRAL BANDPASS

The fundamental absorption band of HCl occurs in the 3.4 μm region. Table 1 lists absorption line parameters for HCl as compiled in the Air Force Geophysics Laboratory (AFGL) 1980 Trace Gas Line Parameter Compilation (Reference 4). Of the lines listed, only those lines from P(9) to R(9) have sufficient strength to contribute significant modulation. Using the AFGL Fast Atmospheric Signature Code (FASCODE) (References 5 and 6) version 1B, calculations of transmittance through a 10 km midlatitude summer atmosphere and a 10,000 parts per million-meter (ppm-m) HCl column were performed. One ppm-m HCl corresponds to an HCl concentration of 1 ppm integrated over a 1 m path. These transmittance spectra were superimposed to allow a preliminary selection to be made of HCl absorption lines which were likely to provide significant modulation while remaining free from interference due to atmospheric gases. The complete transmittance spectra are presented as Appendix A.

Due to relatively strong atmospheric absorption for frequencies greater than 2950 cm^{-1}, only those lines from P(8) to R(2) appear likely to provide useful modulation. In fact, to minimize interference by absorbing atmospheric gases, a bandpass extending from 2690-2870 cm^{-1} appears to be optimal. This bandpass would include all HCl^{35} and HCl^{37} lines from P(1)-P(8).

Although the AFGL line parameter compilation is the most commonly used data base for atmospheric applications, the possibility exists for incorrect line positions and strengths, particularly for regions relatively free of

TABLE 1. HCl ABSORPTION LINE PARAMETERS AS COMPILED BY THE AIR FORCE GEOPHYSICS LABORATORY (REFERENCE 4).

Wavenumber (cm^{-1})	Strength	Halfwidth (cm^{-1})	Ground State Energy	Designation	Isotope
2514.7532	8.778E-24	0.0135	2471.787	P(15)	HCl^{35}
2516.2700	2.656E-23	0.0135	2475.458	P(15)	HCl^{37}
2542.7251	3.565E-23	0.0135	2166.084	P(14)	HCl^{35}
2544.2800	1.081E-22	0.0135	2169.306	P(14)	HCl^{37}
2570.2661	1.309E-22	0.0135	1879.923	P(13)	HCl^{35}
2571.8689	3.979E-22	0.0135	1882.723	P(13)	HCl^{37}
2597.3762	4.343E-22	0.0145	1613.475	P(12)	HCl^{35}
2599.0220	1.322E-21	0.0145	1615.882	P(12)	HCl^{37}
2624.0298	1.298E-21	0.0172	1366.901	P(11)	HCl^{35}
2625.7261	3.959E-21	0.0172	1368.943	P(11)	HCl^{37}
2650.2275	3.490E-21	0.0204	1140.349	P(10)	HCl^{35}
2651.9670	1.066E-20	0.0204	1142.054	P(10)	HCl^{37}
2675.9614	8.420E-21	0.0247	933.954	P(9)	HCl^{35}
2677.7329	2.576E-20	0.0247	935.352	P(9)	HCl^{37}
2701.1921	1.817E-20	0.0337	747.842	P(8)	HCl^{35}
2703.0081	5.568E-20	0.0337	748.963	P(8)	HCl^{37}
2725.9214	3.496E-20	0.0412	582.125	P(7)	HCl^{35}
2727.7800	1.073E-19	0.0412	582.998	P(7)	HCl^{37}
2750.1311	5.962E-20	0.0543	436.902	P(6)	HCl^{35}
2752.0349	1.831E-19	0.0543	437.558	P(6)	HCl^{37}
2773.8240	8.942E-20	0.0642	312.262	P(5)	HCl^{35}
2775.7610	2.749E-19	0.0642	312.731	P(5)	HCl^{37}
2796.9709	1.164E-19	0.0795	208.280	P(4)	HCl^{35}
2798.9431	3.581E-19	0.0795	208.593	P(4)	HCl^{37}
2819.5588	1.285E-19	0.0920	125.018	P(3)	HCl^{35}
2821.5691	3.955E-19	0.0920	125.206	P(3)	HCl^{37}
2841.5864	1.139E-19	0.0952	62.528	P(2)	HCl^{35}
2843.6250	3.508E-19	0.0952	62.622	P(2)	HCl^{37}
2863.0244	6.845E-20	0.0967	20.847	P(1)	HCl^{35}
2865.0979	2.108E-19	0.0967	20.878	P(1)	HCl^{37}
2904.1128	7.294E-20	0.0967	0.0	R(0)	HCl^{35}
2906.2471	2.247E-19	0.0967	0.0	R(0)	HCl^{37}
2923.7307	1.294E-19	0.0952	20.847	R(1)	HCl^{35}
2925.8970	3.985E-19	0.0952	20.878	R(1)	HCl^{37}
2942.7246	1.555E-19	0.0920	62.528	R(2)	HCl^{35}
2944.9141	4.788E-19	0.0920	62.622	R(2)	HCl^{37}
2961.0701	1.502E-19	0.0795	125.018	R(3)	HCl^{35}
2963.2849	4.622E-19	0.0795	125.206	R(3)	HCl^{37}
2978.7539	1.229E-19	0.0642	208.280	R(4)	HCl^{35}
2981.0000	3.781E-19	0.0642	208.593	R(4)	HCl^{37}
2995.7815	8.735E-20	0.0543	312.262	R(5)	HCl^{35}
2998.0471	2.685E-19	0.0543	312.731	R(5)	HCl^{37}
3012.1257	5.460E-20	0.0412	436.902	R(6)	HCl^{35}
3014.4131	1.677E-19	0.0412	437.558	R(6)	HCl^{37}
3027.7729	3.025E-20	0.0337	582.125	R(7)	HCl^{35}
3030.0869	9.282E-20	0.0337	582.998	R(7)	HCl^{37}
3042.7253	1.494E-20	0.0247	747.842	R(8)	HCl^{35}
3045.0591	4.579E-20	0.0247	748.963	R(8)	HCl^{37}
3056.9690	6.604E-21	0.0204	933.954	R(9)	HCl^{35}
3059.3169	2.021E-20	0.0204	935.352	R(9)	HCl^{37}
3070.4910	2.619E-21	0.0172	1140.349	R(10)	HCl^{35}
3072.8501	8.003E-21	0.0172	1142.054	R(10)	HCl^{37}
3083.2725	9.344E-22	0.0145	1366.901	R(11)	HCl^{35}
3085.6499	2.851E-21	0.0145	1368.943	R(11)	HCl^{37}
3095.3293	3.005E-22	0.0135	1613.475	R(12)	HCl^{35}
3097.7041	9.152E-22	0.0135	1615.882	R(12)	HCl^{37}
3106.6125	8.729E-23	0.0135	1879.923	R(13)	HCl^{35}
3109.0039	2.653E-22	0.0135	1882.723	R(13)	HCl^{37}
3117.1450	2.293E-23	0.0135	2166.084	R(14)	HCl^{35}
3119.5400	6.956E-23	0.0135	2169.306	R(14)	HCl^{37}
3126.8894	5.459E-24	0.0135	2471.787	R(15)	HCl^{35}
3129.3030	1.652E-23	0.0135	2475.458	R(15)	HCl^{37}
3135.8750	1.179E-24	0.0135	2796.848	R(16)	HCl^{35}
3138.2830	3.560E-24	0.0135	2800.996	R(16)	HCl^{37}

strong absorption lines. OptiMetrics has observed such line position errors in a previous study involving gas filter correlation spectroscopy for HF detection (Reference 7). Since relatively minor errors in line position can result in sizable amounts of unexpected interference modulation, an attempt was made to verify the long-path transmittance predictions of FASCODE. Long-path (5.08 km) transmittance data obtained by Dowling et al. (Reference 8) for humid midlatitude summer conditions indicate that most of the HCl lines from P(1) to P(8) are free from interference. Figure 3 indicates the positions of the HCl lines superimposed on the measured transmittance spectra.

Based on these calculations, two interference filters were selected from a catalog of off-the-shelf filters. The spectral response tracings of these filters are provided in Figures 4 and 5.

B. MODULATION FROM EMISSION MODE OPERATION

The modulated radiance resulting from emission mode operation was calculated assuming a uniform HCl cloud 1 km in diameter. The concentration of HCl gas in the cloud was assumed to be 1 ppm and 10 ppm for the two preliminary cases considered. A midlatitude summer environment (T = 294 K, P_{H_2O} = 14.3 torr) was assumed. The background path was assumed to be an 80-degree zenith angle slant path to space, with clear atmospheric conditions. Between the HCl cloud and the GFCS instrument a 1 km attenuating atmosphere was assumed.

For the preliminary study, the HCl in the cloud was assumed to be at a temperature of 300 K. The correlation cell contained 2 atm-cm of HCl. This was considered an optimistic test of the estimated conditions expected to be encountered in an actual field test.

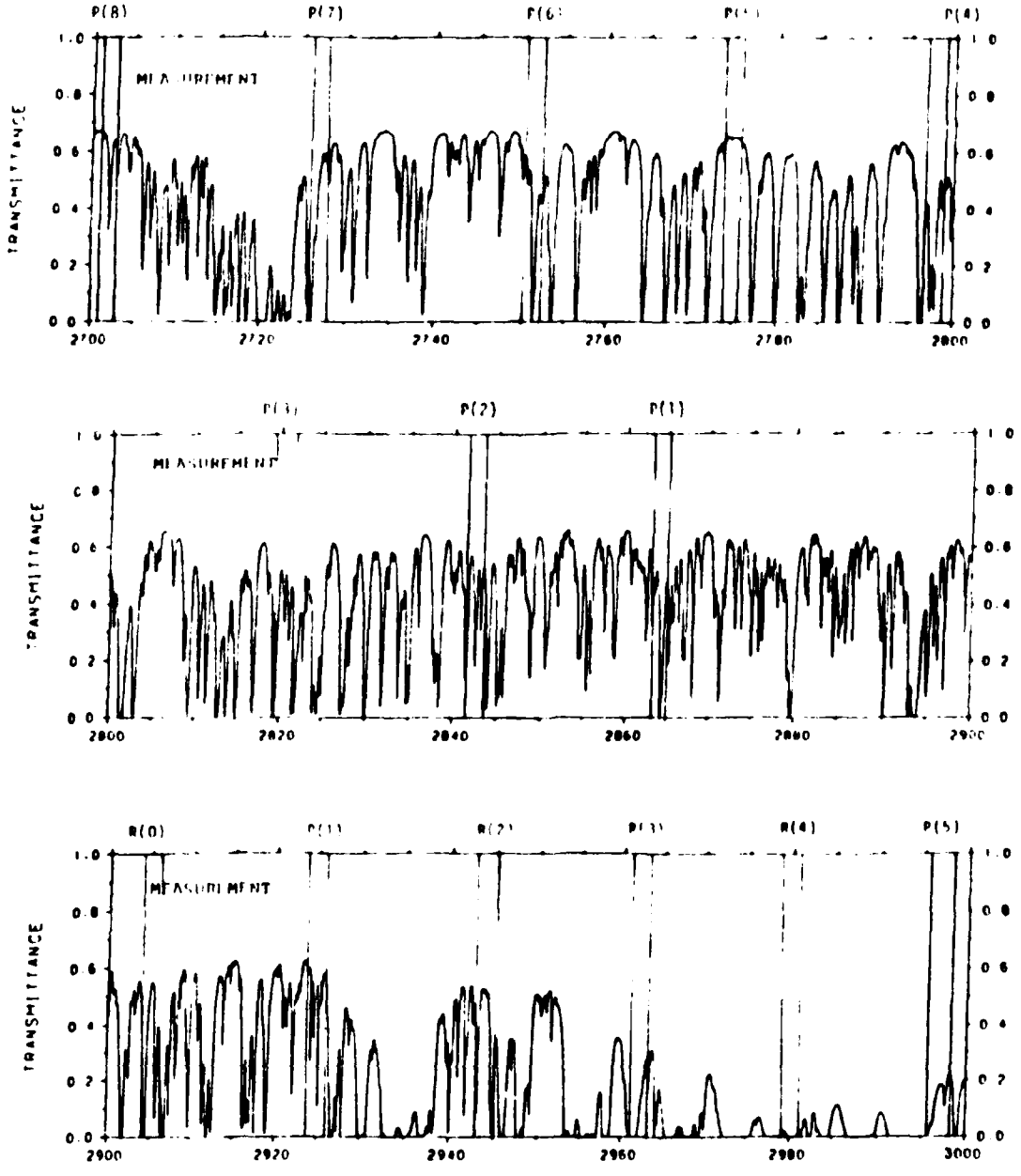

CONDITIONS: 5.08 KM PATH, T = 26.7 C, P_{H_2O} = 21.6 TORR

Figure 3. Comparison of HCl Absorption Lines with Measured Long-Path Transmittance from Dowling, et al., Analysis of Atmospheric Interferometer Data (Reference 8).

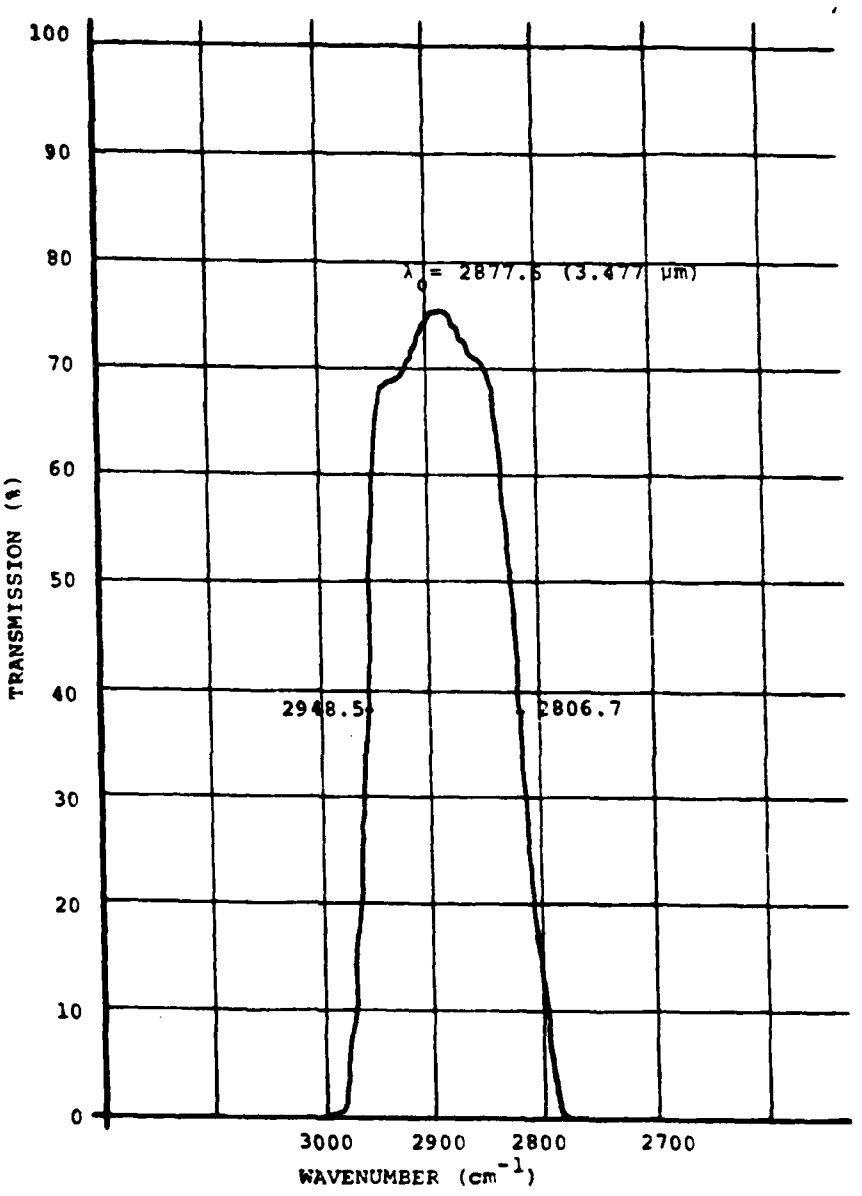

Figure 4. Spectral Response of Interference Filter including HCl Lines P(3)-R(2).

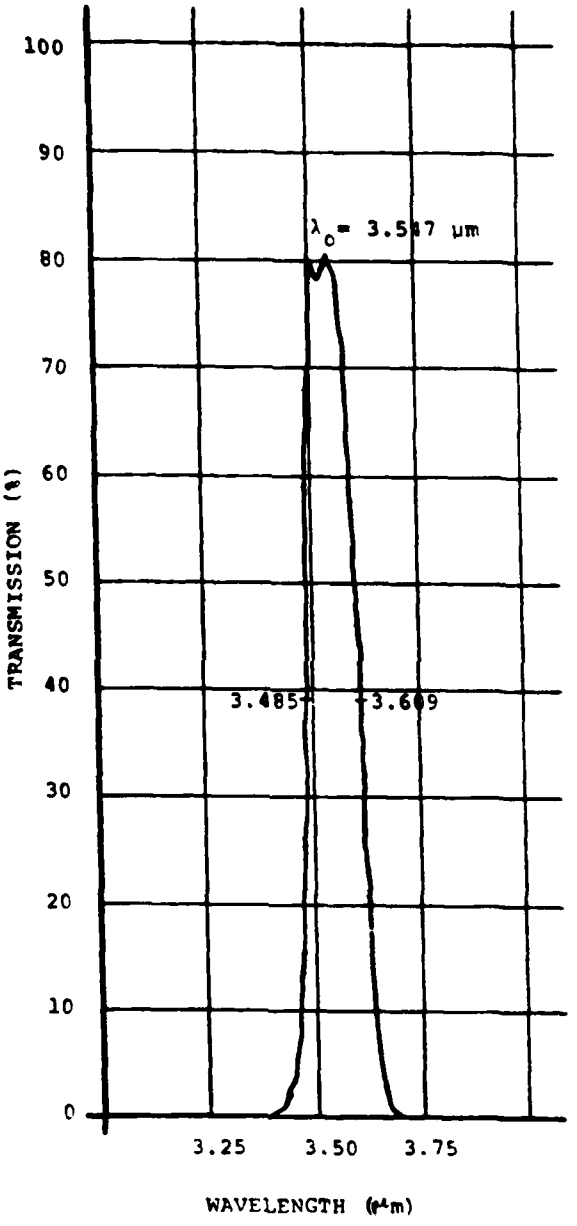

Figure 5. Spectral Response of Interference Filter Including HCl Lines P(1)-P(5).

The results of the calculations of modulated radiance are displayed in Table 2. These calculations were performed using transmittance and radiance spectra computed using FASCODE 1B.

C. MODULATION FROM ABSORPTION MODE OPERATION

Calculations were performed using FASCODE to obtain absorption coefficients for HCl in gas cells, HCl at typical atmospheric conditions, and atmospheric gases. Calculations were performed for HCl in gas cells assuming 1 atm pressure and temperatures from 257 K to 373 K. Calculations for HCl at typical atmospheric conditions corresponded to 1 ppm concentration for a 1 km path at 257 K, 294 K, and 300 K. Atmospheric absorption coefficients were calculated for a standard sub-Arctic winter model atmosphere, a standard tropical atmosphere, and midlatitude summer atmospheres with water vapor concentrations of 5 torr, 14.3 torr, and 20 torr.

For the purpose of obtaining modulation estimates, absorption coefficients were calculated for frequencies from 2630-3120 cm^{-1} at increments of 0.02 cm^{-1}. Modulation estimates could then be obtained by specifying the filter bandpass, correlation cell length, atmospheric path length, HCl concentration in parts per million, and the appropriate set of absorption coefficients. These estimates assumed that the absorption coefficients calculated from the standard set of conditions could be scaled up or down to correspond to the appropriate column density for the absorbing gas of interest. It was also assumed that there is uniform system response over the filter bandpass.

TABLE 2. CALCULATION OF MODULATED RADIANCE IN EMISSION MODE OPERATION.

HCl Column Density (ppm-m)	Radiance ($\mu W/cm^2$-ster)		
	Correlation Cell	Reference Cell	Modulated
0	3.226	2.853	0
1,000	3.354	3.074	.093
10,000	3.394	3.272	.255

Conditions: 2690-2850 cm^{-1} bandpass
Correlation cell 2.0 atm-cm HCl, 294 K, 1013 mb
Midlatitude summer background
80° zenith angle, 300 K plume

1. CORRELATION CELL HCl CONCENTRATIONS

Modulation calculations assuming a 1 km path through a standard midlatitude summer atmosphere at sea level were performed to estimate modulation levels which would be obtained using various different correlation cells. Modulation will vary with the HCl column density in the correlation cell and the temperature of the cell. For the first set of calculations, the HCl column density was varied from 0.25 atm-cm to 2.0 atm-cm. The temperature and pressure of the HCl in the correlation cell were assumed to be 294 K and 1013 mb, respectively. Note that 1 atm-cm of HCl corresponds to a column density of 10,000 ppm-m.

Estimated modulation is plotted in Figures 6 and 7 as a function of HCl column density for midlatitude summer conditions and various column densities of HCl in the correlation cell. Since each GFCS has a minimum detectable modulation which depends on the noise of the instrument, the sensitivity of a given GFCS is improved through use of correlation cells with larger HCl column densities.

Varying the temperature of HCl in the correlation cell affects the modulation in two ways. First, since the molecular number density of any gas is inversely proportional to temperature, as temperature increases the number of HCl molecules in a given cell at 1 atm pressure decreases. Second, the HCl absorption lines broaden at higher temperatures. For 1 atm pressure and temperatures near 300 K, Lorentz (pressure) broadening dominates, however. Therefore, the first effect is in practice the only one which need be considered.

Figures 8-10 display the results of modulation calculations for various correlation cell temperatures using three different bandpasses.

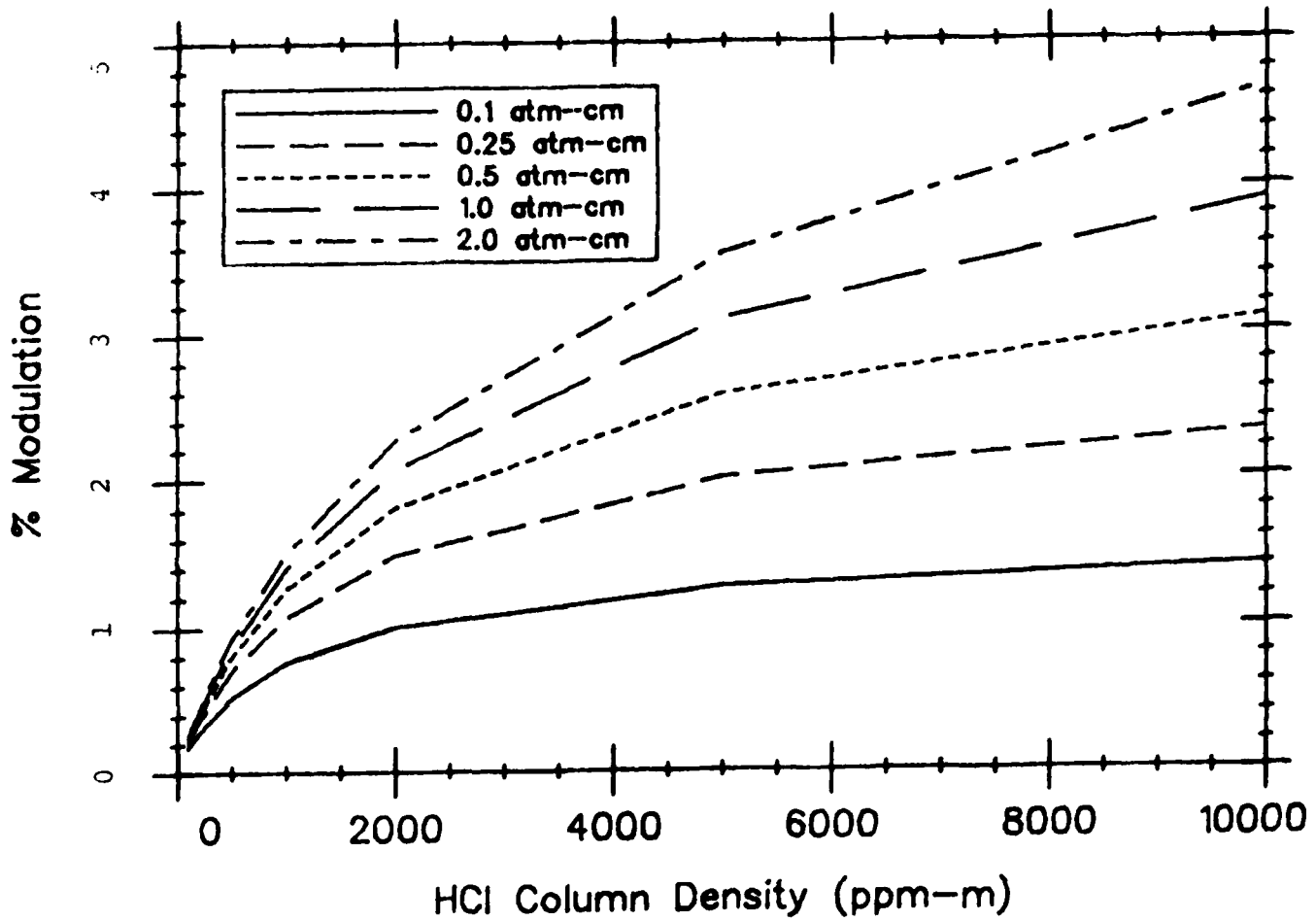

Figure 6. Modulation as a Function of HCl Column Density for Various Amounts of HCl in Correlation Cell. Conditions: Bandpass 2770-2870 cm^{-1}, Midlatitude Summer Conditions, No Interference.

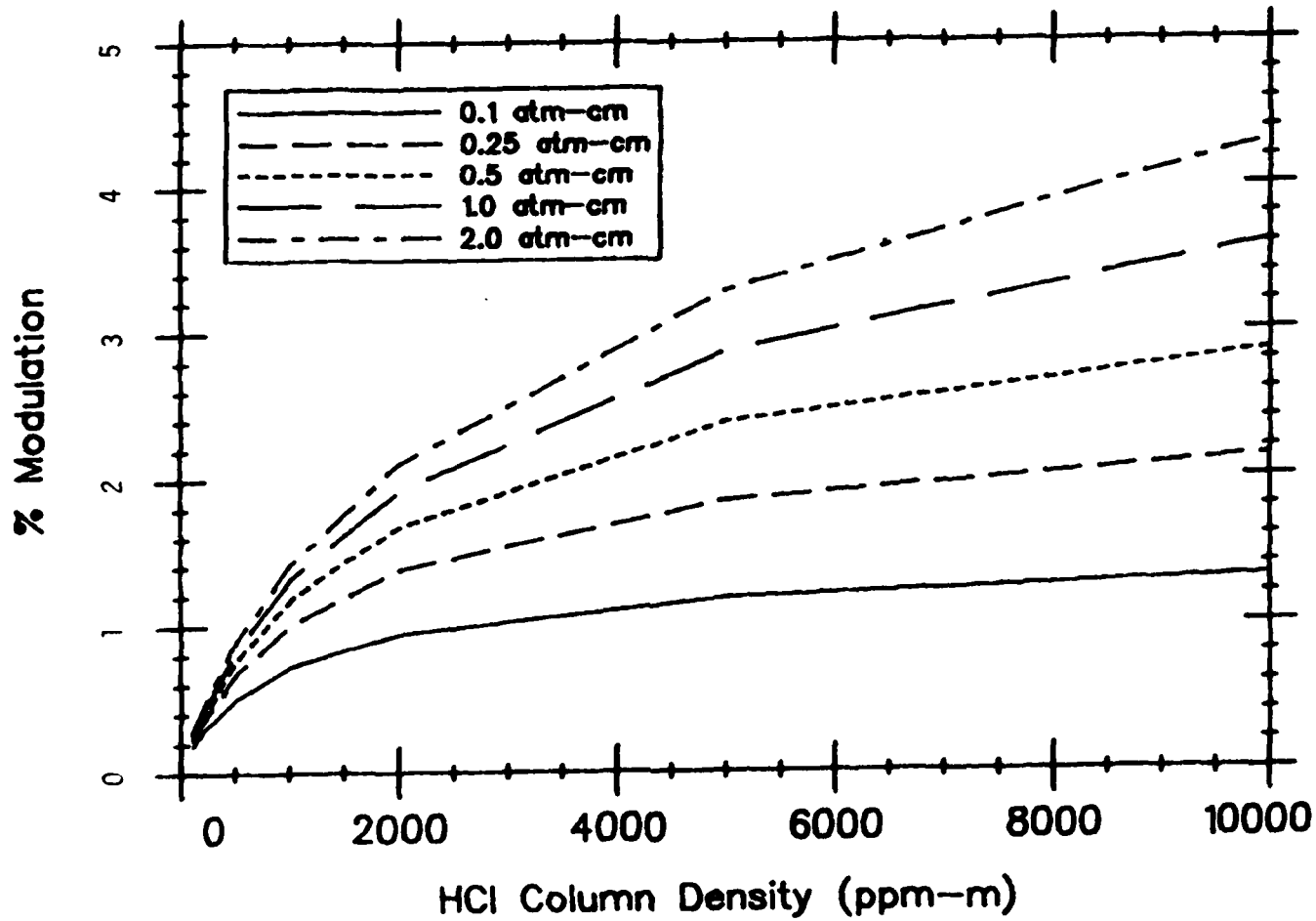

Figure 7. Modulation as a Function of HCl Column Density for Various Amounts of HCl_{-1} in Correlation Cell. Conditions: Bandpass 2806-2948 cm^{-1}, Midlatitude Summer Condition, No Interference.

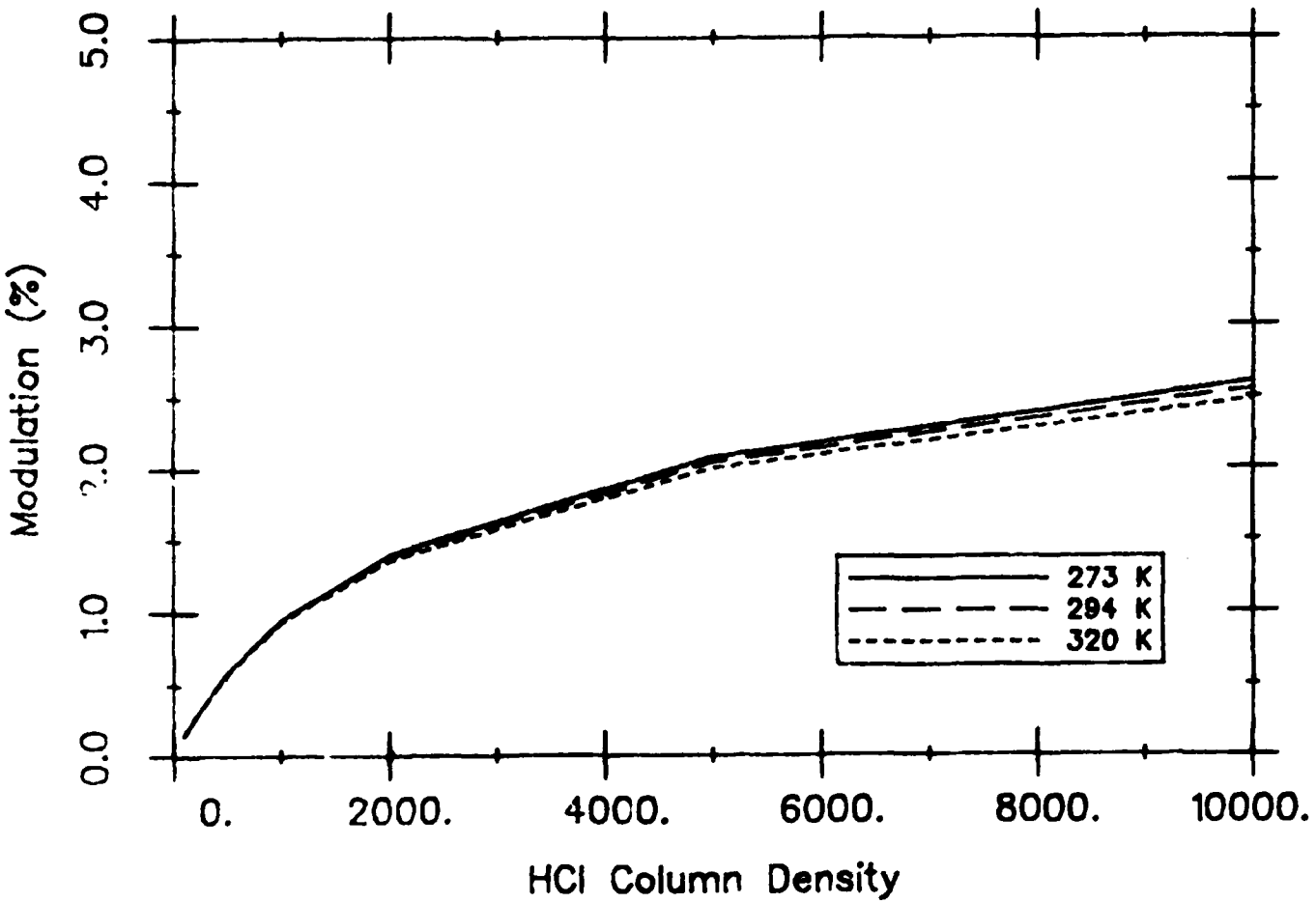

Figure 8. Modulation Versus HCl Column Density for Three Different Temperatures of HCl in Correlation Cell. Conditions: 1 km Atmospheric Path, 2690-2850 cm^{-1} Bandpass, 1 atm-cm HCl in Correlation Cell.

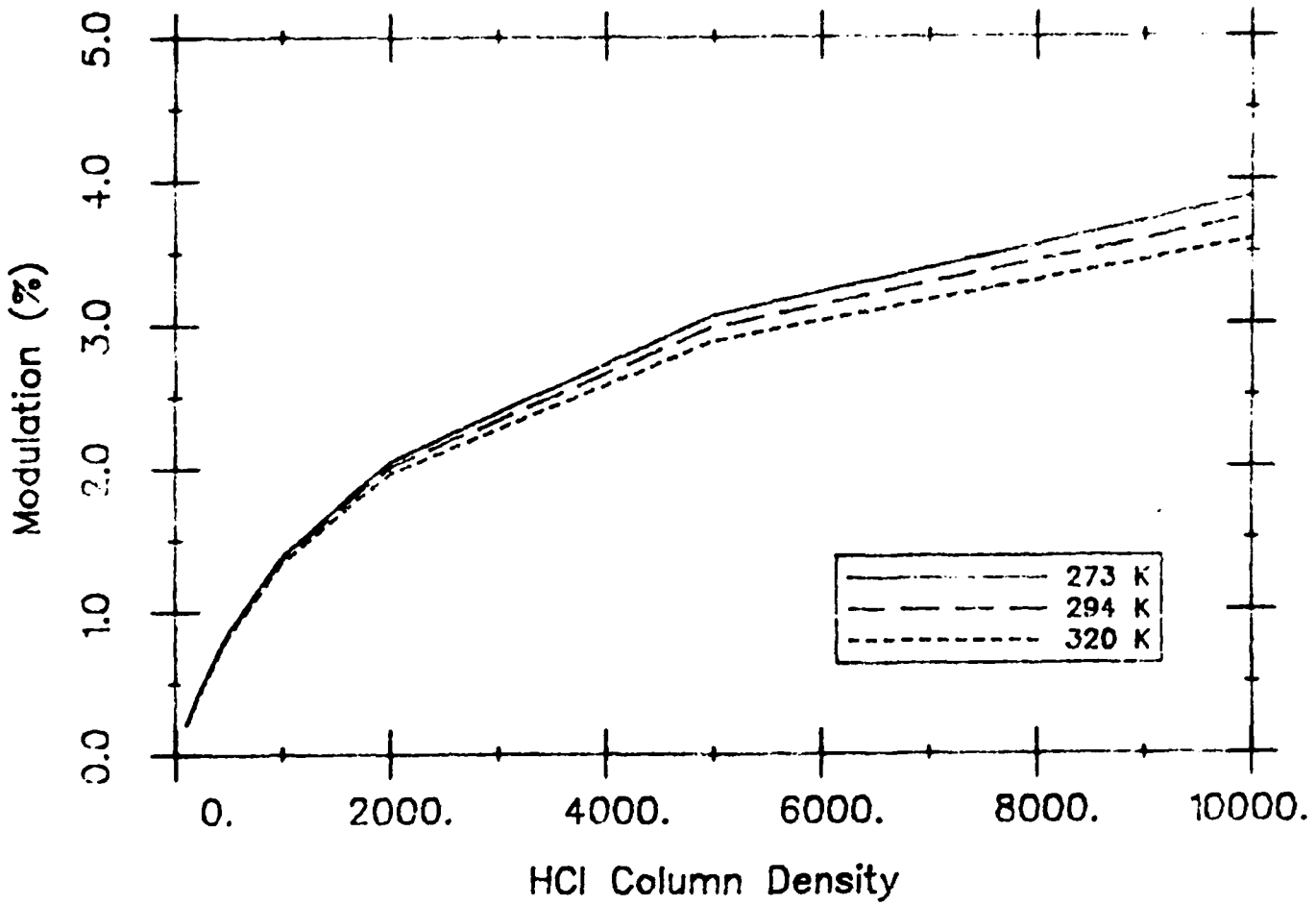

Figure 9. Modulation Versus HCl Column Density for Three Different Temperatures of HCl in Correlation Cell. Conditions: 1 km Atmospheric Path, 2770-2870 cm^{-1} Bandpass, 1 atm-cm HCl in Correlation Cell.

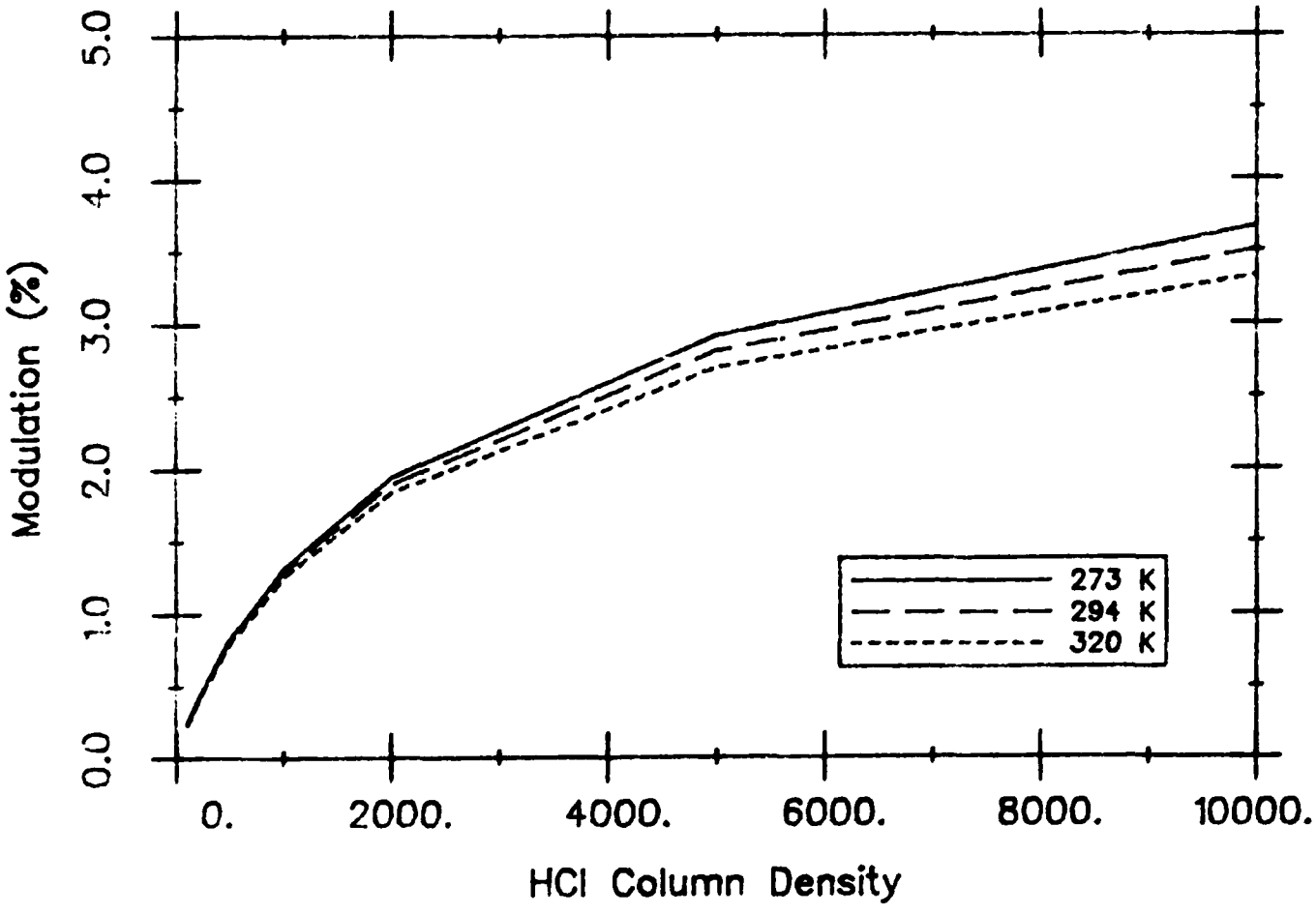

Figure 10. Modulation Versus HCl Column Density for Three Different Temperatures of HCl in Correlation Cell. Conditions: 1 km Atmospheric Path, 2806-2948 cm^{-1} Bandpass, 1 atm-cm HCl in Correlation Cell.

2. INTERFERENCE CALCULATIONS

Modulation may result from the presence of species other than HCl if absorption due to the other species is correlated to HCl absorption. The interfering species may be found in either the ambient atmosphere or in the STS exhaust cloud. Among atmospheric species, water vapor is the only species with significant absorption in the 2600-2950 cm^{-1} region. The STS exhaust cloud consists of HCl gas, water vapor, and aerosols consisting of water, Al_2O_3, and HCl. Since extinction due to aerosols is slowly varying with wavelength, modulation can only result from water vapor and gaseous HCl.

Calculations were performed to estimate the amount of modulation which results from varying the amount of water vapor in the path. By varying the amount of water vapor from 5 torr to 20 torr, the maximum amount of interference resulting from water vapor may be estimated. Figures 11-15 compare the modulation which results from different amounts of HCl while varying the spectral bandpass and correlation cell HCl column density.

The atmospheric path length may also be varied to estimate the modulation which results from interference by atmospheric gases. In Figures 16-21, the atmospheric path length is varied from 1 to 10 km for the same HCl column densities.

As these calculations indicate, interfering gases produce little modulation for the 2770-2870 cm^{-1} and 2690-2850 cm^{-1} bandpasses, but considerably greater modulation for the 2806-2948 cm^{-1} bandpass. The amount of modulation which results from interference may be expressed as an equivalent HCl column density. For an elevation in atmo-

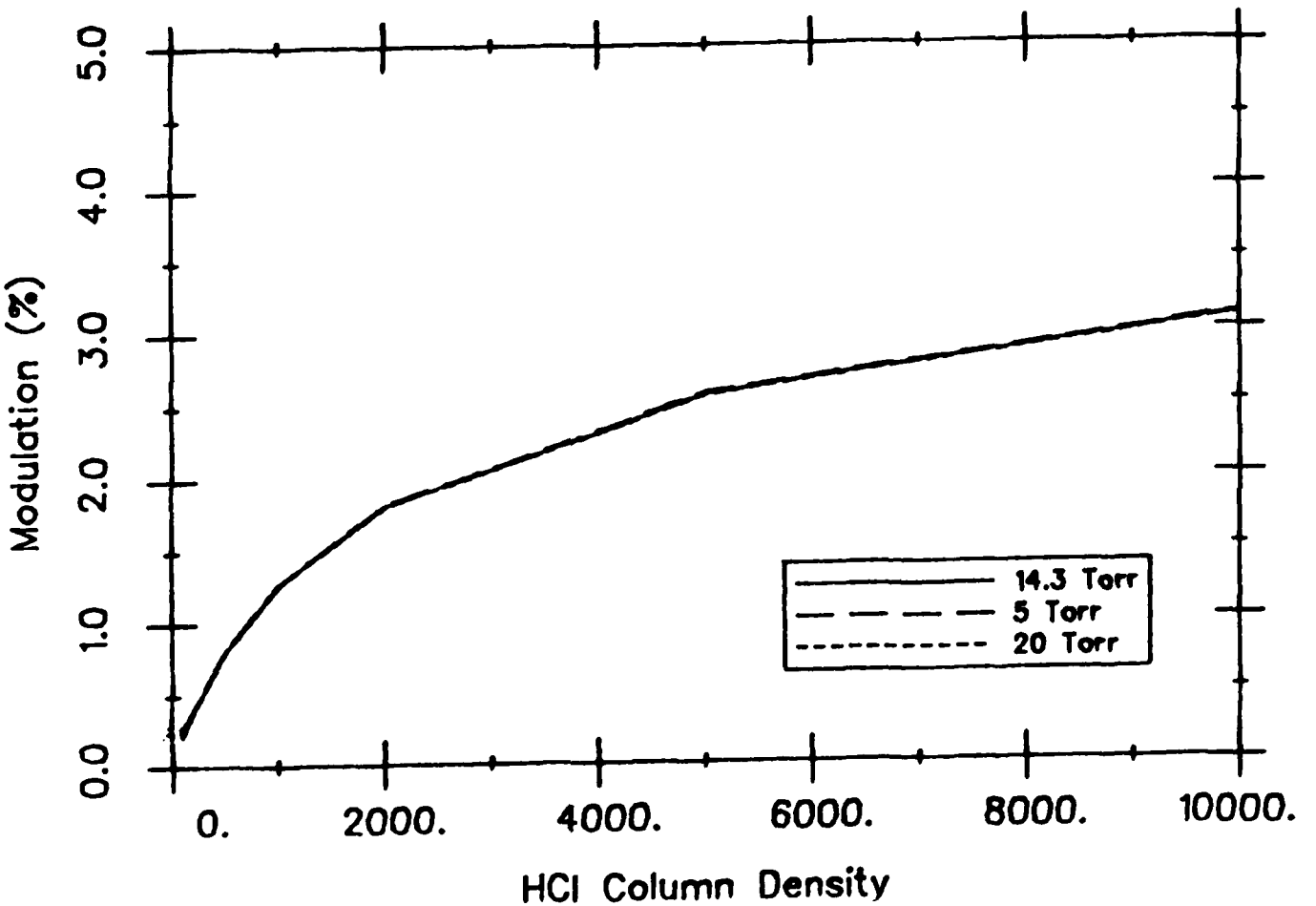

Figure 11. M[illegible]lation Versus HCl Co[illegible] [illegible]ity for [illegible]hree Differ[illegible]t P[illegible]ial Pressures of Water [illegible]apor in the Atmospheri[illegible] A[illegible]dlatitude Summer Atmosphere is Assumed. Conditio[illegible] [illegible] Path, .5 atm-cm HCl in Correlation Cell, 2770-28[illegible] [illegible] Bandpass. The three curves on this plot are app[illegible] [illegible]

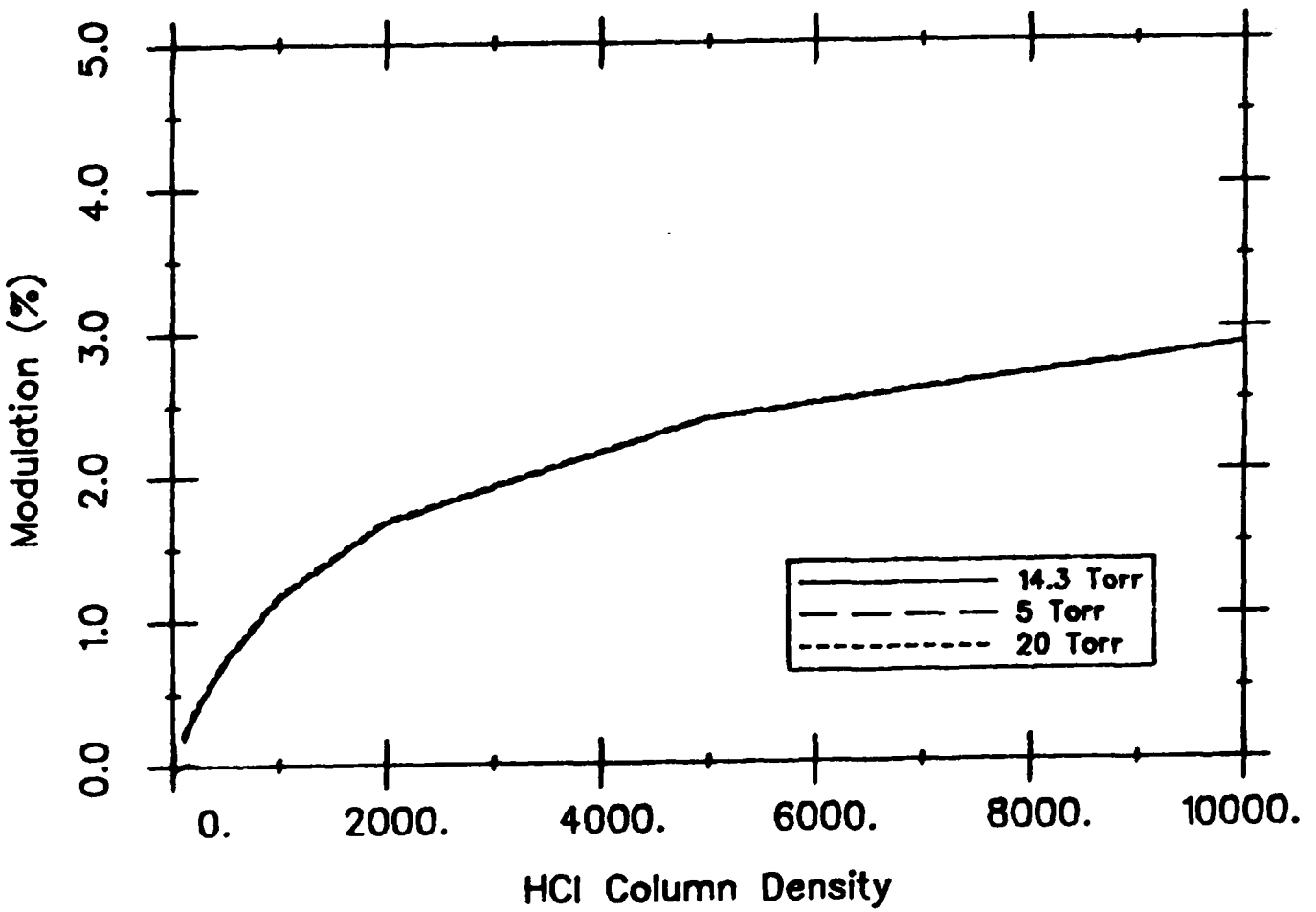

Figure 12. Modulation Versus HCl Column Density for Three Different Partial Pressures of Water Vapor in the Atmospheric Path. A Midlatitude Summer Atmosphere is Assumed. Conditions: 1 km Path, .5 atm-cm HCl in Correlation Cell, 2806-2948 cm^{-1} Bandpass. The three curves on this plot are approximately colinear.

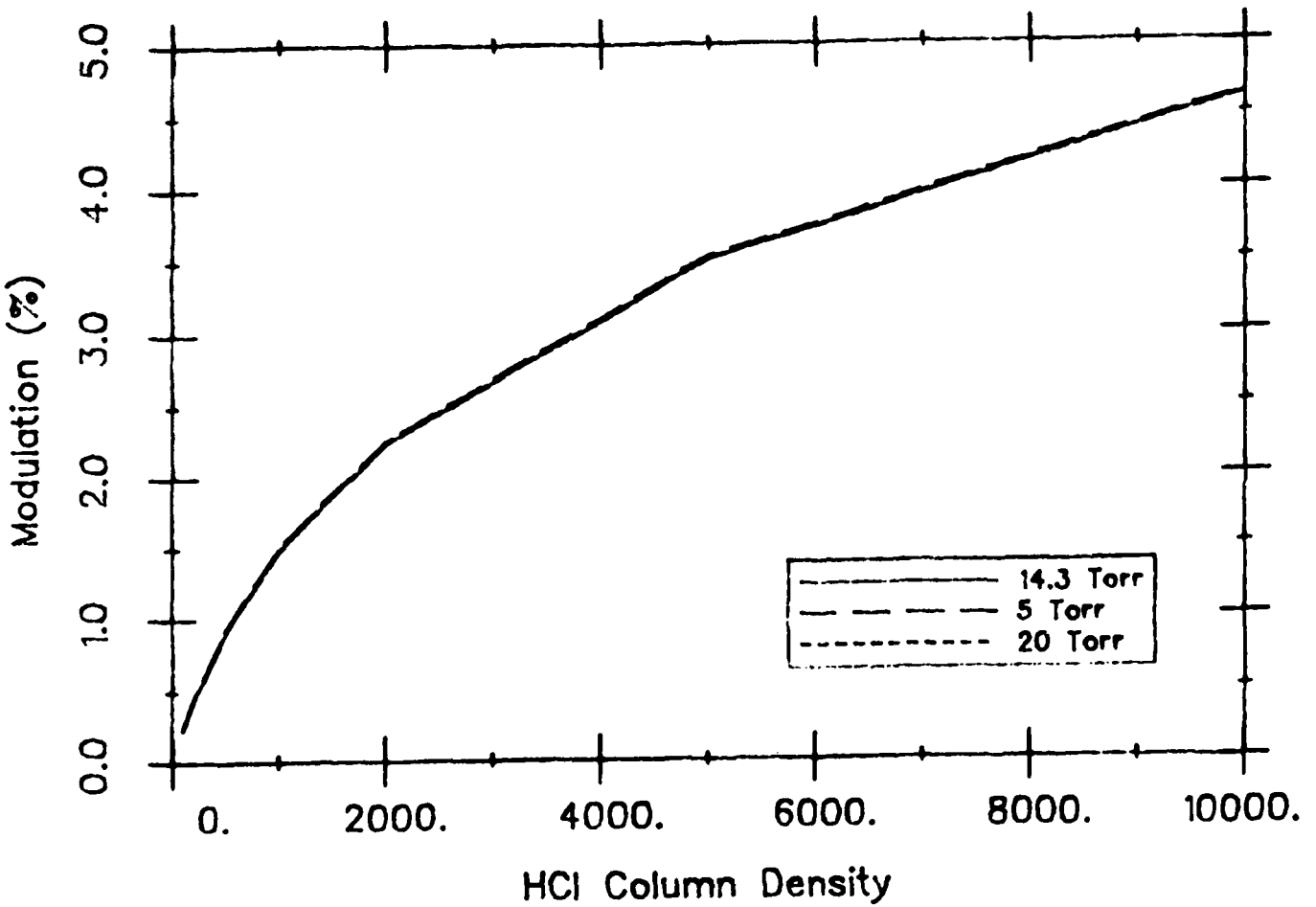

Figure 13. [illegible]lation Versus HCl Column Density for [illegible] Different [illegible]tial Pressures of Water Vapor in the [illegible] A Midlatitude Summer Atmosphere is Assumed. Conditions: [illegible] Path, 2 atm-cm HCl in Correlation Cell, 2770-287[illegible] Bandpass. [illegible] curves [illegible] are [illegible] [illegible]ly [illegible].

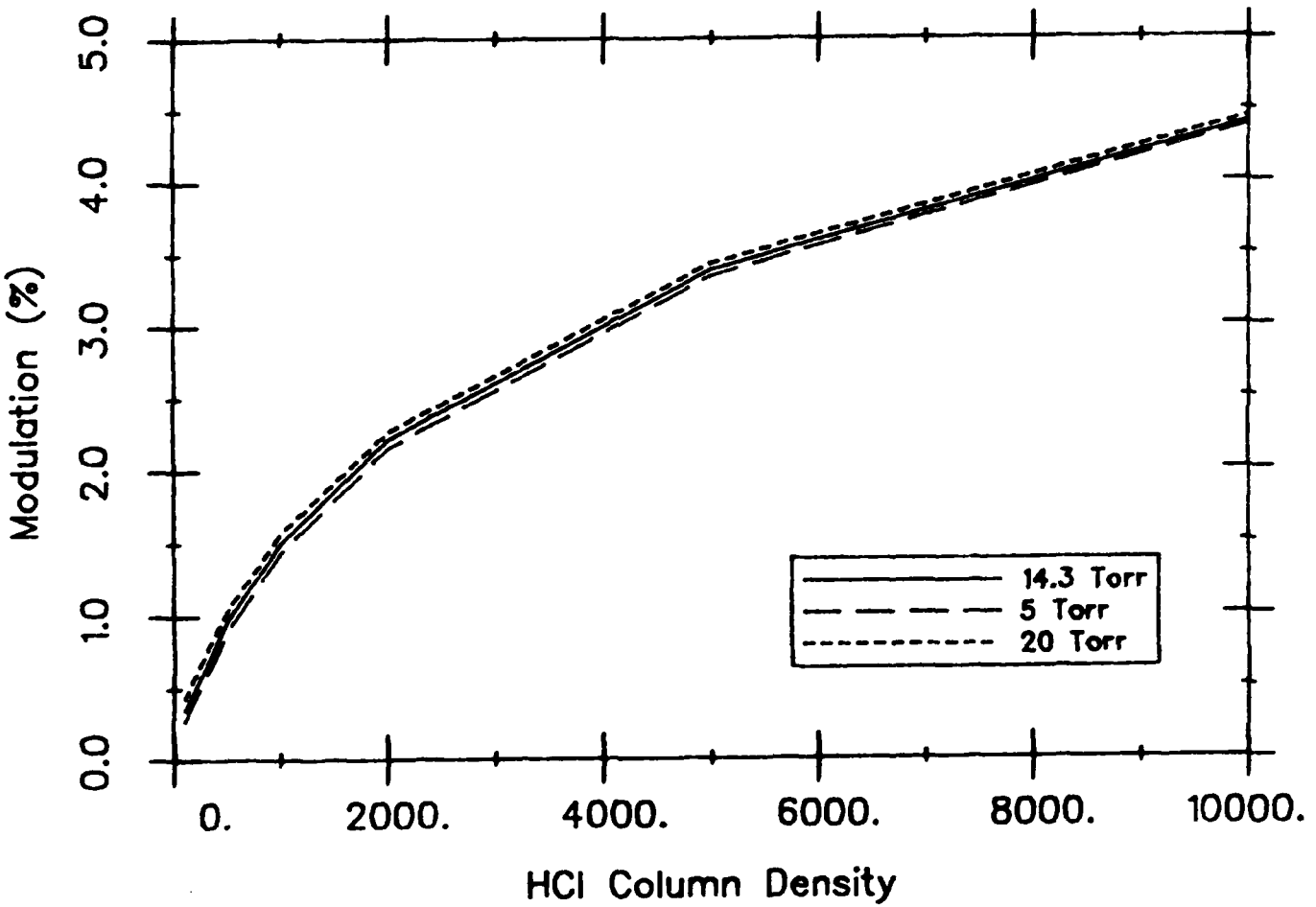

Figure 14. Modulation Versus HCl Column Density for Three Different Partial Pressures of Water Vapor in the Atmospheric Path. A Midlatitude Summer Atmosphere is Assumed. Conditions: 2 km Path, 2 atm-cm HCl in Correlation Cell, 2806-2948 cm^{-1} Bandpass.

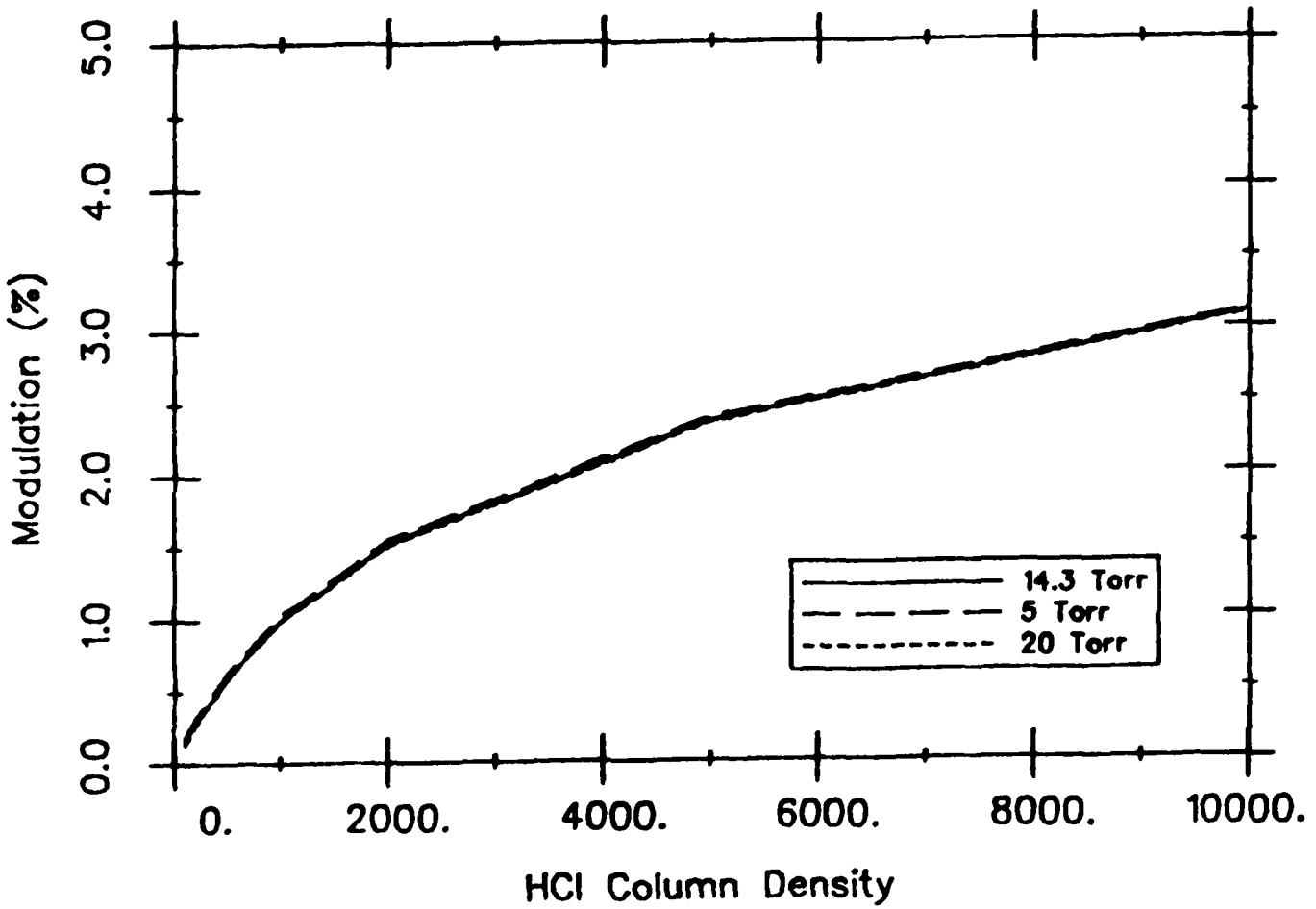

Figure 15 [illegible] Midlatitude Summer Atmosphere is Assumed. Conditions: [illegible] Path, 2 atm-cm HCl in Correlation Cell. 2690-285[illegible]

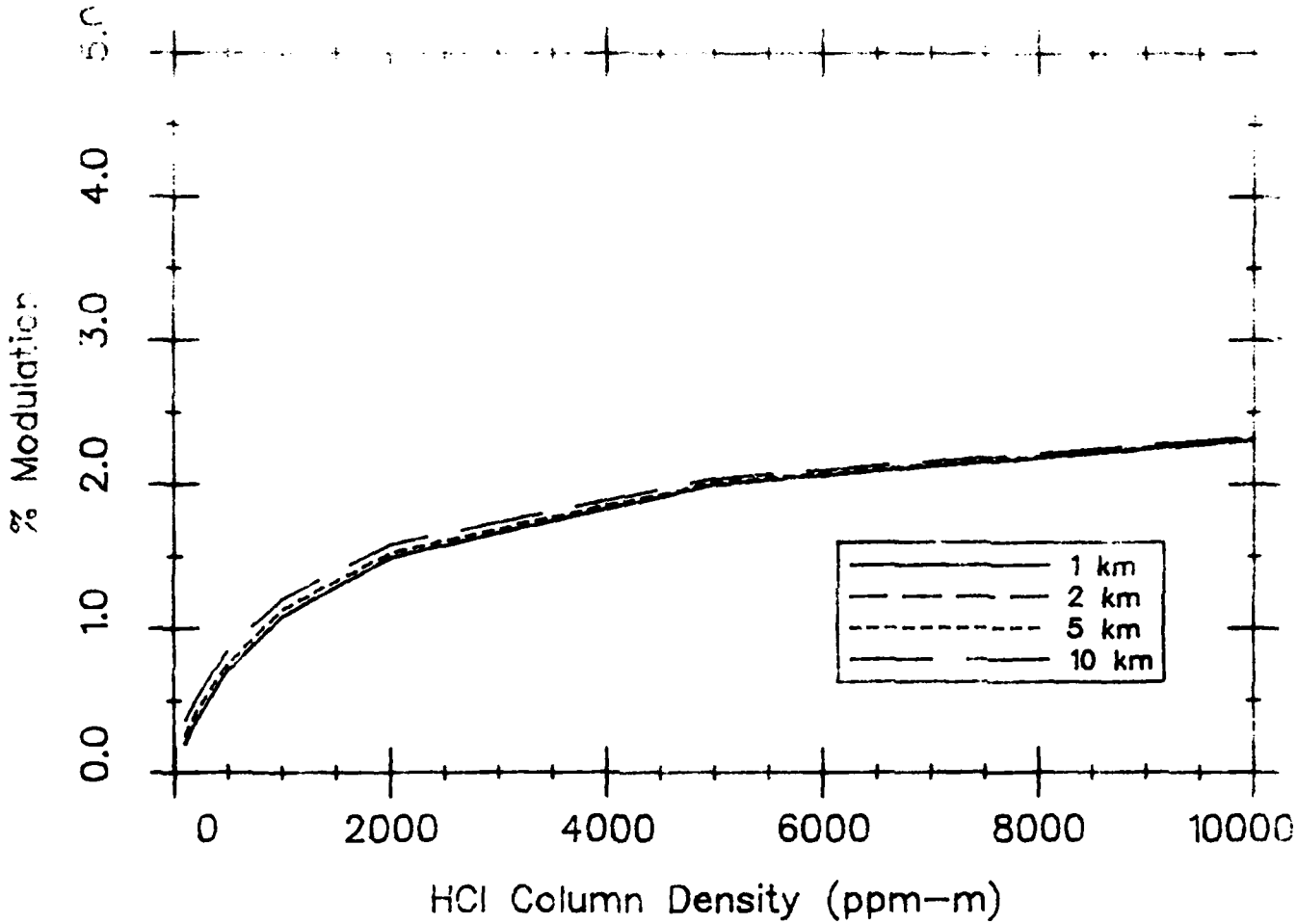

GAS CELL: 1 ATM., 294 K, HCl COLUMN DENSITY 0.25 ATM-CM
FILTER: 2770 - 2870 CM^{-1}

INTERFERING GASES EQUAL TO A MIDLATITUDE SUMMER ATMOSPHERE PATH OF THE GIVEN LENGTH.

Figure 16. Calibration and Interference Estimates, GFCS in Absorption Mode.

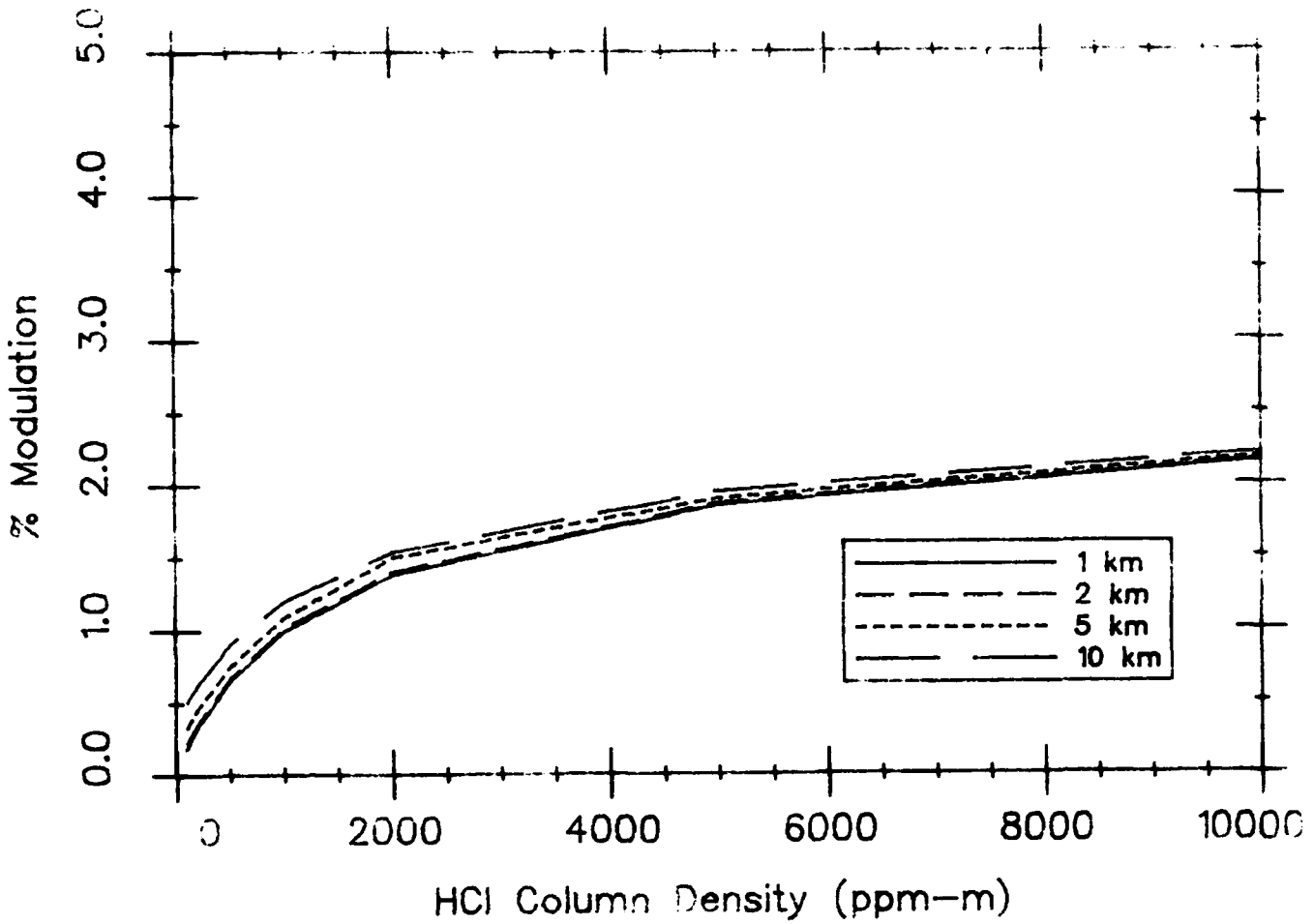

GAS CELL: 1 ATM., 294 K, HCl COLUMN DENSITY 0.25 ATM-CM
FILTER: 2806 - 2948 CM^{-1}

INTERFERING GASES EQUAL TO A MIDLATITUDE SUMMER ATMOSPHERE PATH OF THE GIVEN LENGTH.

Figure 17. Calibration and Interference Estimates, GFCS in Absorption Mode.

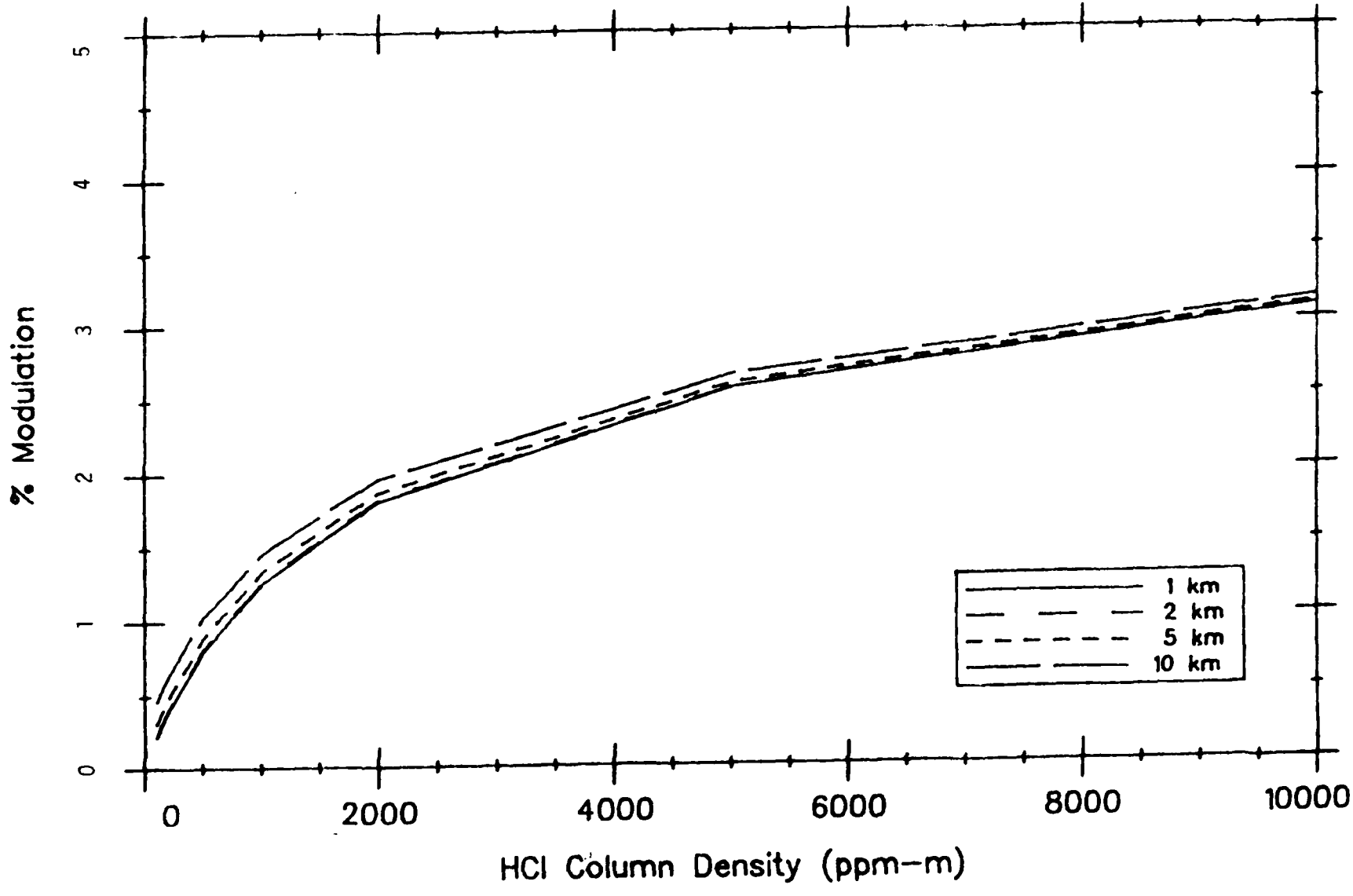

Figure 18. Calibration and Interference Estimates, GFCS in Absorption Mode. Gas Cell: 1 atm., 294 K, HCl Column Density 0.5 atm-cm Filter: 2770-2870 cm-1. Interfering gases Equal to a Midlatitude Summer Atmosphere Path of the Given Length.

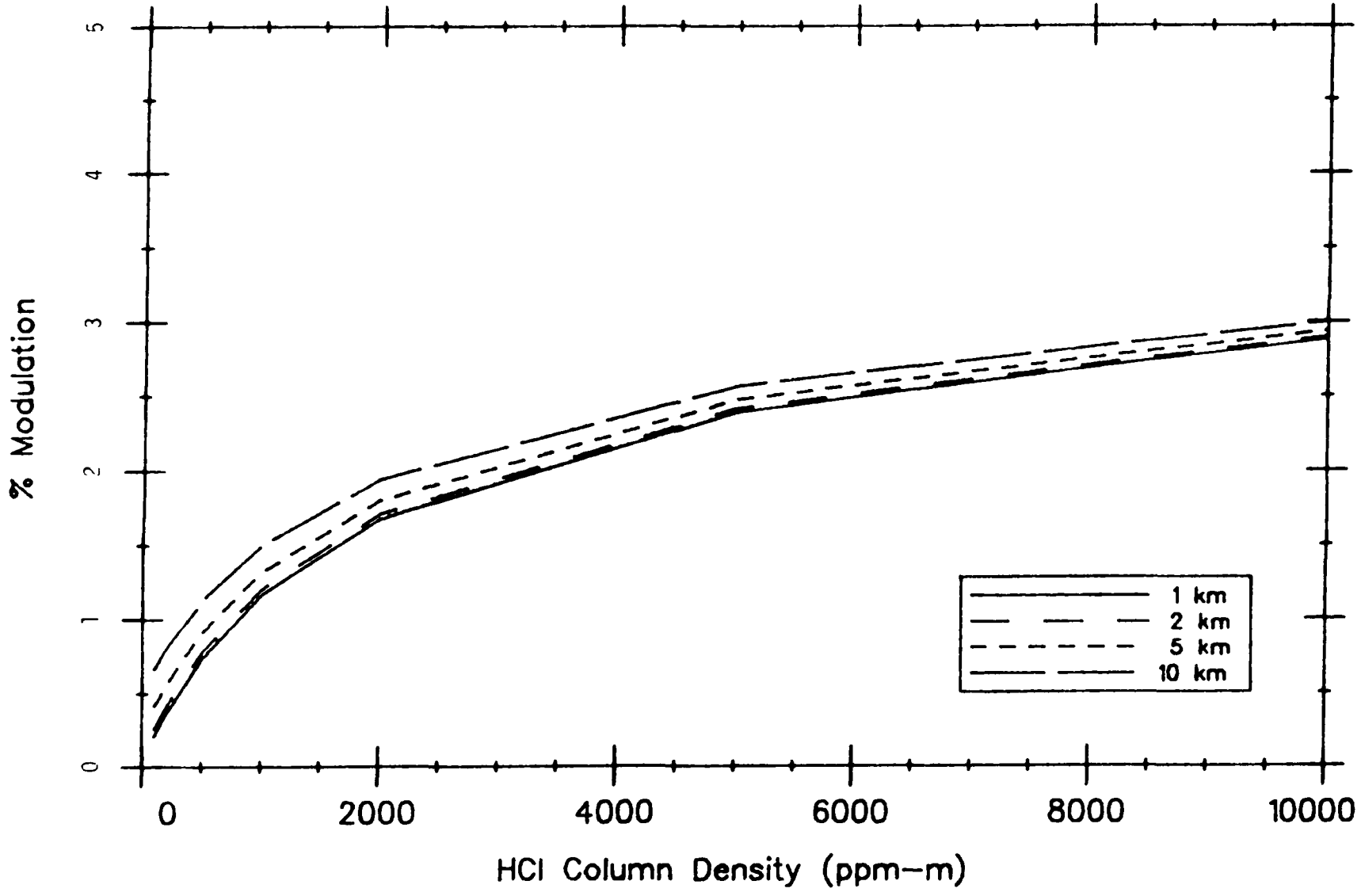

Figure 19. Calibration and Interference Estimates, GFCS in Absorption Mode. Gas Cell: 1 atm., 294 K, HCl Column Density 0.5 atm-cm, Filter: 2806-2948 cm^{-1}. Interfering Gases Equal to a Midlatitude Summer Atmosphere Path of the Given Length.

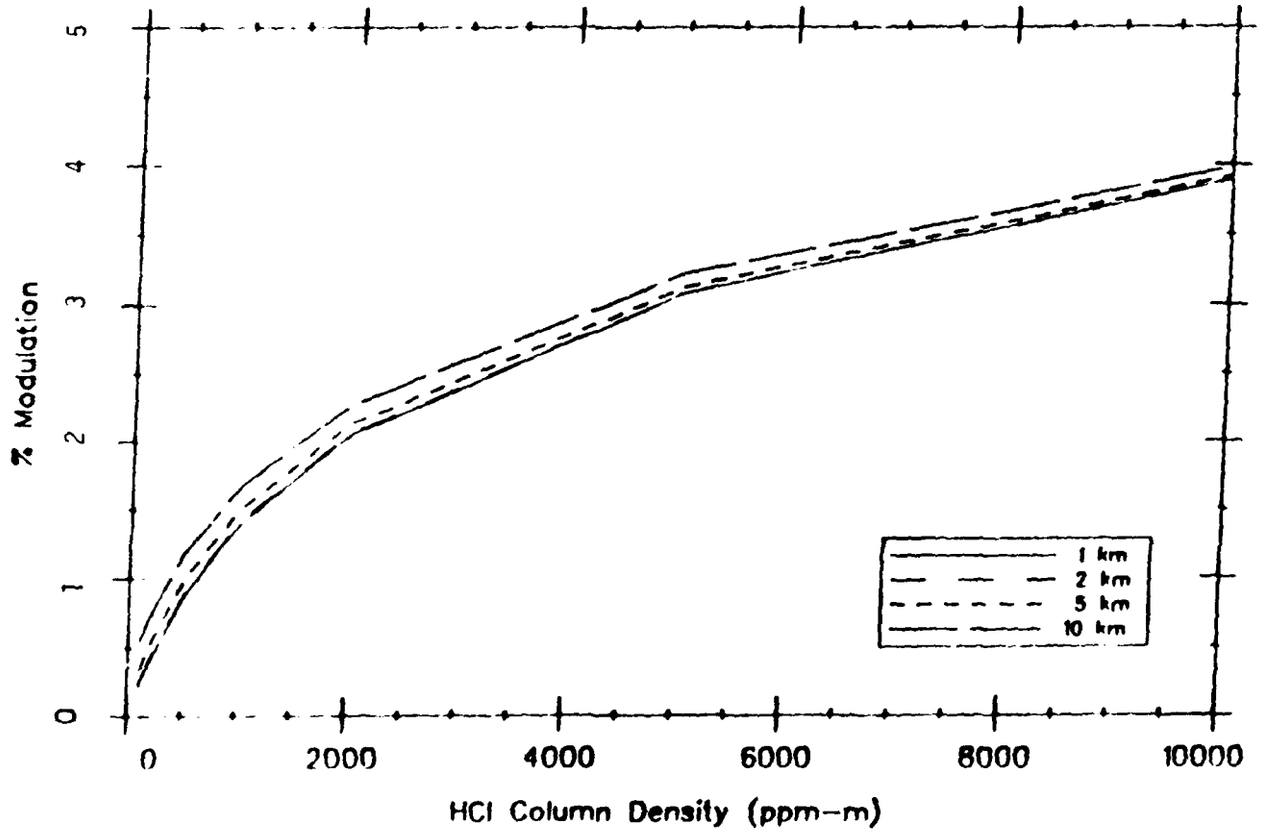

GAS CELL: 1 ATM., 294 K, HCL COLUMN DENSITY 1 ATM-CM
FILTER: 2770 - 2870 CM^{-1}

INTERFERING GASES EQUAL TO A MIDLATITUDE SUMMER ATMOSPHERE PATH OF THE GIVEN LENGTH.

Figure 20. Calibration and Interference Estimates, GFCS in Absorption Mode.

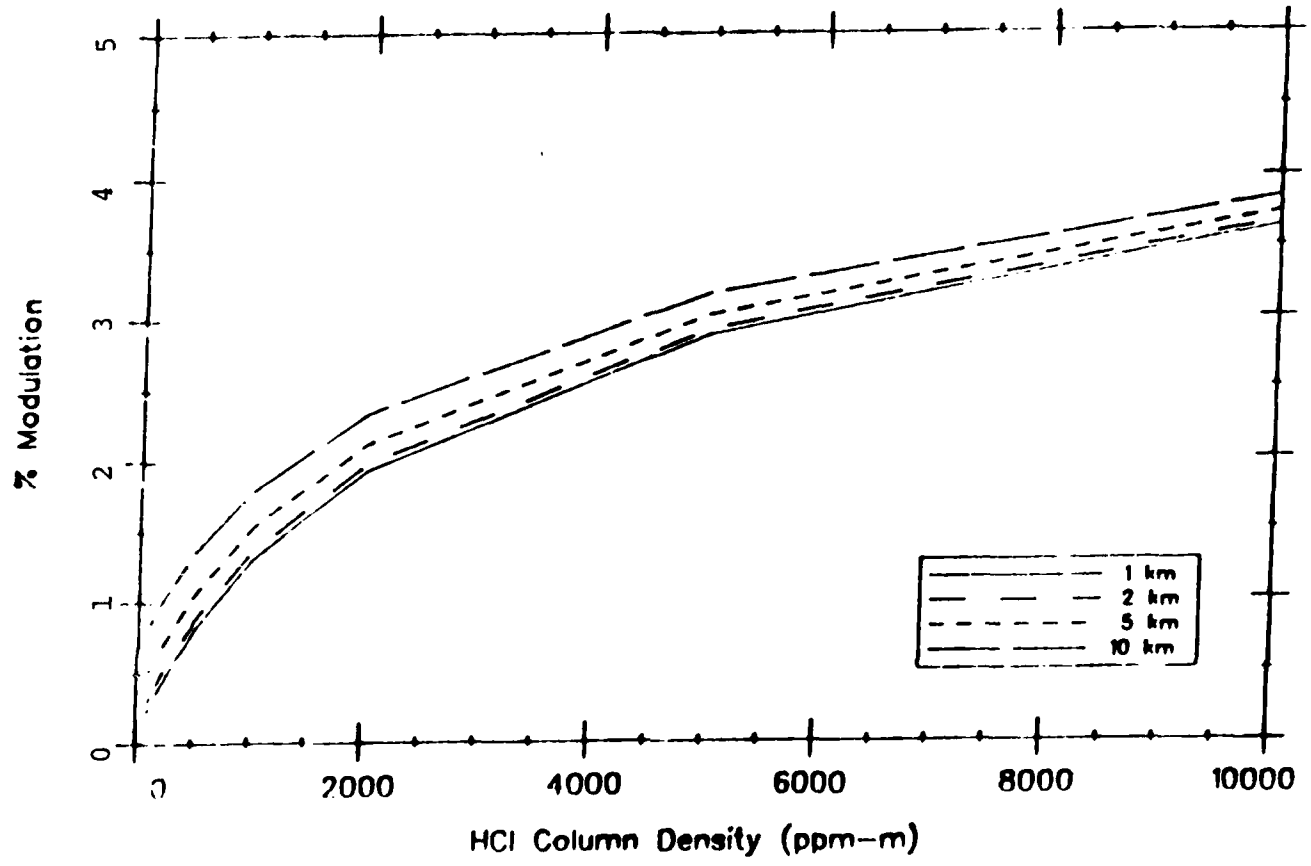

GAS CELL: 1 ATM., 294 K, HCL COLUMN DENSITY 1 ATM-CM
FILTER: 2806 - 2948 CM^{-1}

INTERFERING GASES EQUAL TO A MIDLATITUDE SUMMER ATMOSPHERE PATH OF THE GIVEN LENGTH.

Figure 21. Calibration and Interference Estimates, GFCS in Absorption Mode.

spheric water vapor partial pressure of 15 torr along a 2 km path, the modulation which results using a correlation cell containing 2 atm-cm of HCl is equivalent to 10 ppm-m of HCl for the 2770-2870 cm^{-1} band, but 100 ppm-m of HCl for the 2806-2948 cm^{-1} band. Modulation which may result from water vapor along 10 km paths may approach 1000 ppm-m as a worst case for the latter bandpass. Selecting a correlation cell with HCl column density of .25 atm-cm and a filter with 2770-2870 cm^{-1} bandpass will limit interference due to atmospheric gases along a 10 km path to 100 ppm-m of HCl for a path free of HCl and 250 ppm-m for a path with 1000 ppm-m of HCl present.

Table 3 presents a summary of equivalent HCl column density resulting from interference modulation for several selected cases.

3. *AIR TEMPERATURE EFFECTS*

Since the molecular number density of air is reduced at elevated temperatures and the GFCS operating in absorption mode detects HCl molecular column density, to convert modulation to a column density expressed in ppm-m requires calibration for temperature. These calculations have been performed assuming sub-Arctic winter, midlatitude summer, and tropical model atmospheres with the HCl at the ambient temperature of the model atmosphere (257 K, 294 K, and 300 K, respectively). In addition to taking into account air temperatures, these calculations consider the variation in water vapor partial pressure for the given model atmospheres. The results of these calculations are presented in Figures 22-27.

TABLE 3. EQUIVALENT HCl COLUMN DENSITY DUE TO INTERFERING GASES.

Bandpass (cm^{-1})	Atmospheric Path Length (km)	Correlation Cell HCl Concentration (atm-cm)	Atmospheric Water Vapor (torr)	Equiv. HCl Column Density (ppm-m)
2770-2870	1	0.25	14.3	10
	10	0.25	14.3	100
	2	2.0	5.0	50
	2	2.0	20.0	70
2806-2948	1	0.25	14.3	100
	10	0.25	14.3	1000
	2	2.0	5.0	120
	2	2.0	20.0	250

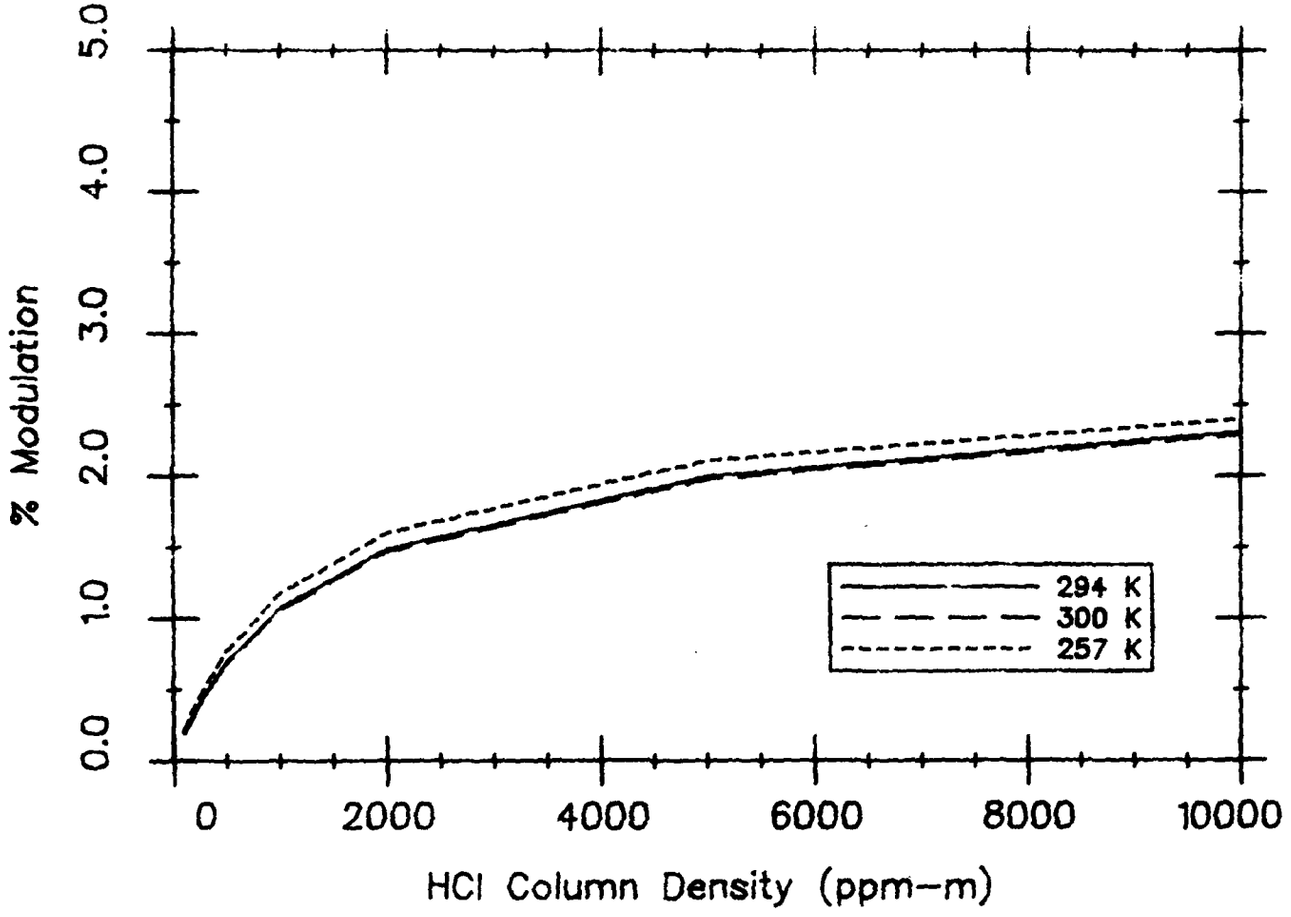

Figure 22. Modulation Resulting from HCl Present in a 1 km Midlatitude Summer (294 K), Tropical (300 K), and Sub-Arctic Winter (257 K) Atmosphere. Conditions: .25 atm-cm HCl in Correlation cell at 294 K, 1013 mb, 2770-2870 cm^{-1} Bandpass.

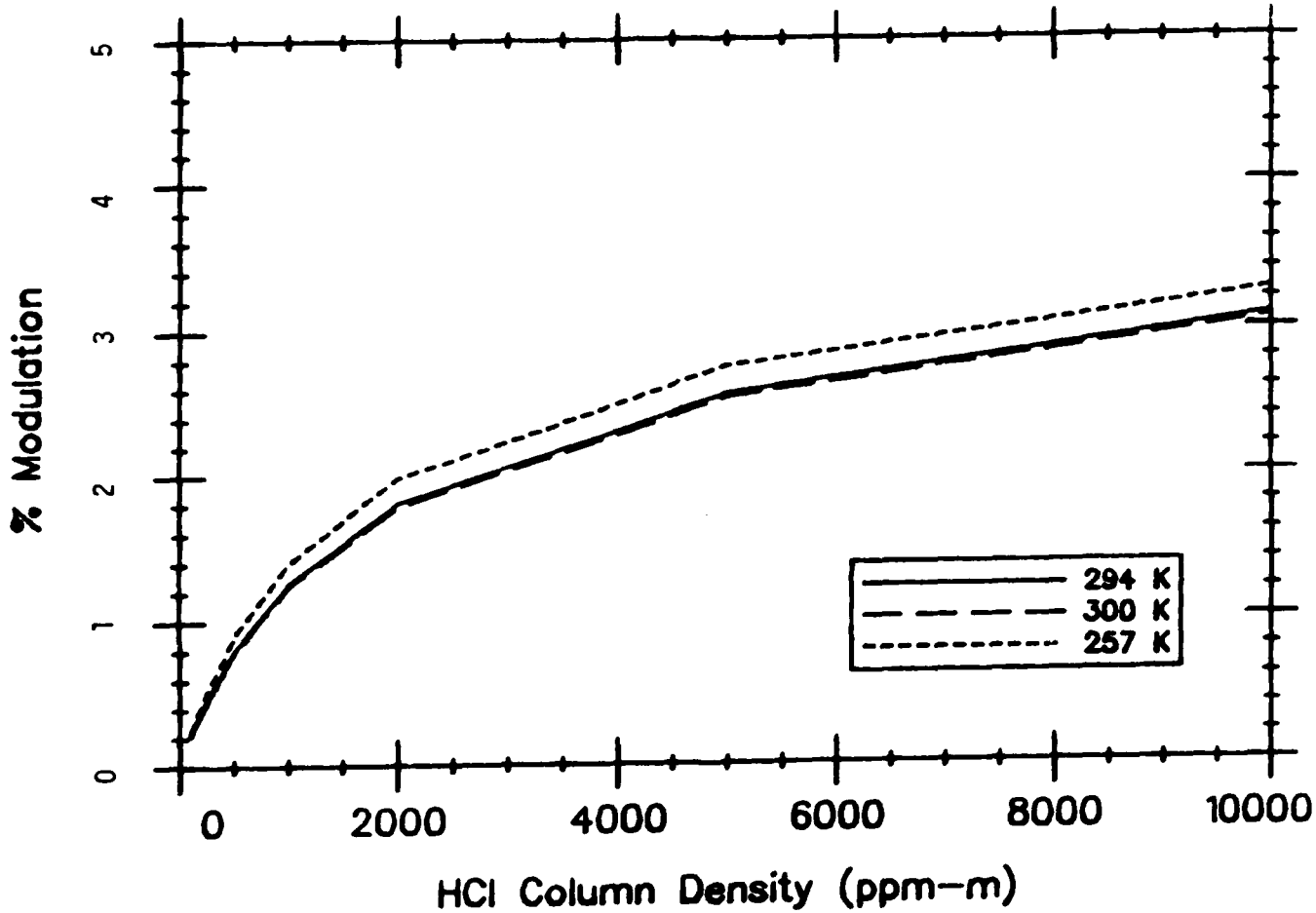

Figure 23. Modulation from HCl Present in a 1 km Midlatitude Summer (294 K), Tropical (300 K), and Sub-Arctic Winter (257 K) Atmosphere. Conditions: .50 atm-cm HCl in Correlation Cell at 294 K, 1013 mb, 2770-2870 cm^{-1} Bandpass.

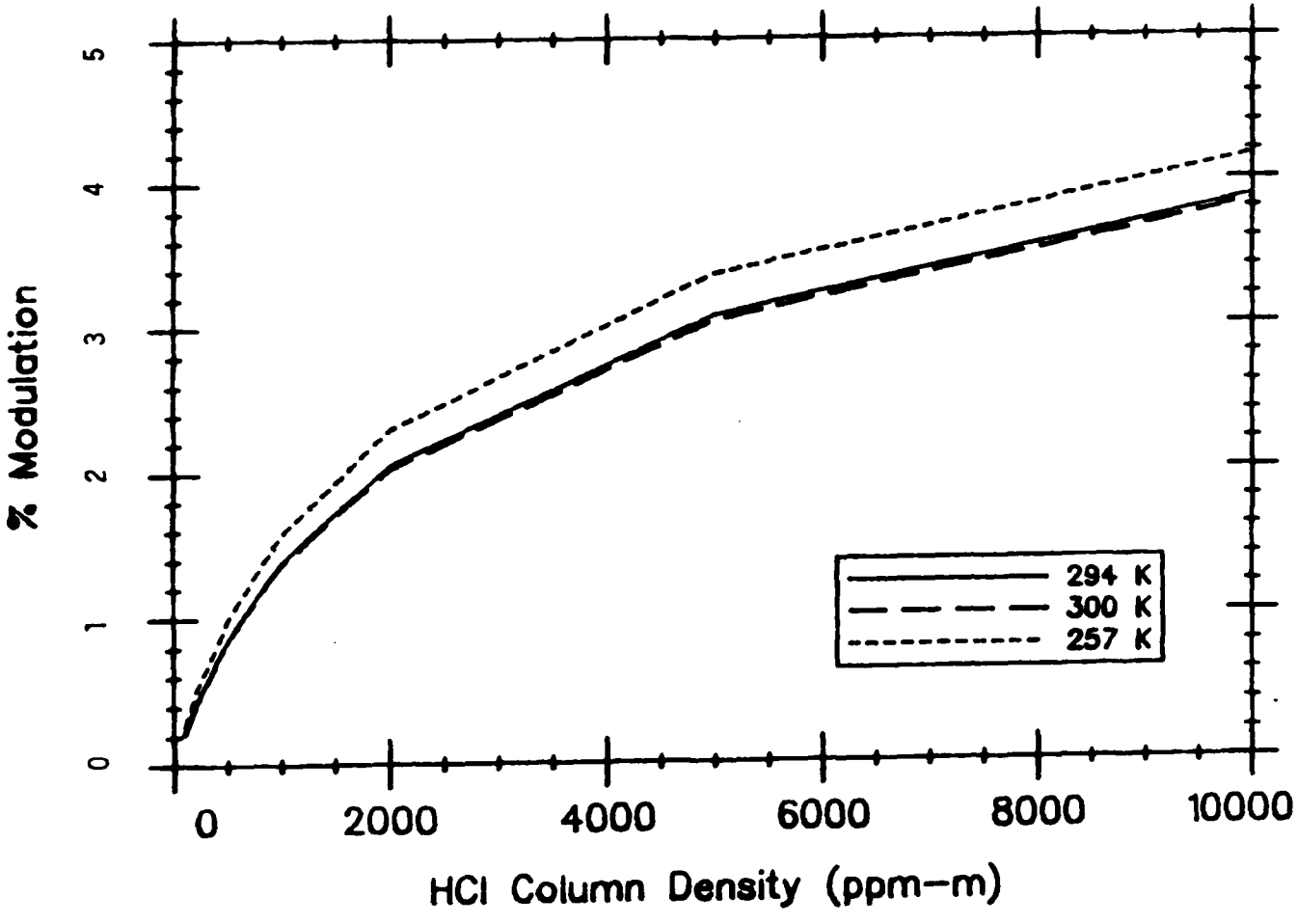

Figure 24. Modulation from HCl Present in a 1 km Midlatitude Summer (294 K), Tropical (300 K), and Sub-Arctic Winter (257 K) Atmosphere. Conditions: 1.0 atm-cm HCl in Correlation Cell at 294 K, 1013 mb, 2770-2870 cm^{-1} Bandpass.

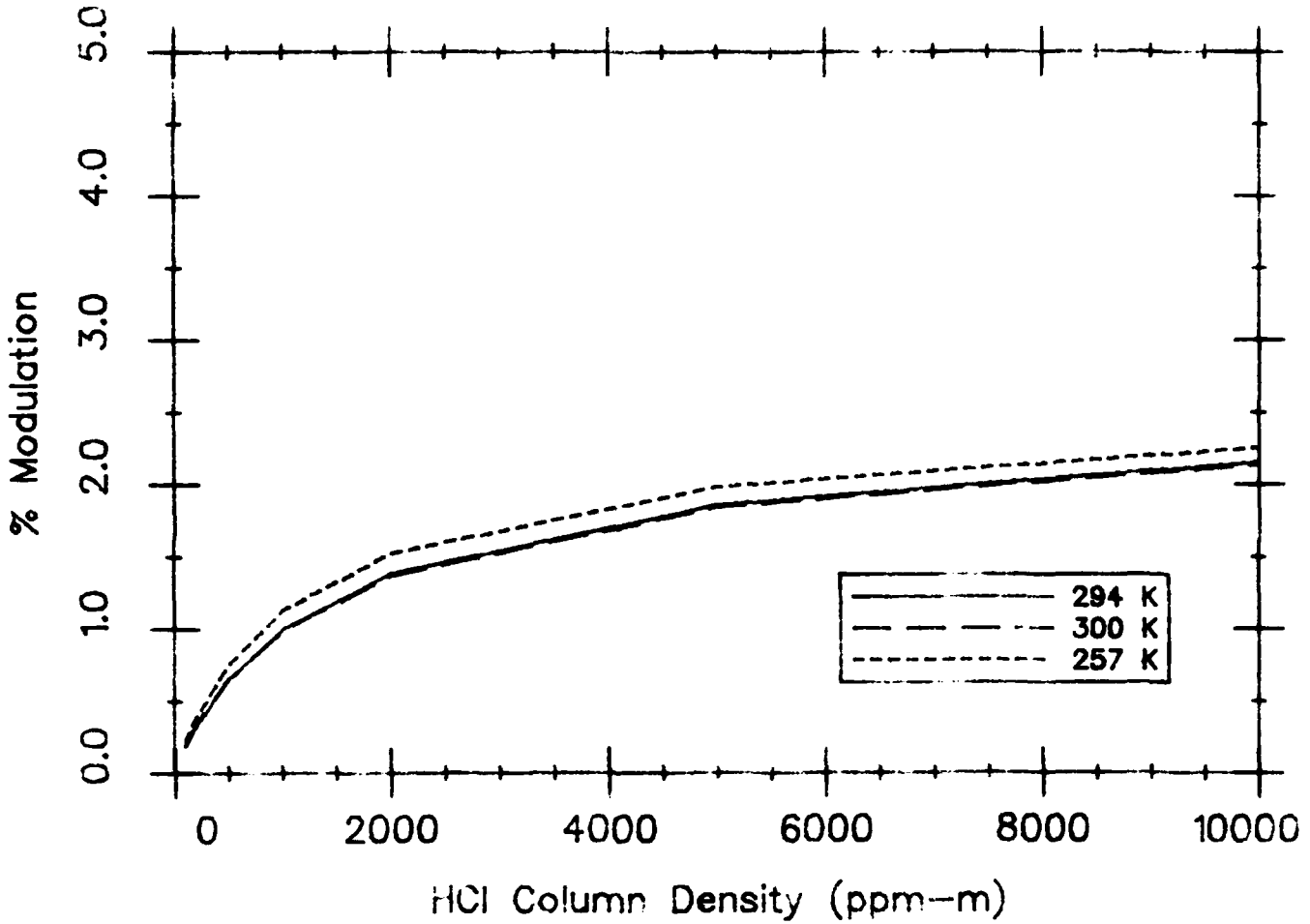

Figure 25. Modulation from HCl Present in a 1 km Midlatitude Summer (294 K), Tropical (300 K), and Sub-Arctic Winter (257 K) Atmosphere. Conditions: .25 atm-cm HCl in Correlation Cell at 294 K, 1013 mb, 2806-2948 cm^{-1} Bandpass.

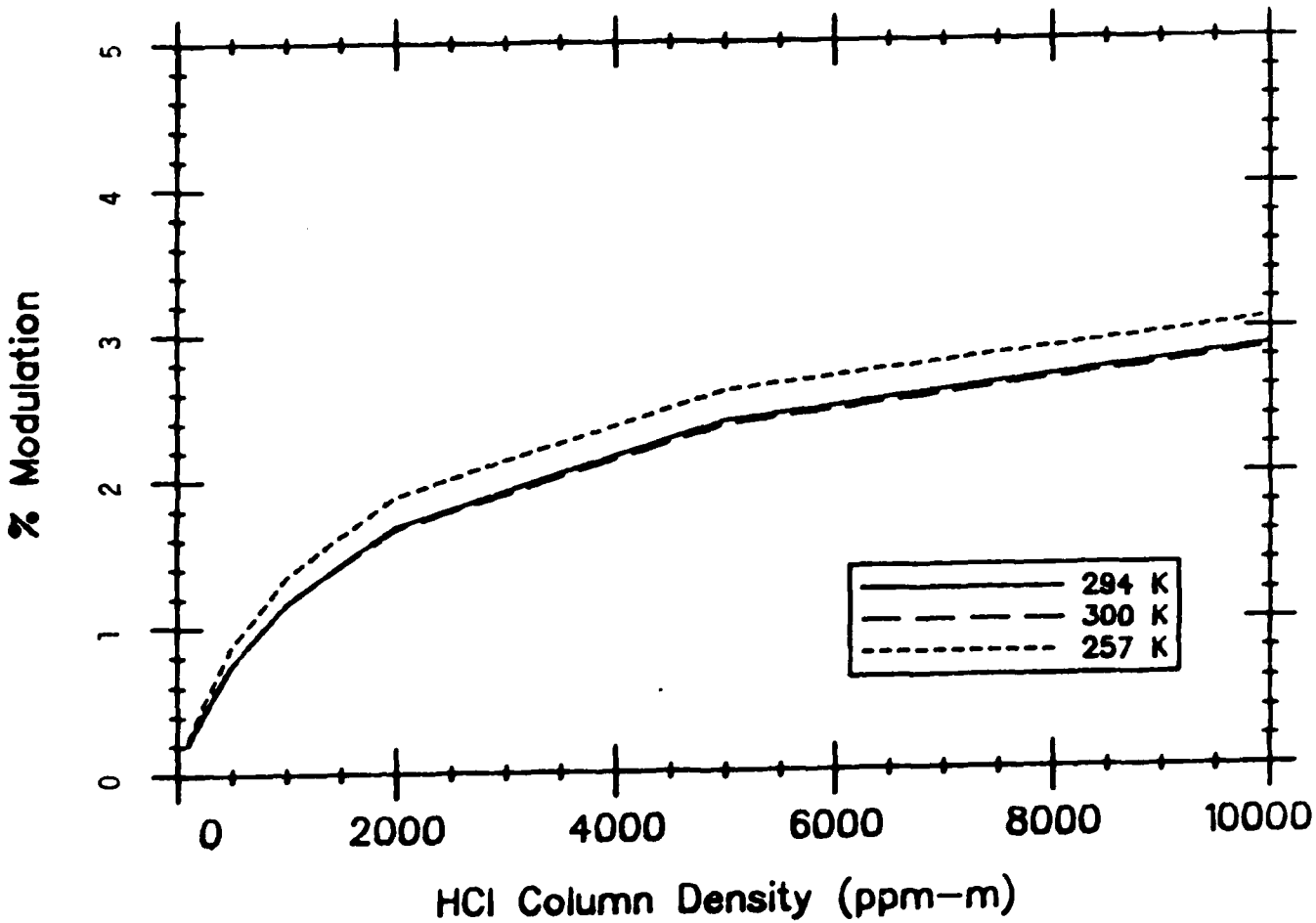

Figure 26. Modulation from HCl Present in a 1 km Midlatitude Summer (294 K), Tropical (300 K), and Sub-Arctic Winter (257 K) Atmosphere. Conditions: .50 atm-cm HCl in Correlation Cell at 294 K, 1013 mb, 2806-2948 cm^{-1} Bandpass.

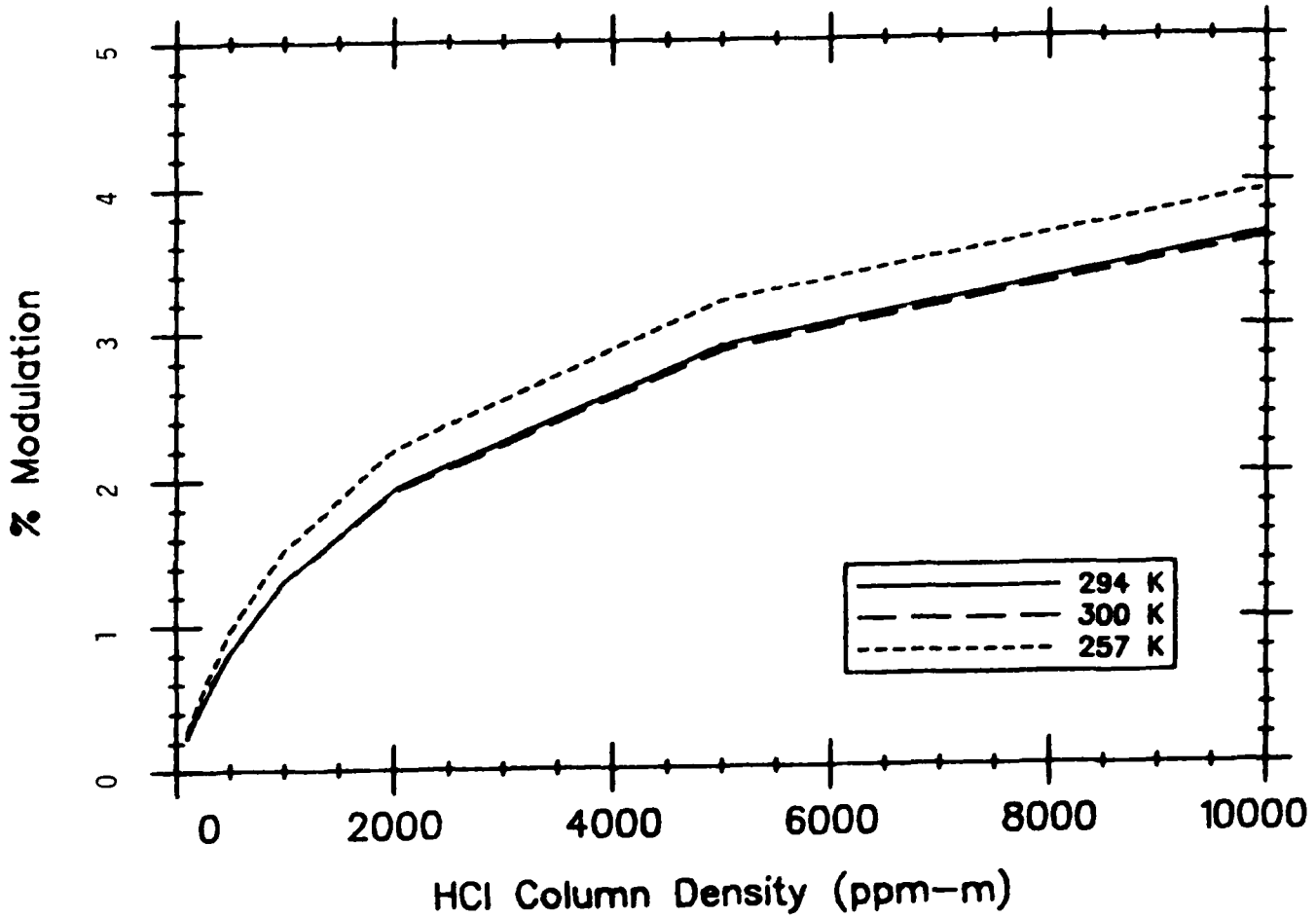

Figure 27. Modulation from HCl Present in a 1 km Midlatitude Summer (294 K), Tropical (300 K), and Sub-Arctic Winter (257 K) Atmosphere. Conditions: 1.0 atm-cm HCl in Correlation Cell at 294 K 1013 mb, 2806-2948 cm^{-1} Bandpass.

SECTION IV
PRELIMINARY INSTRUMENT FEASIBILITY STUDIES

A. USE OF INFRAMETRICS IMAGER DETECTING HCl EMISSIONS

The Inframetrics Model 525 3-5 μm imager has been proposed as an imaging detector for use in an HCl GFCS. The nominal specifications for the instrument are described in Table 4.

TABLE 4. SPECIFICATIONS FOR INFRAMETRICS MODEL 525.

Minimum Detectable ΔT	0.2 C @ 300 K
Field of View	14° x 18°
Spectral Range, Nominal	3-5 μm
Detector	HgCdTe
Detector Coolant	LN_2
Frame Rate	30 Hz
Resolvable Elements per Line	250
Lines per Frame	200
Instantaneous Field of View	2 mr

When viewing a 300 K blackbody source, the minimum detectable temperature (MDT) difference is 0.2 C. This translates into a differential radiance of 1.4×10^{-6} W/cm^2-sr, assuming a uniform 3-5 μm spectral bandpass. Because the MDT characteristic implies frame averaging over the eye integration time of 0.2 seconds, the single-frame noise equivalent radiance (NER) is 3.5×10^{-6} W/cm^2-sr.

Since the single frame NER is greater than the modulation radiance expected in emission mode, it is clear that

the Inframetrics imager will not be acceptable for emission mode operation. While frame-averaging over N frames has the potential to reduce the NER by $\sqrt{N}$, changing radiance levels within the scene will limit the usefulness of this approach to very small values of N.

One possibility for increased sensitivity which might permit use of a commercial imager is to detect scattered solar radiation passing through an HCl cloud. The GFCS instrument operates in absorption mode when using this source. Estimates of modulation which might result in this mode are calculated in the next section.

B. SCATTERING OF SOLAR RADIATION

Solar radiation may be scattered into the line of sight by aerosols in the launch cloud or ambient atmospheric aerosols. For an HCl GFCS detecting atmospheric radiation, solar radiation scattered into the line of sight may be greater in magnitude than radiation emitted by gases along the path. This provides the opportunity to increase the modulated signal by viewing HCl absorption of scattered solar radiation.

There are two principal difficulties with this mode of operation. First, the amount of solar radiation scattered into the line of sight is dependent on the scattering angle. Only for small scattering angles ($\theta < 30$ degrees) will the modulation be sufficiently large to be useful. Second, when using the STS launch cloud as the scattering medium, it is difficult to quantify the gaseous HCl concentration. Assumptions must be made concerning the distribution of gaseous HCl relative to the aerosol. In addition, for a launch cloud dense enough to provide reasonable scattering, the large optical depth will mask absorption by gaseous HCl.

Calculations were performed to estimate the amount of radiation scattered into the line of sight by a cumulus cloud background and a cloud of aerosol from a typical STS launch. The particle size distributions used to represent the aerosols are presented in Figures 28 and 29. Mie scattering calculations were performed to obtain the scattering and extinction coefficients and phase functions for the two cases. The refractive indices used in the cumulus cloud case were those of liquid water, while a 4 M HCl solution was used to represent the shuttle launch cloud.

The results of the Mie scattering calculations served as inputs to the computer code, FCLOUD (Reference 9). This code predicts the amount of solar radiance scattered into the line of sight by an ellipsoidal cloud. Figures 30 and 31 provide estimates of solar radiance scattered into the path as a function of scattering angle for a cumulus cloud background and an HCl aerosol cloud.

For a 15 degree scattering angle, the radiance scattered into the path by a cumulus cloud background is approximately equal to 2.61×10^{-5} $W/cm^2\text{-}sr\text{-}cm^{-1}$ at a wavelength of 2800 cm^{-1}. Assuming 2 percent modulation over a 100 cm^{-1} bandpass, the modulated scattered path radiance is equal to 5.2×10^{-5} $W/cm^2\text{-}sr$. However, if the scattering angle increases to 60°, the path radiance decreases by an order of magnitude. Since the radiance of a 300 K blackbody at the same wavelength is 4.1×10^{-8} $W/cm^2\text{-}sr\text{-}cm^{-1}$, the scattered radiance will dominate the emitted radiance.

Path radiance due to scattering by an HCl cloud at a 30 degree scattering angle is equal to 6.5×10^{-8} $W/cm^2\text{-}sr\text{-}cm^{1}$. This is comparable to the emitted path radiance. As a result, it appears that solar radiation scattered by an HCl cloud is not likely to significantly increase the signal available, but will need to be taken into consideration for emission mode calibration.

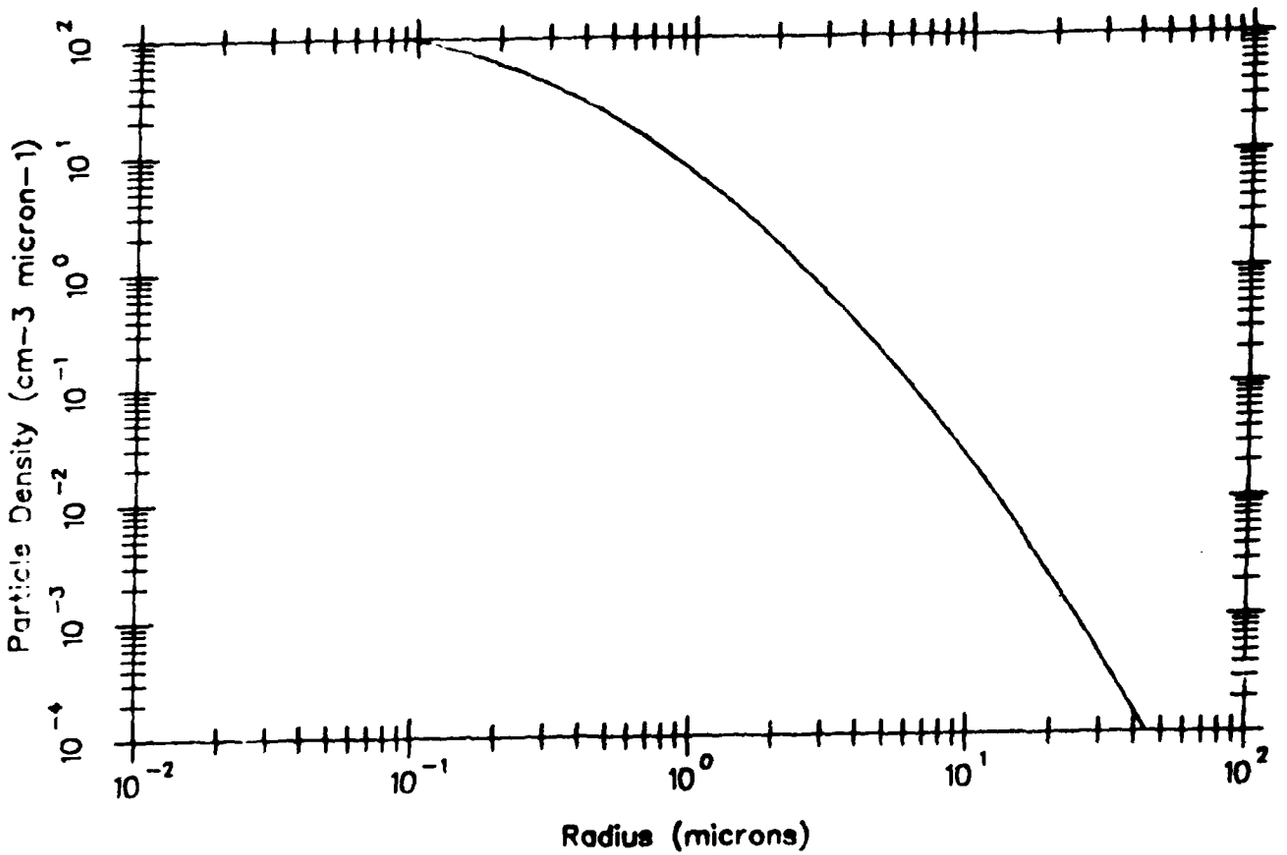

Figure 28. Particle Size Distribution Used to Represent STS Launch Cloud.

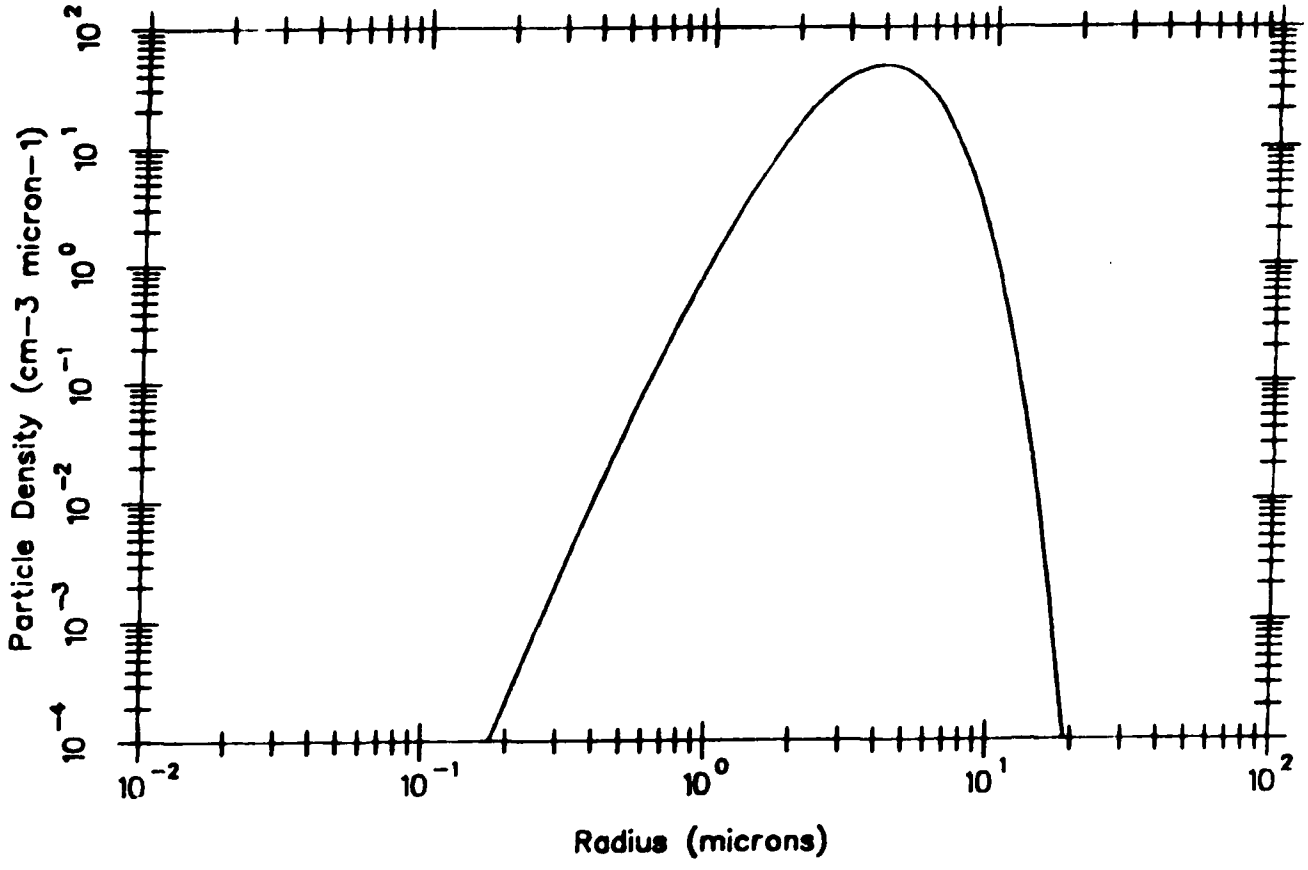

Figure 29. Particle Size Distribution Used to Represent Cumulus Cloud.

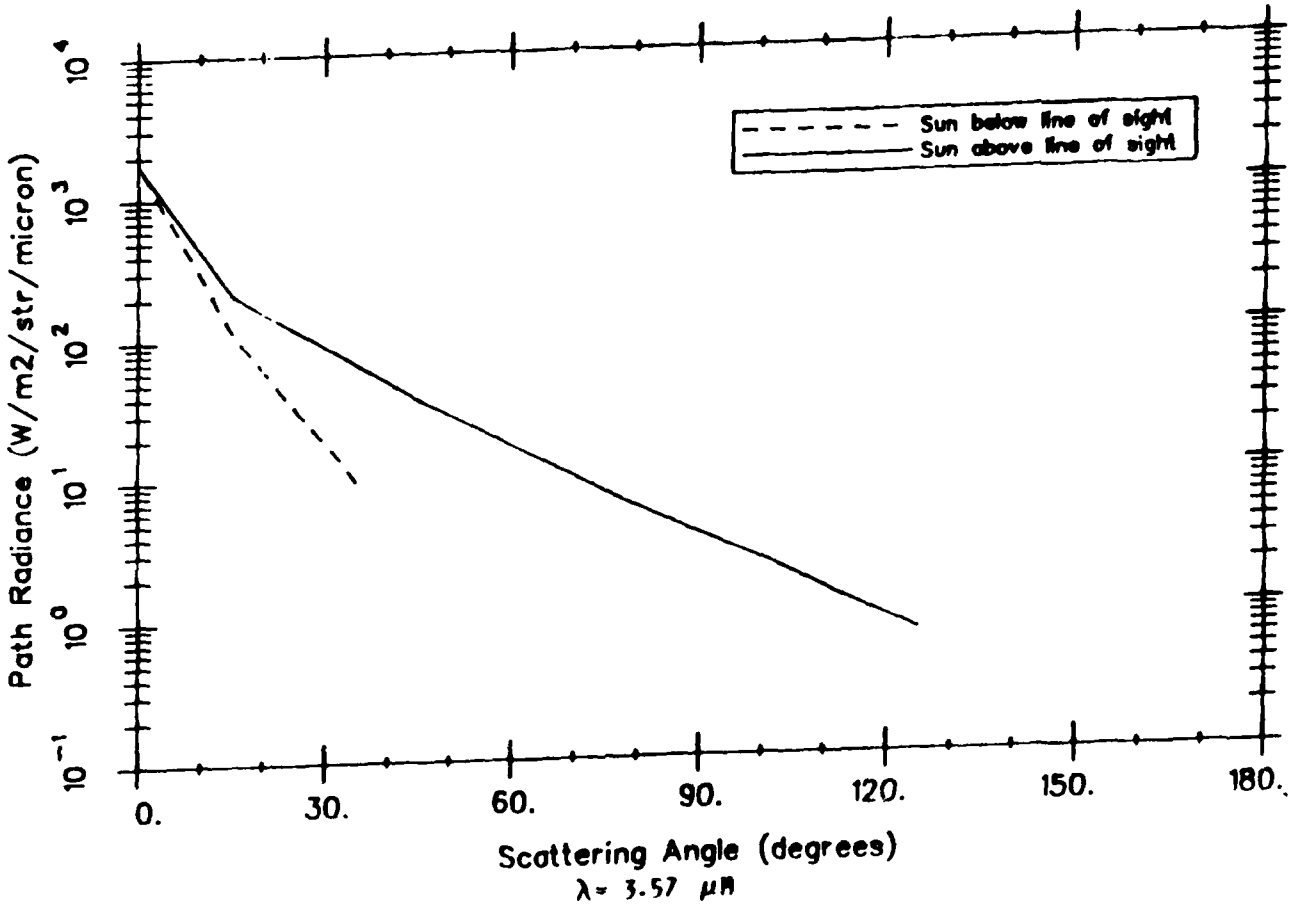

Figure 30. Scattered Solar Radiance for a Cumulus Cloud Background.

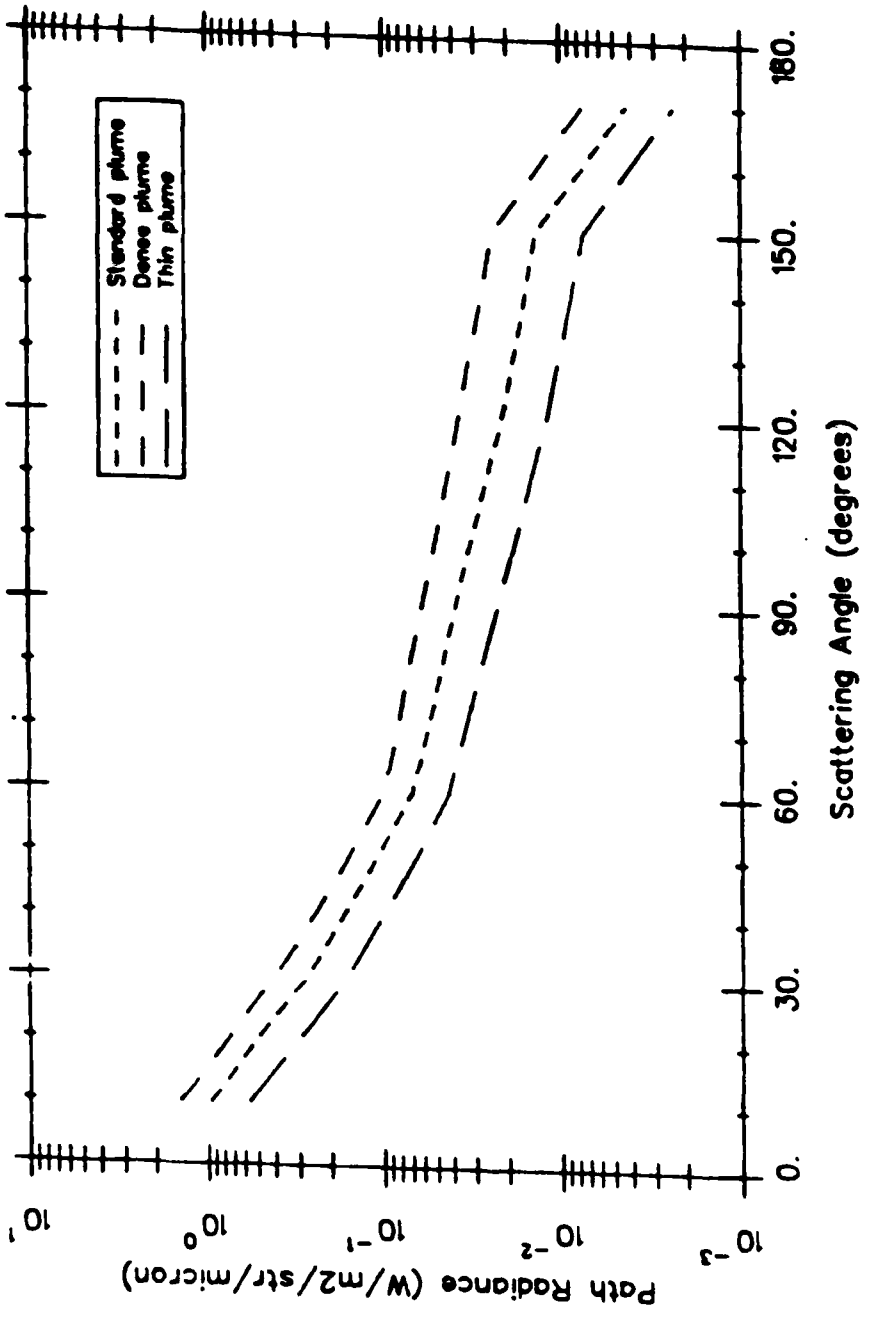

Figure 31. Solar Radiance Scattered by STS Launch Cloud. Conditions: λ= 3.57 um, Visible Extinction Coefficient= .25, .5, 1.0 km^{-1} for Thin, Standard, and Dense Plume, Single-Scattering Albedo= .595.

(The reverse of this page is blank.)

SECTION V

LABORATORY DEMONSTRATION OF GFCS IN ABSORPTION MODE

A. SYSTEM DESIGN

Figure 32 displays a typical optical system design for a GFCS operating in absorption mode. The optical path to the retroreflector in the laboratory demonstration is approximately 5.5 m. In an actual field test, the optical path would be greater than 1 km. The main difference in extrapolating lab results to field test performance predictions will be reduced source radiance at the detector due to increased beam divergence (resulting mainly from retroreflector imperfections) and reduced atmospheric transmittance.

The source used in the GFCS is a halogen lamp. By adjusting the voltage supplied to the filament, the operating temperature of the lamp may be varied over a range extending from approximately 2000-3000 K. As the radiance from a 3000 K blackbody source is approximately 10^4 times greater than ambient atmospheric radiance at 3.5 μm, detected source radiance will be several hundred times greater than path radiance.

B. SYSTEM PERFORMANCE

The GFCS was operated in a lab environment with cells containing various amounts of HCl used as samples. Both modulation and transmitted radiance were plotted as a function of time. In the first series of tests, the system was operated with a 1.5 cm correlation cell filled with 25 kP of HCl and 75 kP of N_2. This concentration of HCl is not to be

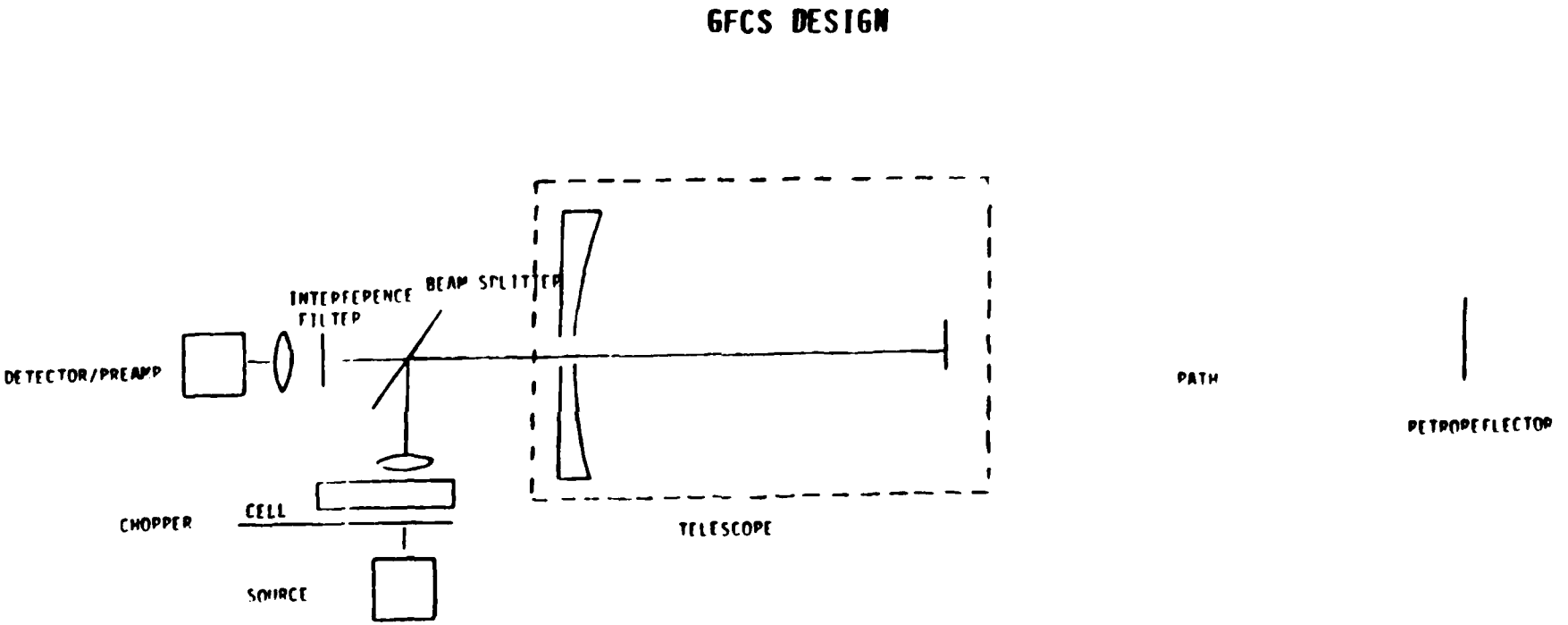

Figure 32. Optical System Design for GFCS Operating in Absorption Mode.

used as a basis for estimating modulation, however, for two reasons:

1. The procedure for filling the cells introduces uncertainties in partial pressure of HCl on the order of 10 percent, which is considerably greater than the uncertainties in modulation due to instrument noise or interfering gases.

2. The quantity of HCl in the cell decreases with time due to leakage and/or chemical reactions with the cell.

In an actual field test, the quantity of HCl would be measured spectroscopically before and after the test. This technique will allow much more accurate estimates of the HCl concentration and establish limits on the reduction in HCl with time. For the purpose of the laboratory demonstration, however, this was not done.

Four sample cells were filled with different quantities of HCl to demonstrate the modulation which results from different concentrations of HCl in the path. In addition, several spectrally neutral attenuators were used to demonstrate the instrument's response to noncorrelating attenuation as would occur for an aerosol cloud.

Figure 33 demonstrates the response of the GFCS to the four HCl sample cells. The GFCS displays signals which are proportional to transmittance and modulation as a function of time. The instrument is balanced initially by adjusting the gain of the amplifiers so that the signal recorded with the correlation cell in place is equal to the signal with the reference cell in place.

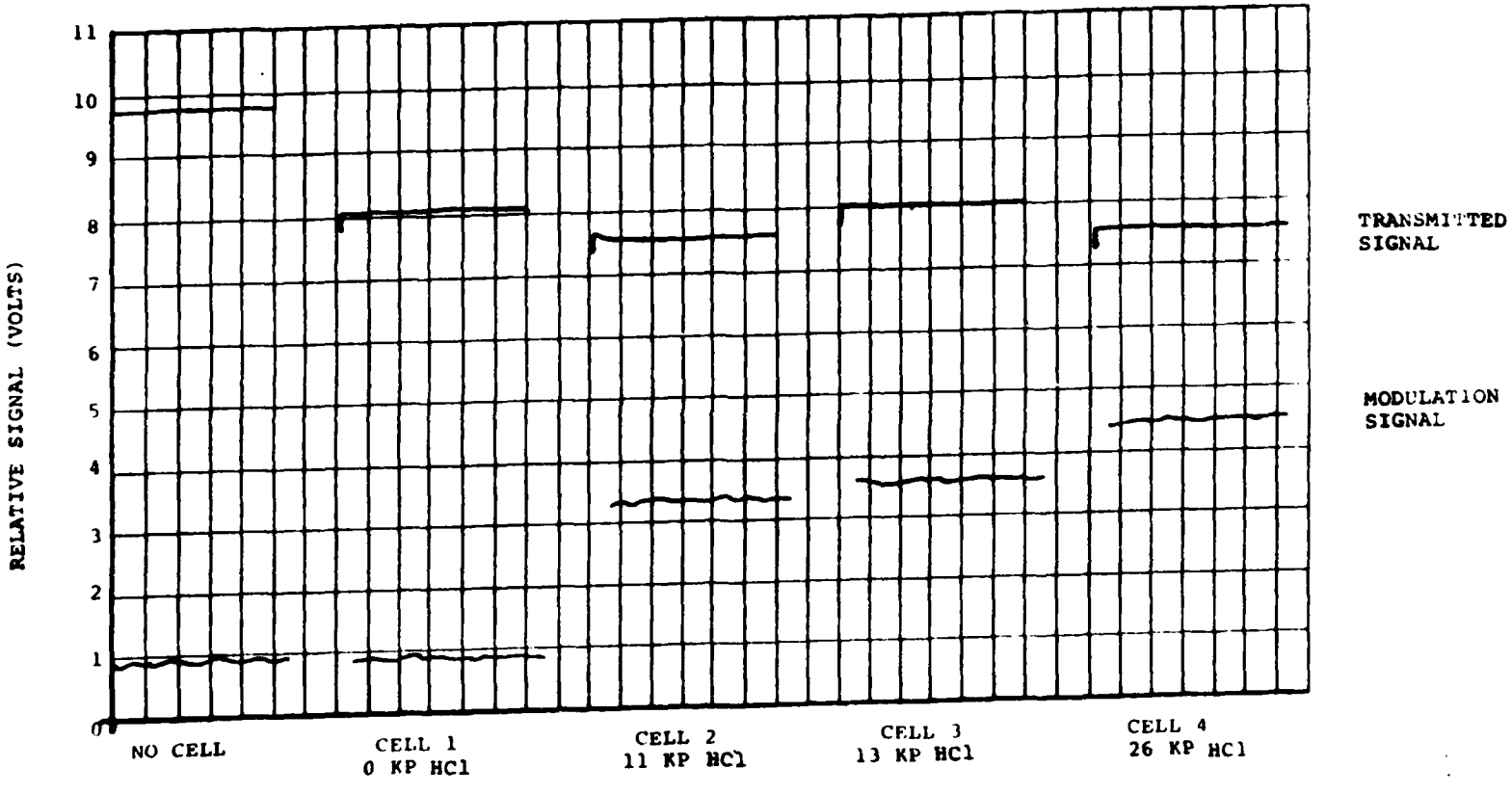

Figure 33. Transmitted Signal (Upper Curve) and Modulation (Lower Curve) for Clean Air and Four Cells with 0 kp, 11 kp, 13 kp, and 26 kp HCl.

The amount of noise in the detected signal can be observed to be less than 0.1 percent of the total signal with no attenuator in place. The GFCS can be adjusted to integrate the detected signal over time constants varying from 1 second to 60 seconds. In this manner, the signal-to-noise ratio can be improved by a factor equal to $\sqrt{60}$. The modulation noise is about an order of magnitude greater, relative to the modulation signal, than the noise in the transmitted signal. This is largely due to the difference in two nearly equal signals.

The output of the GFCS with the insertion of the neutral attenuators in the beam is presented in Figure 34. The maximum modulation resulting from the presence of the attenuators is approximately equal to the signal noise. Due to the short path length of the laboratory demonstration, it was not possible to calculate the discrimination ratio for interference by atmospheric gases such as water vapor. From theoretical calculations, the discrimination ratio should be in excess of 10^6 for water vapor.

The modulation may be calibrated by varying the balance setting and observing the modulation signal and average transmitted energy signal. With the system in balance,

$$\bar{\tau}_c = a_b \bar{\tau}_r \tag{5}$$

and

$$S_b = \bar{\tau}_c + a_b \bar{\tau}_r \tag{6}$$

where

a_b = amplifier setting with instrument balanced
S_b = transmitted signal with instrument balanced

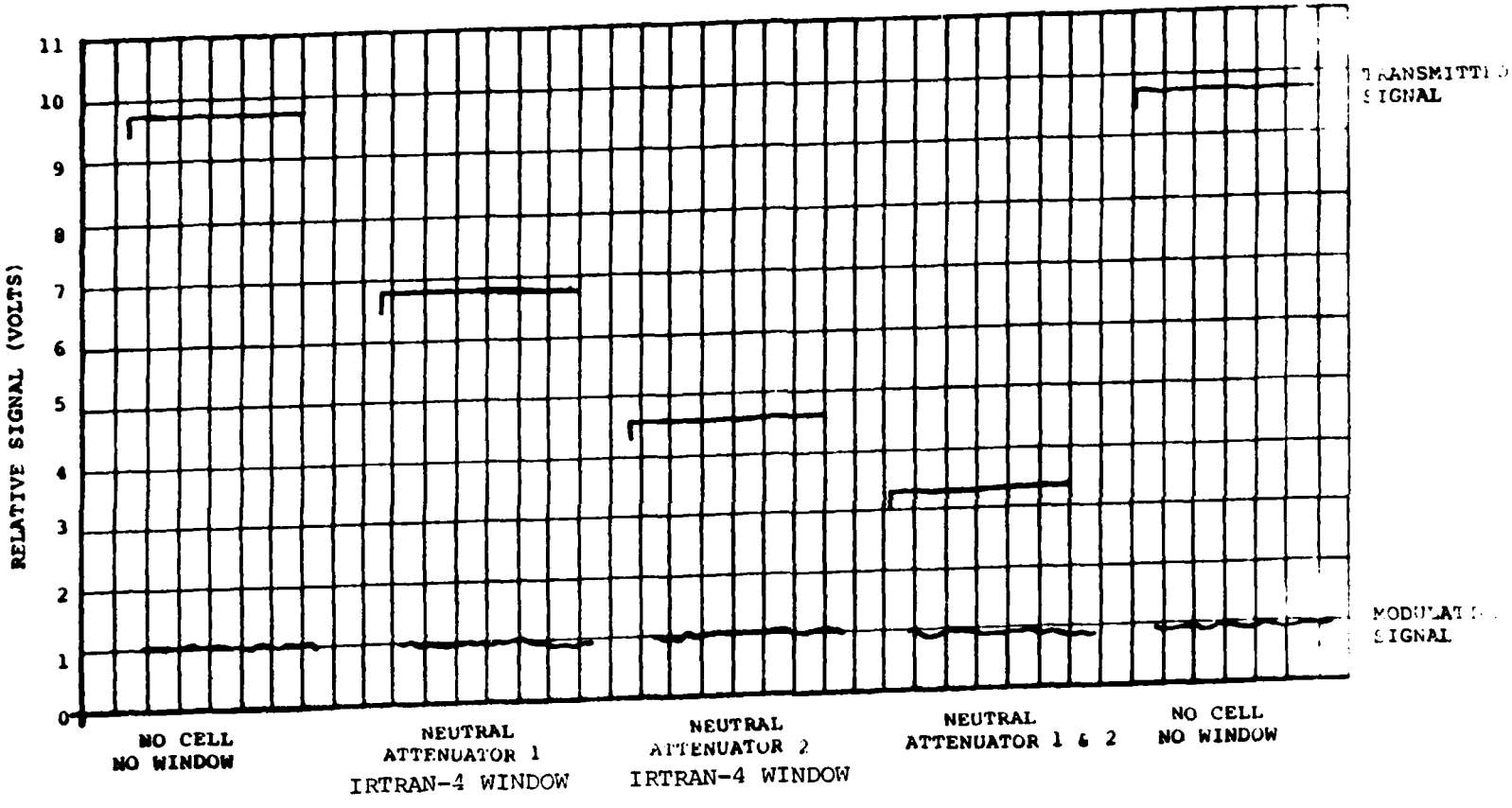

Figure 34. Transmitted Signal (Upper Curve) and Modulation Signal (Lower Curve) for Clean Air and Three Neutral Attenuators.

With the system out of balance,

$$S_u = \bar{\tau}_c + a_u \bar{\tau}_r$$

$$M_u = (\bar{\tau}_c - a_u \bar{\tau}_r) \; / \; (\bar{\tau}_c + a_u \bar{\tau}_r) \qquad (7)$$

where

a_u = amplifier setting with instrument unbalanced

M_u = modulation signal

S_u = transmitted signal with instrument unbalanced

By appropriate substitution, the modulation signal may be expressed in terms of the average transmitted signals, S_u and S_b

$$M_u = (S_b - S_u)/S_u \qquad (8)$$

The calculated modulation may then be compared to the size of the signal as output by the GFCS. The result is a 1.31 percent modulation per volt of output signal with the modulation gain set at 100 percent of full scale. If the modulation gain is adjusted to a smaller scale, the modulation per volt would decrease proportionately. For example, if the modulation gain is set to the 20 percent of full-scale setting, the calibration factor is 0.26 percent modulation per volt of output signal.

Modulation may also be calibrated by measuring the voltage from the detector with an oscilloscope and solving

the equation for modulation. Using this technique, a modulation of 1.45 percent/volt was estimated. This technique is only accurate to about 20 percent, however, since the uncertainty in each signal as read from the oscilloscope is approximately 15 percent of the difference between the signals.

The modulation measured by the GFCS may be compared to the modulation predicted in the theoretical calculations to demonstrate the linearity of the system. Figures 35 and 36 provide two examples of the modulation comparisons. Note that the primary uncertainty is in the theoretical modulation, which results from not knowing the exact quantity of HCl in the correlation cell and sample cells. In an actual field experiment, very accurate measurements of HCl concentrations would be made both before and after the test.

It is important to recall that modulation is a nonlinear function of HCl column density. As a result, measured modulation must be related back to the theoretical curves of modulation versus HCl column density for quantifying HCl. In an actual field test, the appropriate calibration curves would be called up by a computer program interfaced to the GFCS to display HCl concentrations in real time. The computer could also compensate for variations in path length, temperature, water vapor concentration, correlation cell HCl concentration, and spectral bandpass.

A potential source of error which must be recognized in actual field operation is scattering of modulated source radiation into the detector field of view. Figure 37 demonstrates the potential problem. Although system design can minimize the amount of scattered radiation detected, it cannot be completely eliminated.

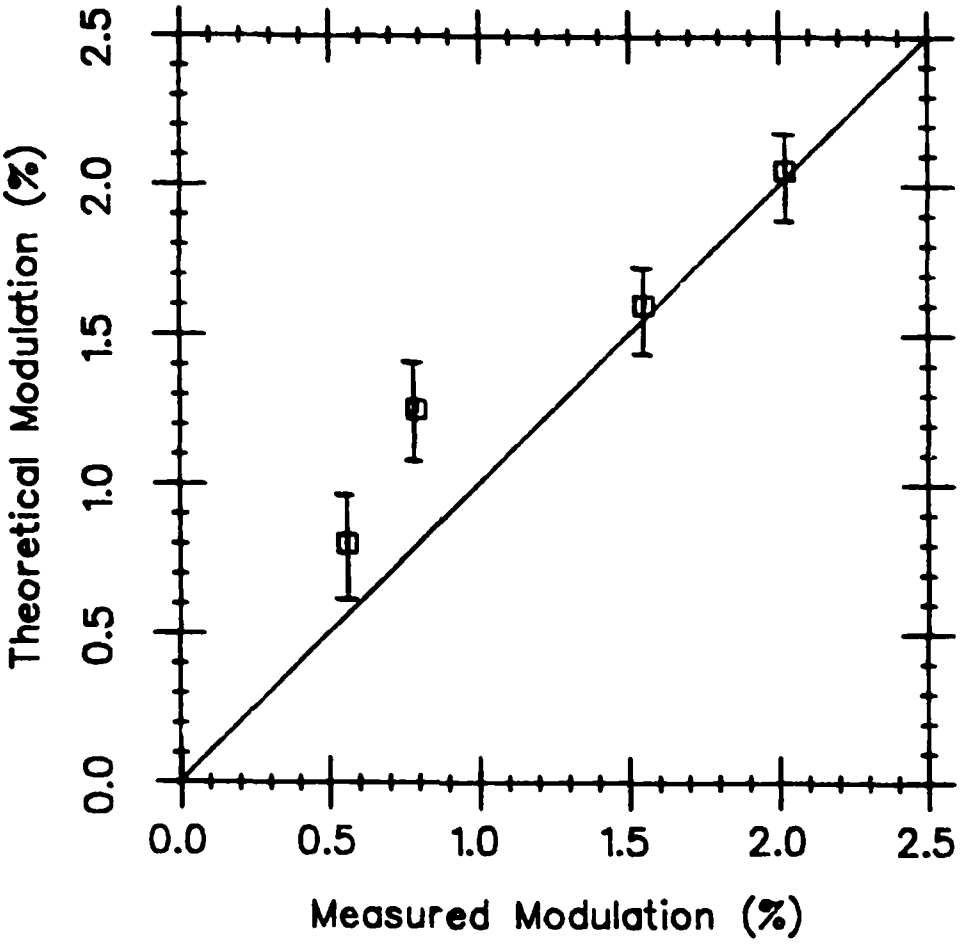

Figure 35. Theoretical Versus Measured Modulation, Bandpass 2770-2870 cm^{-1}, 0.37 atm-cm HCl in Correlation Cell. The Low Measured Modulation for the First Two Points is Probably Due to Leakage of HCl from the Cells.

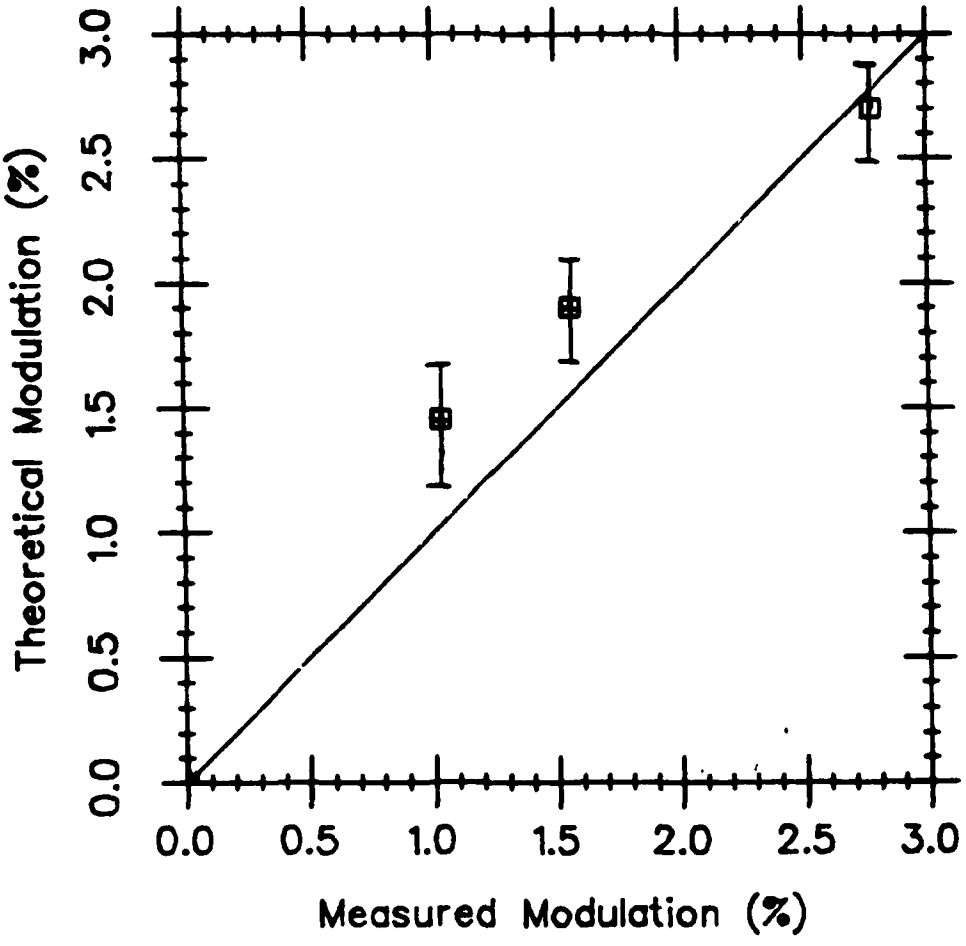

Figure 36. Theoretical Versus Measured Modulation, Bandpass 2806-2948 cm^{-1}, 0.75 atm-cm HCl in Correlation Cell. Again, Leakage of HCl is Probably the Cause of Low Measured Modulation for the First Two Points.

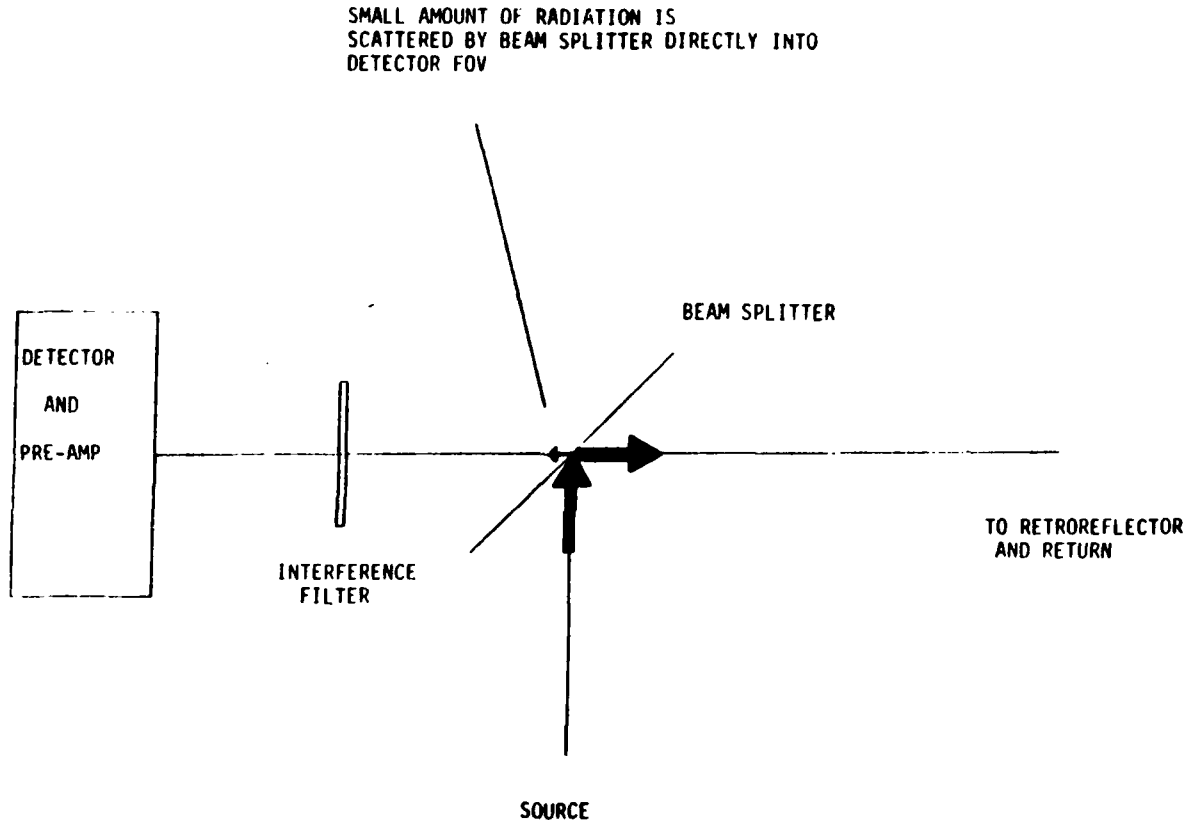

Figure 37. Scattering of Source Radiation Directly into Detector Field of View by Beam Splitter.

The presence of such scattered radiation causes the modulation function to become

$$M = \frac{(\bar{\tau}_{ac} + S\bar{\tau}_c) - a_1\bar{\tau}_r(\bar{\tau}_a+S)}{(\bar{\tau}_{ac}+S\bar{\tau}_c) + a_1\bar{\tau}_r(\bar{\tau}_a+S)} \tag{9}$$

$$= \frac{\bar{\tau}_{ac}-a_1\bar{\tau}_r\bar{\tau}_a + S(\bar{\tau}_c - a_1\bar{\tau}_r)}{\bar{\tau}_{ac}+a_1\bar{\tau}_r\bar{\tau}_a + S(\bar{\tau}_c+ a_1\bar{\tau}_r)}$$

where

$\bar{\tau}_{ac}$ = band average transmittance for atmosphere-correlation cell path

$\bar{\tau}_a$ = band average atmospheric transmittance

$\bar{\tau}_c$ = band average correlation cell transmittance

$\bar{\tau}_r$ = band average reference cell transmittance

a_1 = amplifier gain used for balancing

S = scattering parameter

If the system is balanced, $\bar{\tau}_c = a_1\bar{\tau}_r$ and the scattering term in the numerator cancels out. Therefore, no false modulation will result from inclusion of this term. However, the scattering term will always cause the total detected signal (the denominator) to be larger than would be the case in the absence of scattering. As a result, the modulation will be underestimated. This can be taken into account, however, in instrument calibration, with the computer fitting the calibration points to a theoretical calibration curve with S as an error parameter.

The performance of the GFCS in a laboratory environment may be measured by a number of different figures-of-merit. Table 5 summarizes these objective indicators of the system's performance. The system performs within an order of magnitude of the best GFCS systems constructed for scientific applications which utilize rotating mirrors instead of a rotating gas cell and have higher throughput.

TABLE 5. PERFORMANCE ESTIMATES OF GFCS IN LABORATORY TESTS. CONDITIONS: 2770-2870 cm^{-1} BANDPASS

Noise-equivalent modulation	4×10^{-5}
Noise-equivalent HCl column density	10 ppm-m
Interference modulation (max.)	$<10^{-4}$
Signal-to-noise @ 1540 ppm-m HCl	158
Estimated minimum detectable HCl	30 ppm-m
Discrimination ratio, HCl vs H_2O (theoretical)	10^6

SECTION VI
FIELD SYSTEM DESIGN

The results of the laboratory test and theoretical calculations may be combined to estimate the performance of several alternate designs for field systems. Three different field system configurations were studied:

1. A high-sensitivity gas filter correlation imager detecting HCl emissions,

2. A high-sensitivity gas filter correlation imager detecting HCl absorption of solar radiation scattered into the field of view, and

3. One or more gas filter correlation spectrometers and an array of retroreflectors deployed so as to measure HCl absorption along a number of lines of sight.

The relative advantages and disadvantages of each of these systems are described below.

A. HIGH-SENSITIVITY IMAGER OPERATING IN EMISSION MODE

A carefully designed instrument can detect HCl emissions for ambient temperatures near 300 K. Such a system requires a high etendue, maximum spectral bandpass, slow sampling rate, and high mechanical stability. A nonimaging sensor operating in emission mode has been developed (Reference 10) with the ability to detect HCl at a theoretical level of 300 ppm-m. The specifications for such a system are described in Table 6.

TABLE 6. SPECIFICATIONS FOR GFCS OPERATING IN EMISSION MODE FOR HCl DETECTION, PRODUCED BY BARRINGER RESEARCH, LTD. (REFERENCE 10).

Detector	Thermoelectrically cooled (243 K) PoSe
Detector area	.04 cm^2
D^*	7×10^9
Responsivity	10^4 V/W
Detector solid angle	0.63 sr
Optical transmission	0.033
Light etendue	3.3×10^{-4} cm^2 sr
System bandwidth	0.16 Hz
Spectral filter center	3.6 μm
Spectral bandwidth	0.15 μm
Min. detectable gas	300 ppm-m
Noise equiv. radiance	4.9×10^{-8} W/cm^2-sr

To operate as an imager with reasonable sensitivity, the sensor must scan along a line perpendicular to the motion of the cloud, with the scan line forming a gate through which the cloud must pass. The composite scan lines then form an image of the cloud. This procedure is illustrated in Figure 38.

Several design modifications may be made to improve sensitivity for use in imaging mode. For example, eliminating beam splitters and using a PbS detector cooled to 77K will increase sensitivity considerably. The design specifications are listed in Table 7.

The theoretical performance of the imager described above may be estimated by computing the noise equivalent power (NEP) and comparing this to the in-band modulation power reaching the detector. The NEP may be computed from:

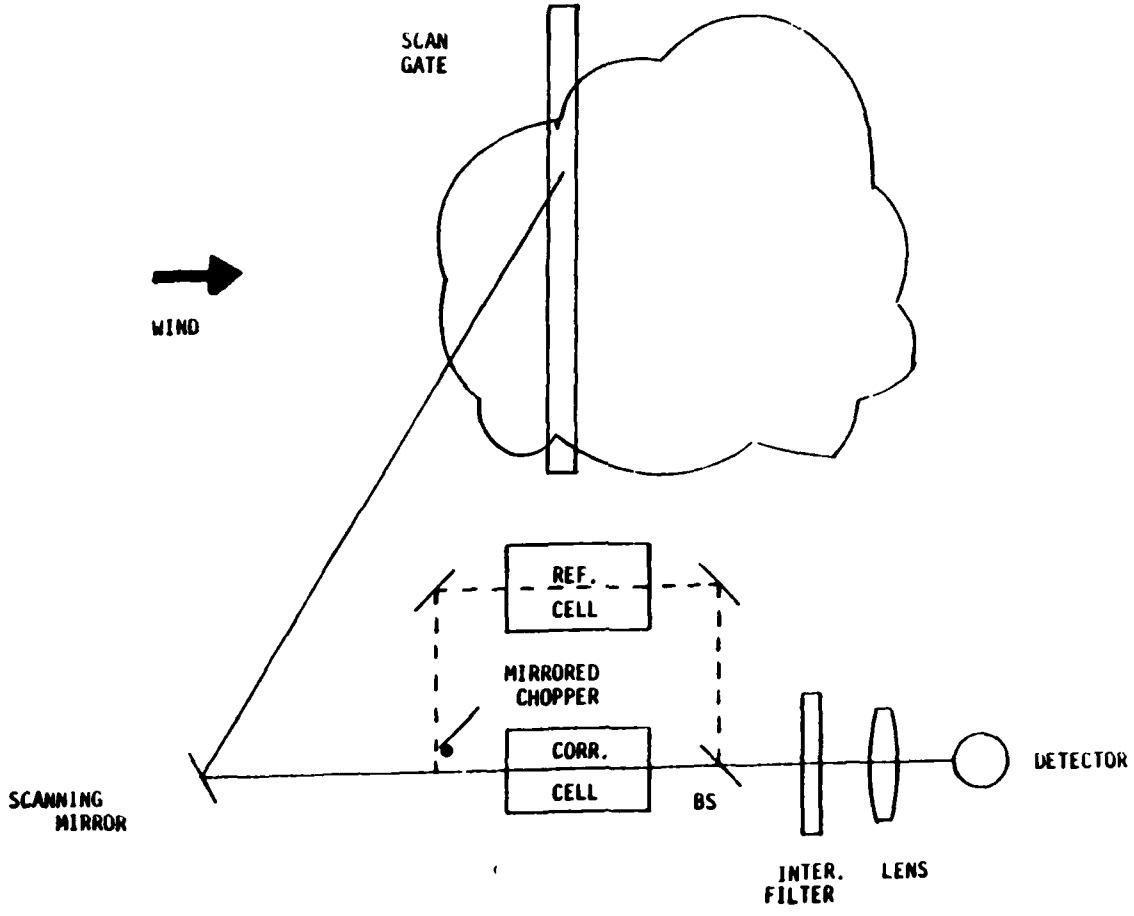

Figure 38. Design for a GFCS which Maps a Cloud by Successive Linear Scans Perpendicular to Wind Vector.

TABLE 7. DESIGN SPECIFICATIONS FOR HIGH-SENSITIVITY LINE SCANNER FOR HCl DETECTION.

Detector	LN_2 cooled (77k) PbS
Detector area	.0016 cm^2
D*	1×10^{11}
Bandpass	3.5 - 3.7 μm
Field of view	0.5 radians
IFOV	4.0 mr
Optics	5 cm, f/2, 50% transmittance
System Bandwidth	100 Hz

$$NEP = \frac{\sqrt{A_d f}}{D^*} = 2.5 \times 10^{-8} \text{ W} \qquad (10)$$

where

A_d = area of detector
f = bandwidth

The in-band modulation power, assuming a 1000 ppm-m HCl concentration viewed against a clear, ambient background through a gas cell containing 2 atm-cm of HCl at 294 K is 9.3×10^{-8} W which implies a signal to noise ratio of 4.

An alternate design would involve replacing the single detector with a linear detector array. This would permit the sensitivity to be improved by $\sqrt{N}$, where N is the number of detectors. This design would increase both the cost and the technological risk of such a system, however.

Since the amount of modulation detected in emission mode is smaller than the amount of modulation in absorption mode, the signal to noise ratio and minimum detectable HCl quantity will be poorer than in absorption mode. Calibration problems will also exist, since aerosols in the shuttle exhaust cloud will tend to mask HCl emissions, resulting in an underestimation of HCl. There is also an ambiguity which results from broadband emission and scattering sources in the path versus increased temperature of atmospheric gases in the path. As emission mode operation requires very accurate measurements of temperature along the path for calibration, the presence of a high optical depth aerosol cloud

which scatters solar radiation into the line of sight can make it impossible to measure the temperature radiometrically.

The difficulties in calibrating the GFCS operating in emission mode can be offset somewhat by modeling the aerosol and environment and including these parameters in calibration calculations. However, such a procedure introduces significant uncertainties in the final result.

The use of a GFCS in emission mode should therefore be assumed to provide an indication that a minimum level of HCl is present rather than an accurate quantification of the amount present.

B. GFCS DETECTING SCATTERED SOLAR RADIATION

The GFCS detecting scattered solar radiation would be designed similar to the GFCS for emission mode operation, but the system would view a brightly lighted cloud background rather than a cold sky background for maximum sensitivity. The geometry is described in Figure 39.

Assuming a 15-degree scattering angle, the modulation power reaching the detector for this system is 5.2×10^{-5} w/cm^2-sr, which implies a signal-to-noise ratio of 2000 for a 1000 ppm-m HCl cloud. For a 60-degree scattering angle, the signal-to-noise ratio is reduced by a factor of 10. Both sets of calculations assume a cumulus cloud with an optimal particle size distribution to maximize solar scattering.

Solar scatter mode has the advantage that the GFCS system operates in absorption mode. Therefore, calibration is considerably easier than for emission mode operation. However, the requirement that a brightly lit cloud background be present is a formidable disadvantage. In addi-

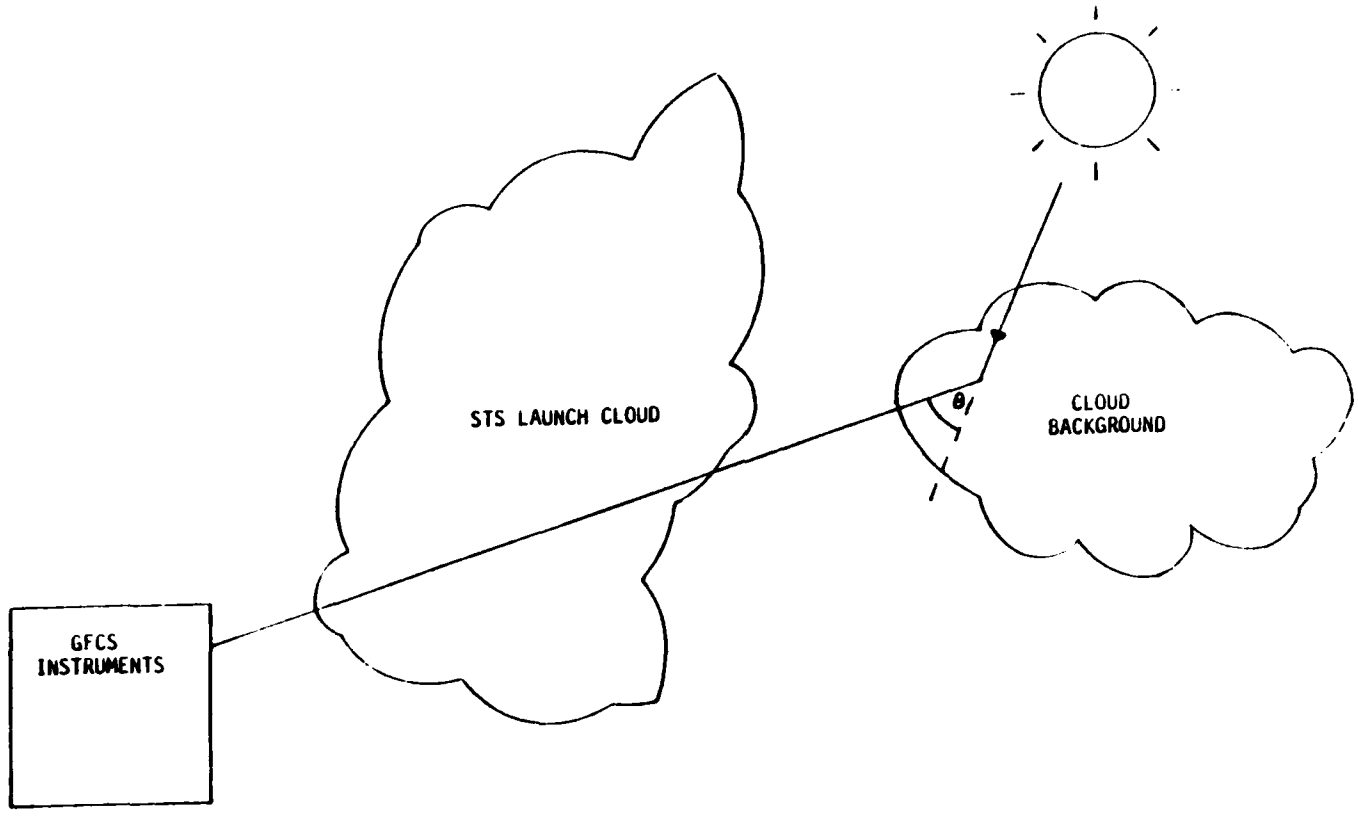

Figure 39. Geometry Required for Detection of HCl Absorption of Scattered Solar Radiation by a GFCS. The Instrument Sensitivity is a Strong Function of the Scattering Angle, θ .

tion, the signal-to-noise ratios may vary across a scene depending on the cloud background. It may therefore be difficult to quantify the sensitivity of the instrument.

C. GFCS OPERATING IN ABSORPTION MODE ALONG SEVERAL LINES OF SIGHT

The alternative with the least technological risk and the potential for maximum sensitivity to HCl is to deploy an array of retroreflectors and one or more GFCS instruments to measure HCl concentrations along several lines of sight. The system can involve a single GFCS which scans over several lines of sight or one GFCS instrument per line of sight. Figures 40 and 41 illustrate the two geometries.

The output from the GFCS instrument(s) can be digitized and processed by computer to display a plot of HCl concentration profile versus time. The sensitivity of the system should be comparable to or better than the sensitivity recorded in the laboratory, which indicated better than 30 ppm-m of HCl was detectable. Interference by water vapor over a 1 km path is less than 40 ppm-m equivalent HCl concentration, and this can be compensated for by the computer program. A few design modifications (using a cooled PbS detector, improving mechanical stability and system throughput by using a rotating mirror rather than a rotating gas cell, obtaining an interference filter with bandpass from 2690-2870 cm^{-1}) should more than offset the loss in sensitivity caused by going to longer path lengths.

The major difficulty with this approach is that it requires appropriate geometry for setting up the GFCS lines of sight and deployment of the system in advance of the launch. If the wind direction should change after deployment of the retroreflectors, the shuttle exhaust cloud may miss the lines of sight entirely. In addition, HCl detec-

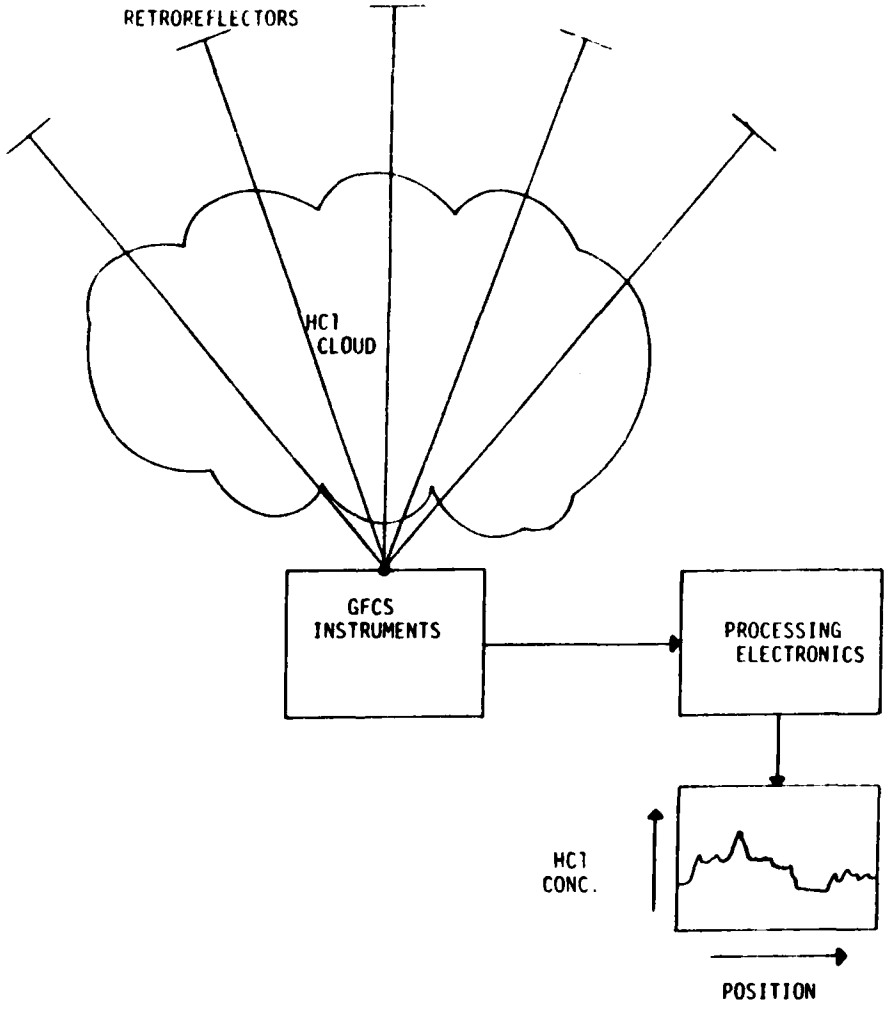

Figure 40. Geometry for GFCS System which Scans Over Several Lines of Sight.

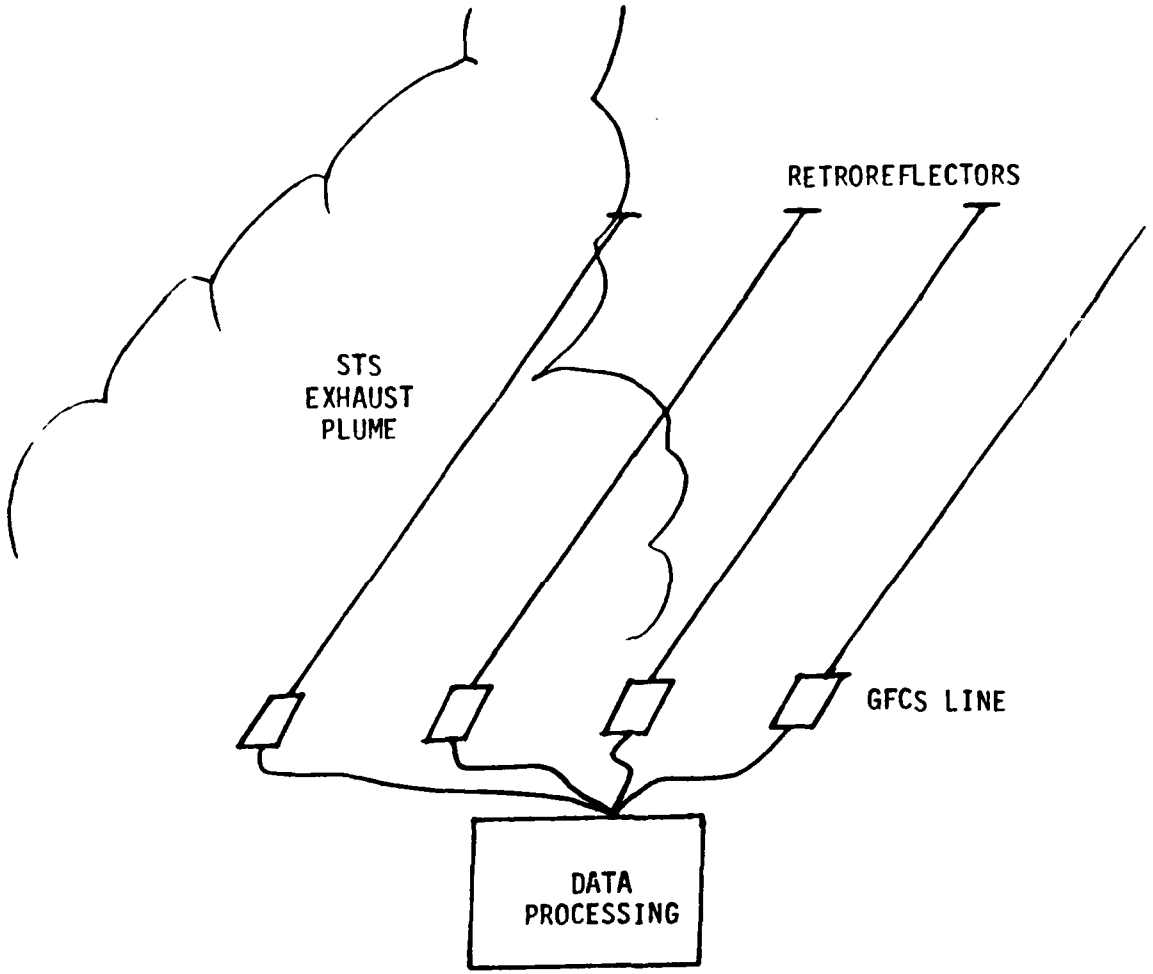

Figure 41. Multiple GFCS Approach to Map HCl Cloud.

tion could only be done near ground level unless the site geometry at VAFB were favorable.

D. SUMMARY

The relative advantages and disadvantages of each instrument are summarized in Table 8. In addition, a comparison of predicted sensitivity of each instrument is provided in Table 9.

Complicated trade-offs appear to exist when balancing instrument sensitivity, technological risk, ease of use, cost and system reliability in evaluating alternative designs. Gas filter correlation instruments have been proven to be useful for HCl detection operating in all three modes (emission, solar source absorption, GFCS source absorption). From the standpoint of sensitivity and technological risk, the multiple LOS GFCS system appears best. From the standpoint of ease of use in a field test, a system detecting either HCl emissions or scattered solar radiation is preferred.

TABLE 8. ADVANTAGES AND DISADVANTAGES OF THE VARIOUS GAS FILTER CORRELATION APPROACHES TO HCl DETECTION.

A. High Sensitivity Imager Operating in Emission Mode

Advantages

1. Does not require high radiance source.
2. Simple optical design.
3. Does not require special geometry.

Disadvantages

1. Masking by HCl aerosol influences calibration.
2. Modulated radiance a function of plume temperature.
3. Solar scattered radiation from cloud background may cause modulation reversal.
4. Correlation cell temperature must be accurately known.
5. Low signal-to-noise makes quantification difficult.
6. High cost and technological risk if a PbS staring array is required.

B. GFCS Detecting Solar Scattered Radiation

Advantages

1. Higher radiance, signal-to-noise than thermal emission if brightly-lit cloud background is present.
2. Operates in absorption mode, permitting easier calibration.
3. Can measure HCl along elevated line of sight.

Disadvantages

1. Requires special geometry, presence of backlit cloud.
2. Radiance varies spatially and temporally across scene, causing signal-to-noise variations.
3. Field test deployment must predict location of plume.

C. GFCS Operating in Absorption Mode Along Several Lines of Sight

Advantages

1. Highest signal-to-noise.
2. Straightforward calibration.
3. Little or no technological risk.

Disadvantages

1. More complicated field test deployment, including setting up retroreflectors based on meteorological predictions.
2. Sampling lines dependent on site geometry.
3. Only near-surface concentrations measurable unless favorable geometry.

TABLE 9. MAXIMUM THEORETICAL SENSITIVITY OF VARIOUS PROPOSED FIELD INSTRUMENTS.

	Signal-to-noise ratio for detection of:		
	Emission Mode HCl		Solar Scattered Radiation
	1,000 ppm-m	10,000 ppm-m	60° scattering angle 1,000 ppm-m
Inframetrics Model 525 Six-Frame Average	<1	<1	4
High-Sensitivity PbS Scanner	3.5	10	200
High-Sensitivity PbS Staring Array (100 Elements)	35.	100	2000

Laboratory GFCS in absorption mode:

Signal-to-noise ratio of 158 (maximum) achieved for detection of 1540 ppm-m of HCl.

(The reverse of this page is blank.)

SECTION VII
CONCLUSIONS AND RECOMMENDATIONS

1. A gas filter correlation approach for HCl detection should utilize the P-branch HCl lines located from 2690-2870 cm^{-1} for maximum sensitivity and minimum interference by atmospheric species. The minor interference which results from water vapor molecules over paths several km in length can be removed by modeling the environment, particularly if relative humidity is known.

2. Correlation cell HCl concentration should be adjusted so that the path-integrated HCl partial pressure is between 0.25 atm-cm and 1.0 atm-cm. The total pressure and temperature in the gas cell should be near ambient. Larger quantities of HCl may be used to maximize sensitivity, while smaller quantities will maximize specificity to HCl.

3. HCl quantities of 500-10,000 ppm-m are expected to be present for typical lines of sight through the STS exhaust cloud. The fraction of the HCl found in the gaseous phase is expected to vary between 20 percent and 70 percent of total HCl, depending primarily on relative humidity.

4. Commercial 3-5 μm infrared imagers such as the Intrametrics Model 525 cannot provide sufficient sensitivity to detect HCl emissions.

5. Detecting HCl absorption of solar radiation scattered by a cloud background is possible with commercial imagers, but the sensitivity will be low (approximately 500-1000 ppm-m) except under extremely fortuitous conditions. In addition, the requirement that a bright cloud background

be present imposes severe constraints on the instrument's usefulness.

6. A laboratory demonstration of a GFCS detecting HCl absorption of radiation from a halogen lamp indicates sensitivity adequate to quantify HCl at the 30 ppm-m level. The instrument, when properly balanced, is able to discriminate between HCl absorption and broadband absorption. Improvements which might be made to maximize sensitivity to HCl should more than offset the reduction in sensitivity resulting from operation over paths greater than 1 km in length.

7. An imaging GFCS with high sensitivity to HCl can be designed to detect HCl emissions at the 250 ppm-m level. This sensor would operate by scanning the HCl cloud perpendicular to the effective wind vector, creating a gate through which the cloud must pass. The 250 ppm-m sensitivity level is the maximum theoretically possible. An actual system might be a factor of 2-5 poorer in operation. Replacing the single detector element with a linear detector array can improve the sensitivity of this approach by a factor of 10, permitting, theoretically, detection of 25 ppm-m of HCl. Using a linear detector array would substantially increase both the cost and technological risk, however.

8. Due to masking by aerosols, quantifying HCl levels in emission mode may be difficult. It is expected that emission mode operation will at best provide an indication that the quantity of HCl present is above some threshold.

9. The possibility exists that solar radiation may be scattered by aerosols in the atmosphere or STS exhaust cloud into the line of sight. This complicates calibration when detecting HCl emissions. The presence of a cloud background also introduces the possibility that a modulation reversal might take place, resulting in the detection of HCl absorption rather than emission.

10. Detection of scattered solar radiation from a cloud background provides added sensitivity for a GFCS system, but requires an optimal geometry between the instrument, sun, cloud background, and STS launch cloud.

11. A GFCS instrument detecting HCl absorption of radiation from a halogen lamp along several lines of sight provides maximum sensitivity and minimum technological risk, but complicates the field test since an array of retroreflectors or sources must be deployed prior to the launch. The site geometry also limits the utility of this approach.

12. It is recommended that either a high-sensitivity sensor capable of detecting either HCl emission or HCl absorption of scattered solar radiation be developed, or a multiple-LOS GFCS transmissometer system be employed. The final decision should be based on the available site geometry and the levels of HCl detection required by the Air Force.

(The reverse of this page is blank.)

REFERENCES

1. Gregory, G.L., D.C. Woods and D.I. Sebacher, Airborne Measurements of Launch Vehicle Effluent, NASA Technical Paper 2090, National Aeronautics and Space Administration, 1983.

2. Anderson, B.J. and V.W. Keller, Space Shuttle Exhaust Cloud Properties, NASA Technical Paper 2258, National Aeronautics and Space Administration, 1983.

3. Maddrea, G.L., Jr., G.L. Gregory, D.I. Sebacher and D.C. Woods, Airborne Measurements of Launch Vehicle Effluent of STS-2 Launch on November 12, 1981 at Cape Canaveral, Florida, NASA Technical Paper 2260, National Aeronautics and Space Administration, 1984.

4. Rothman, L.S. et al., Applied Optics 20, p. 1323, (1981).

5. Smith, H.J.P. et al., FASCODE-Fast Atmospheric Signature Code, AFGL-TR-0081, U.S. Air Force Geophysics Laboratory, Hanscom AFB, MA, January 1978.

6. Clough, S.A., F.X. Kneizys, L.S. Rothman, and W.O. Gallery, Proc. SPIE 277 Atmospheric Transmission, p. 152 (1981).

7. Chaney, L.W. and T.J. Rogne, An Aluminum Refinery Atmospheric Study Using a Gas Filter Correlation Technique, OptiMetrics, Inc. Technical Report OMI-80-006, Dec. 1980.

8. Dowling, J.A. et al., Analysis of Atmospheric Interferometer Data, OptiMetrics, Inc. Technical Report OMI-102, May 1984.

9. Turner, R.E. "Contrast Transmission Models - Modules FCLOUD and OVRCST," EOSAEL 82 Volume IV Radiative Transfer and Turbulence Effects, ASL-TR-0122, U.S. Army Atmospheric Sciences Laboratory, White Sands Missile Range, NM, Nov. 1982.

10. Ward, T.V. and H.H. Zwick, Applied Optics 14, p. 2896 (1975).

(The reverse of this page is blank.)

APPENDIX A

Transmittance spectrum of HCl superimposed on a 10 km midlatitude summer model atmosphere absorption spectrum. The spectral region extends from 2500 cm^{-1} to 3120 cm^{-1}, corresponding to the fundamental vibrational absorption band of HCl.

Solid line: Transmittance for a 10 km path through a standard midlatitude summer atmosphere at sea level, temperature = 294 K, pressure = 1013 mb.

Dashed line: Transmittance through a cell containing 1.0 atm-cm HCl at 294 K and 1013 mb pressure.

These plots were produced by FASCOD 1B (Reference 6).

(The reverse of this page is blank.)

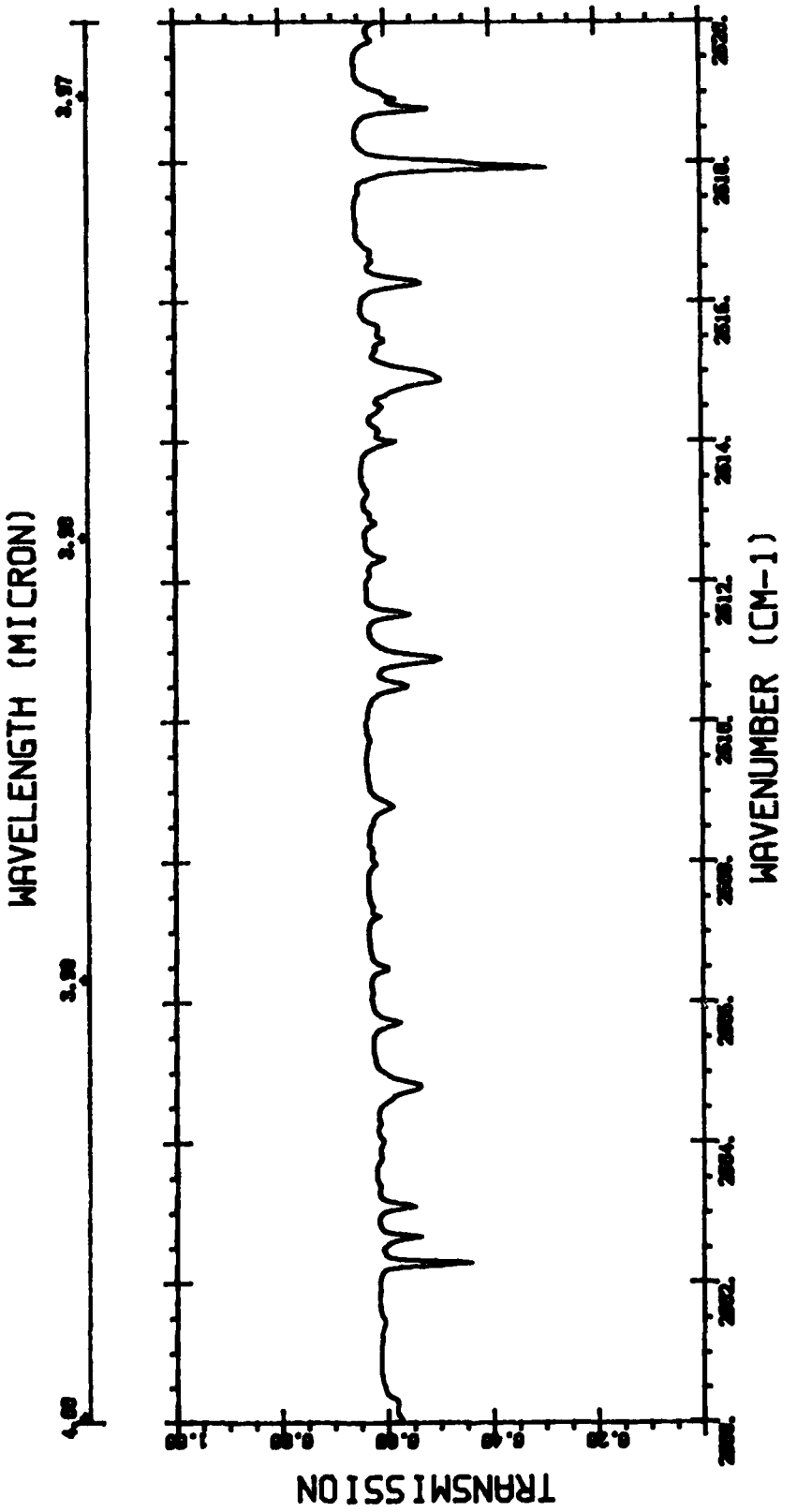
WAVELENGTH (MICRON)
WAVENUMBER (CM-1)
TRANSMISSION

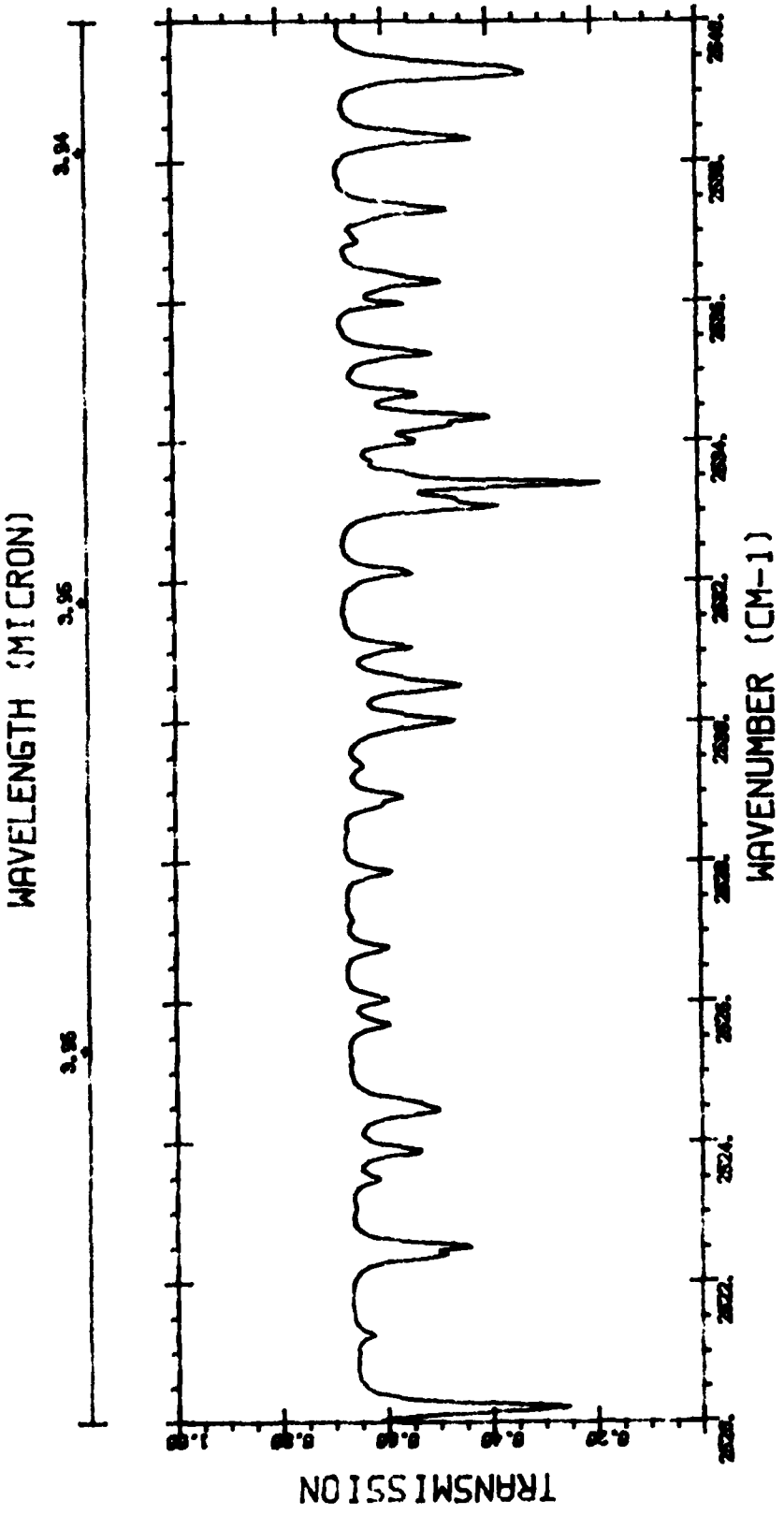
WAVELENGTH (MICRON)
3.94
3.95
3.96
WAVENUMBER (CM-1)
TRANSMISSION

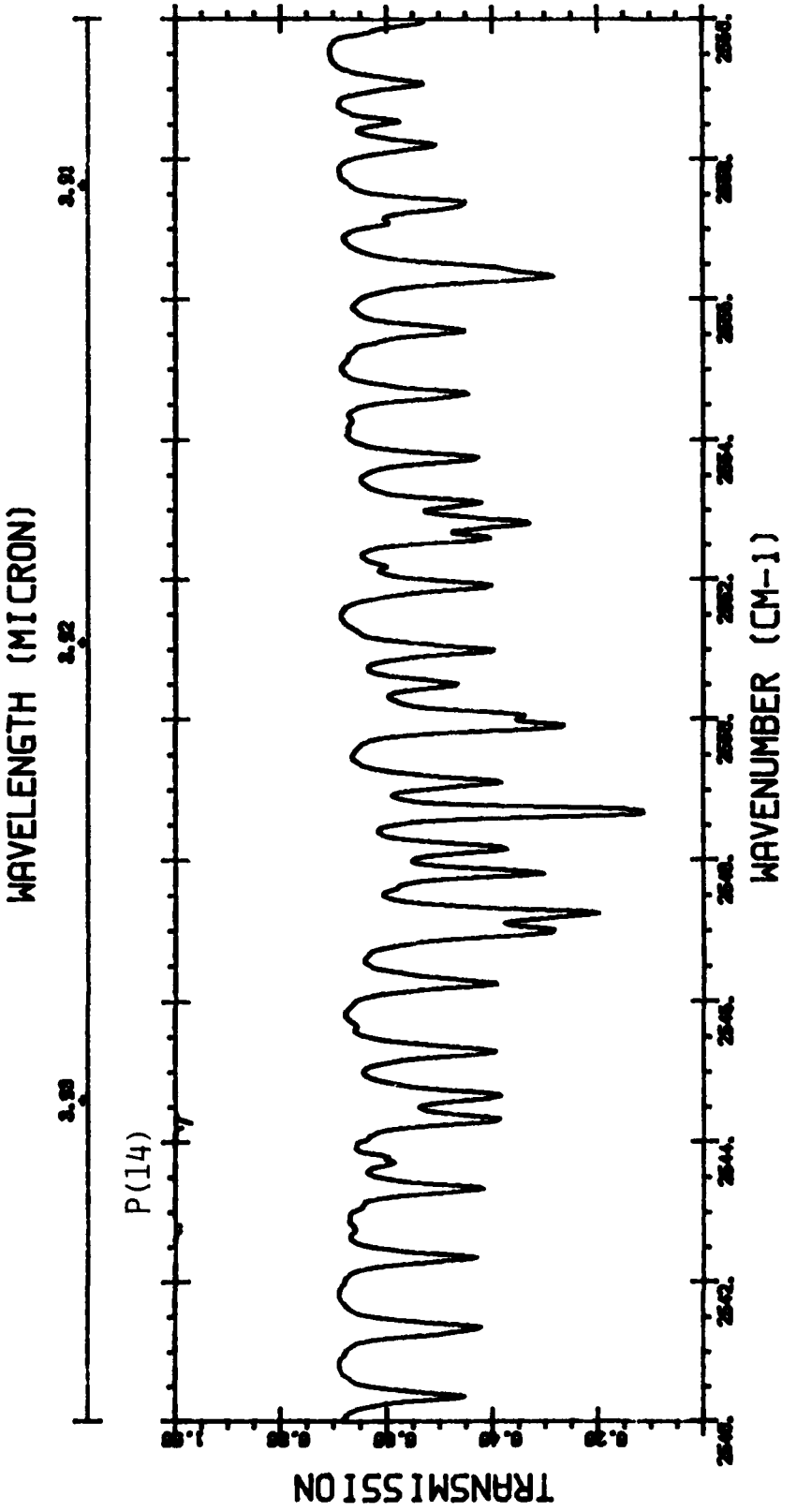
WAVELENGTH (MICRON)
WAVENUMBER (CM-1)
TRANSMISSION
P(14)

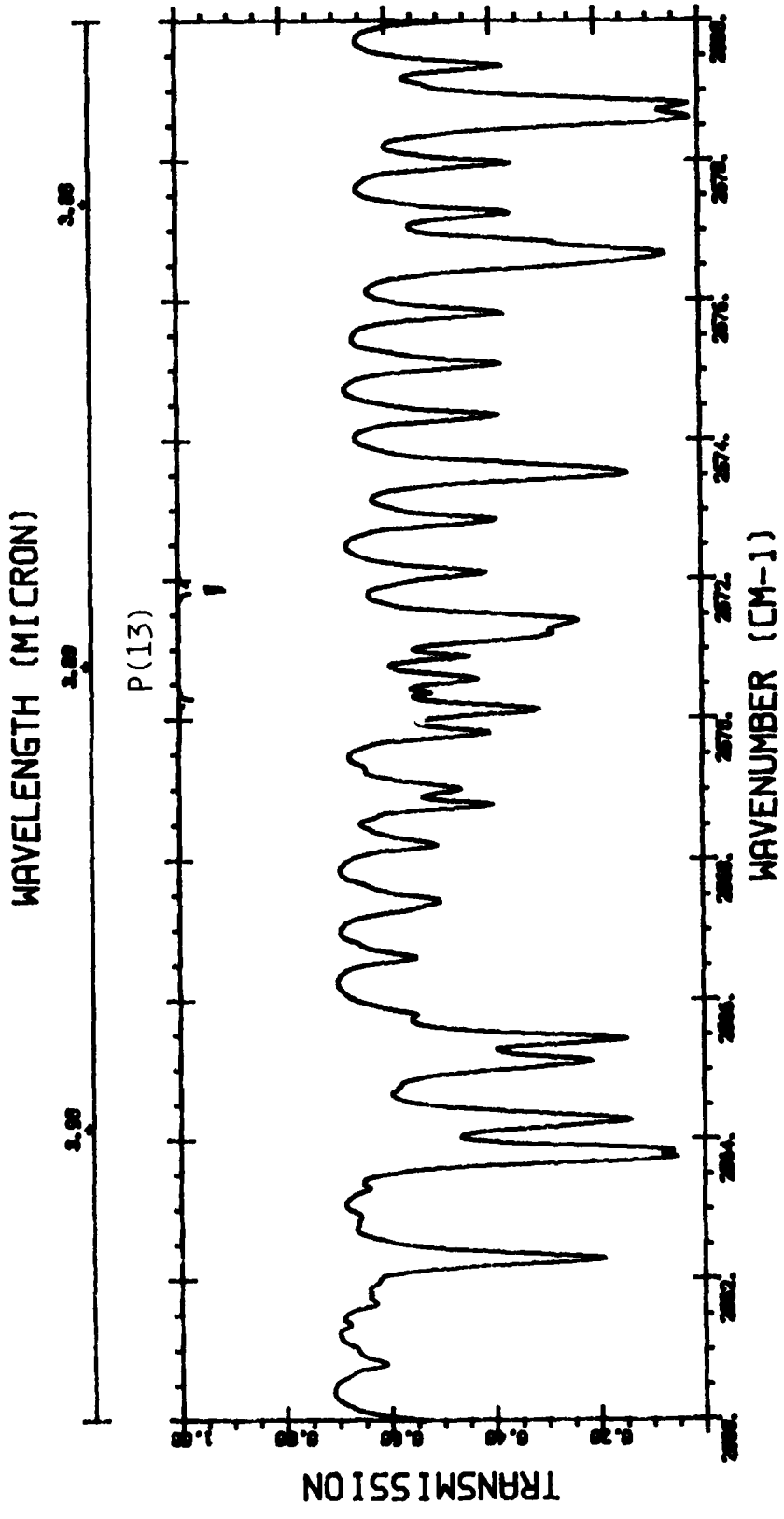
WAVELENGTH (MICRON)
P(13)
WAVENUMBER (CM-1)
TRANSMISSION

AD-A166 386 GAS FILTER CORRELATION IMAGERY FOR HCI MONITORING(U) 2/2
OPTIMETRICS INC ANN ARBOR MI B K MATISE ET AL. JAN 86
OMI-133 AFESC/ESL-RR-85-36 F08635-84-C-0318

UNCLASSIFIED F/G 22/2 NL

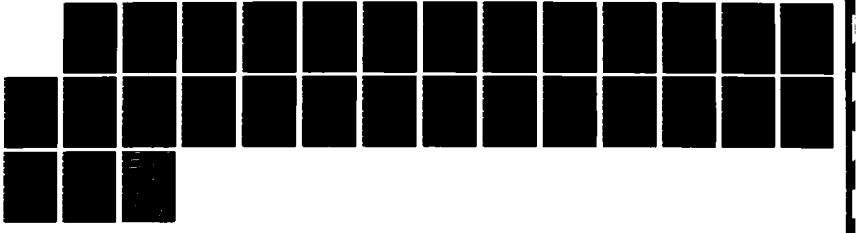

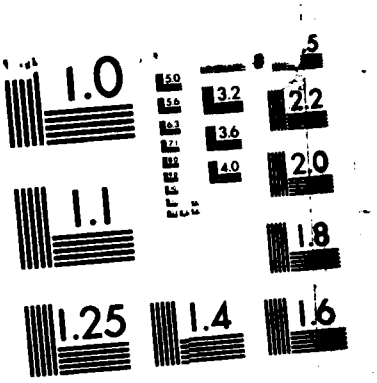

MICROCOPY RESOLUTION TEST CHART
NATIONAL BUREAU OF STANDARDS-1963-A

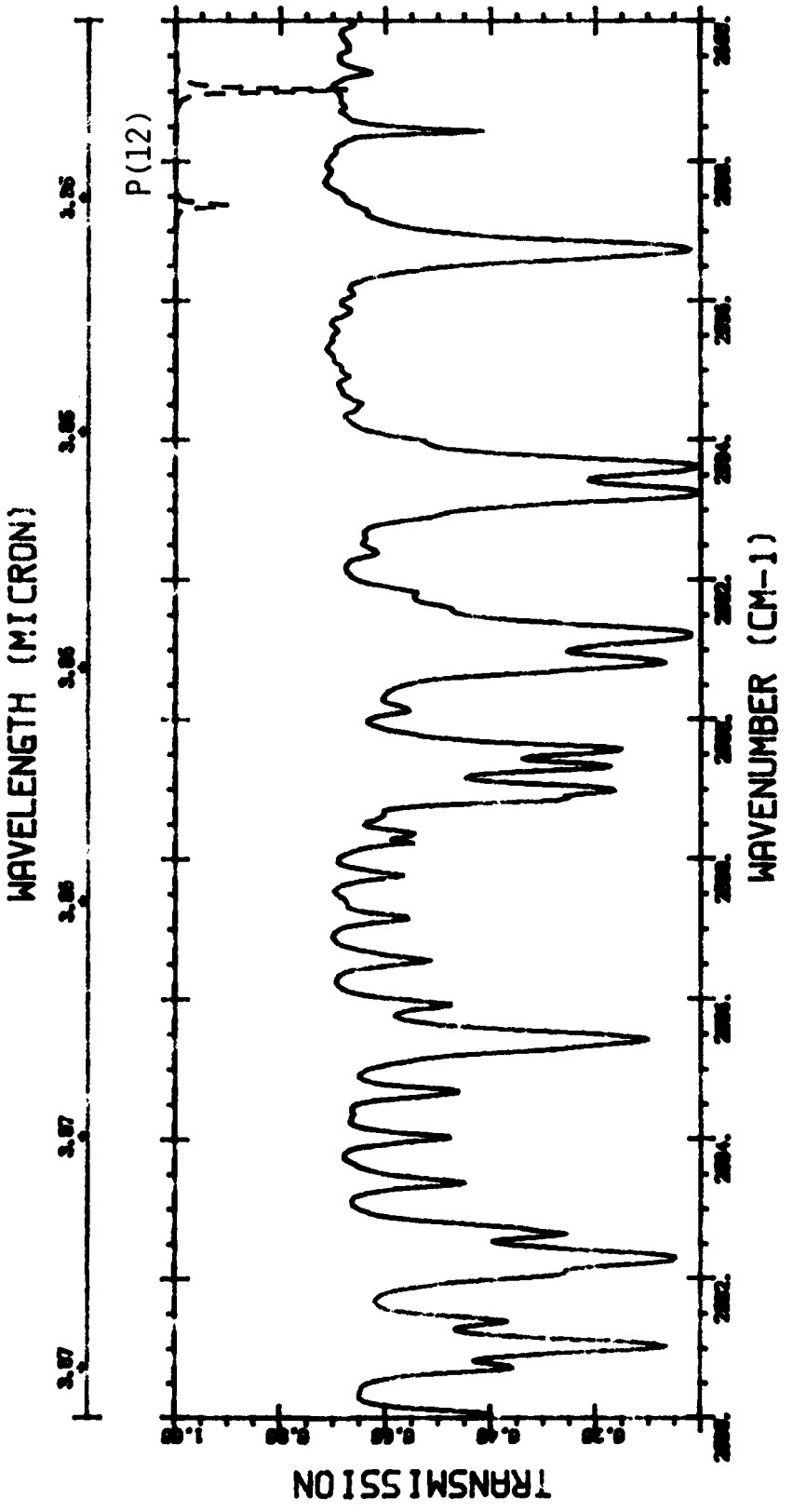
P(12)
WAVELENGTH (MICRON)
WAVENUMBER (CM-1)
TRANSMISSION

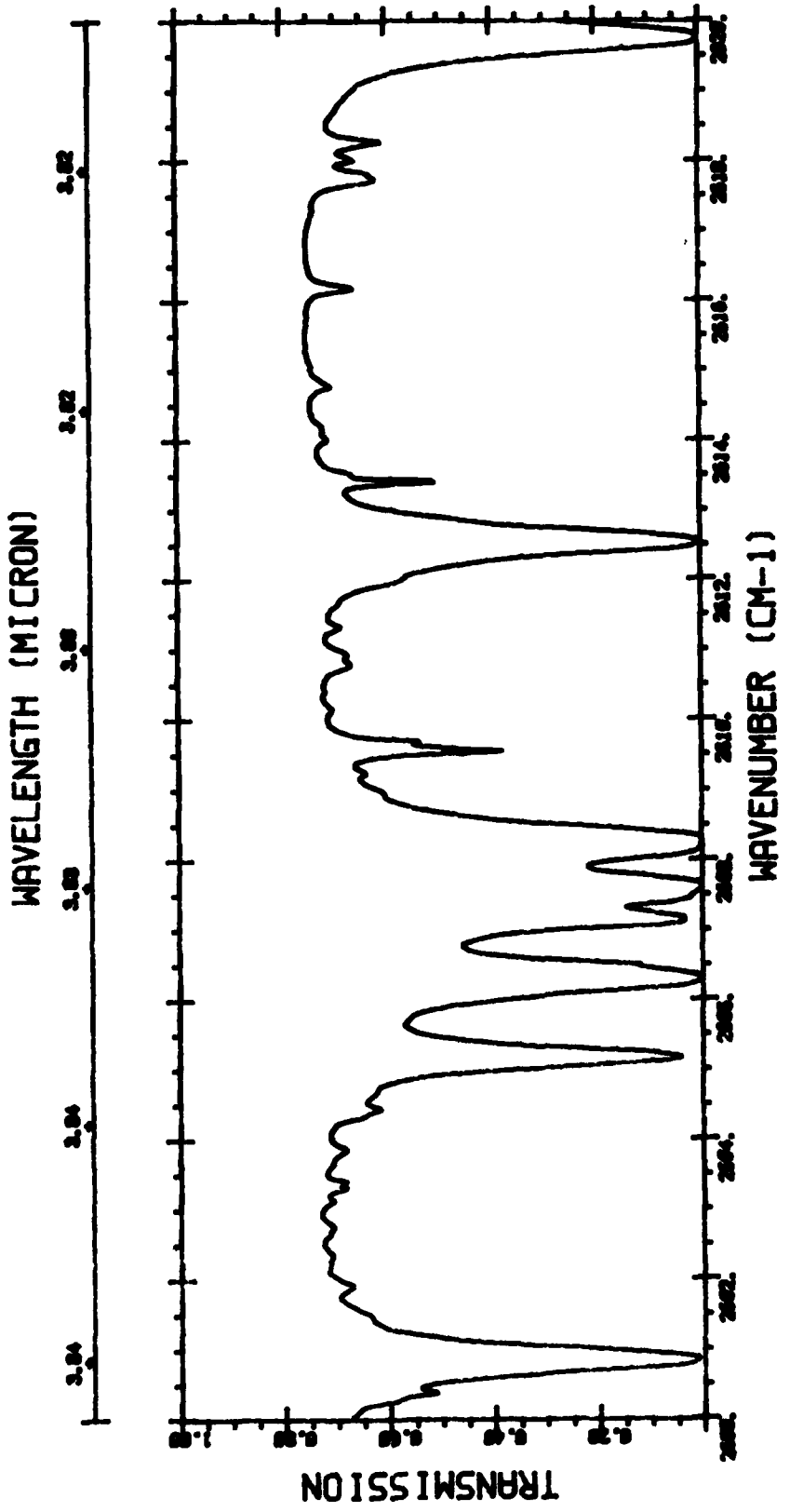
WAVELENGTH (MICRON)
WAVENUMBER (CM-1)
TRANSMISSION

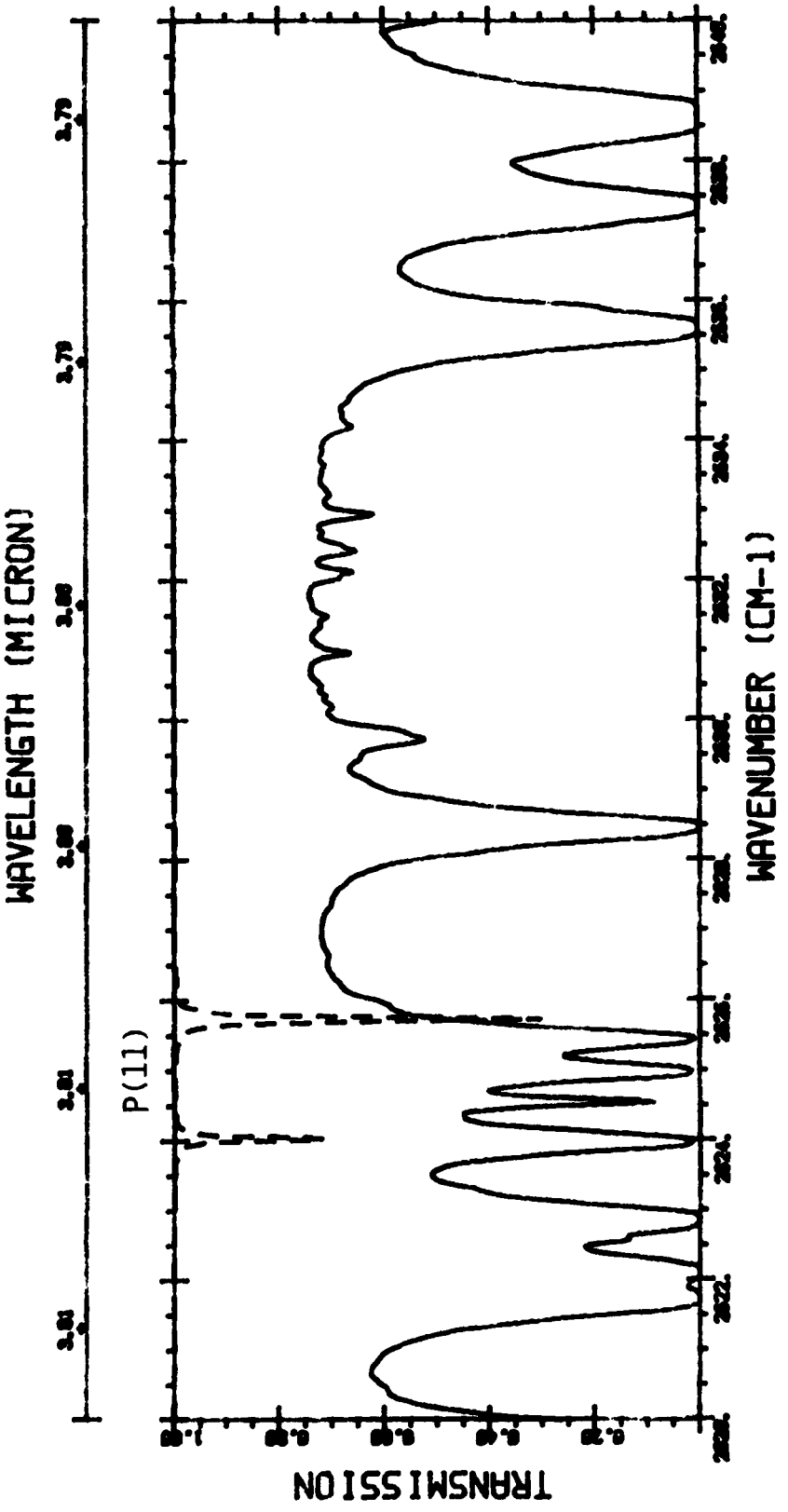
WAVELENGTH (MICRON)
WAVENUMBER (CM-1)
TRANSMISSION
P(11)

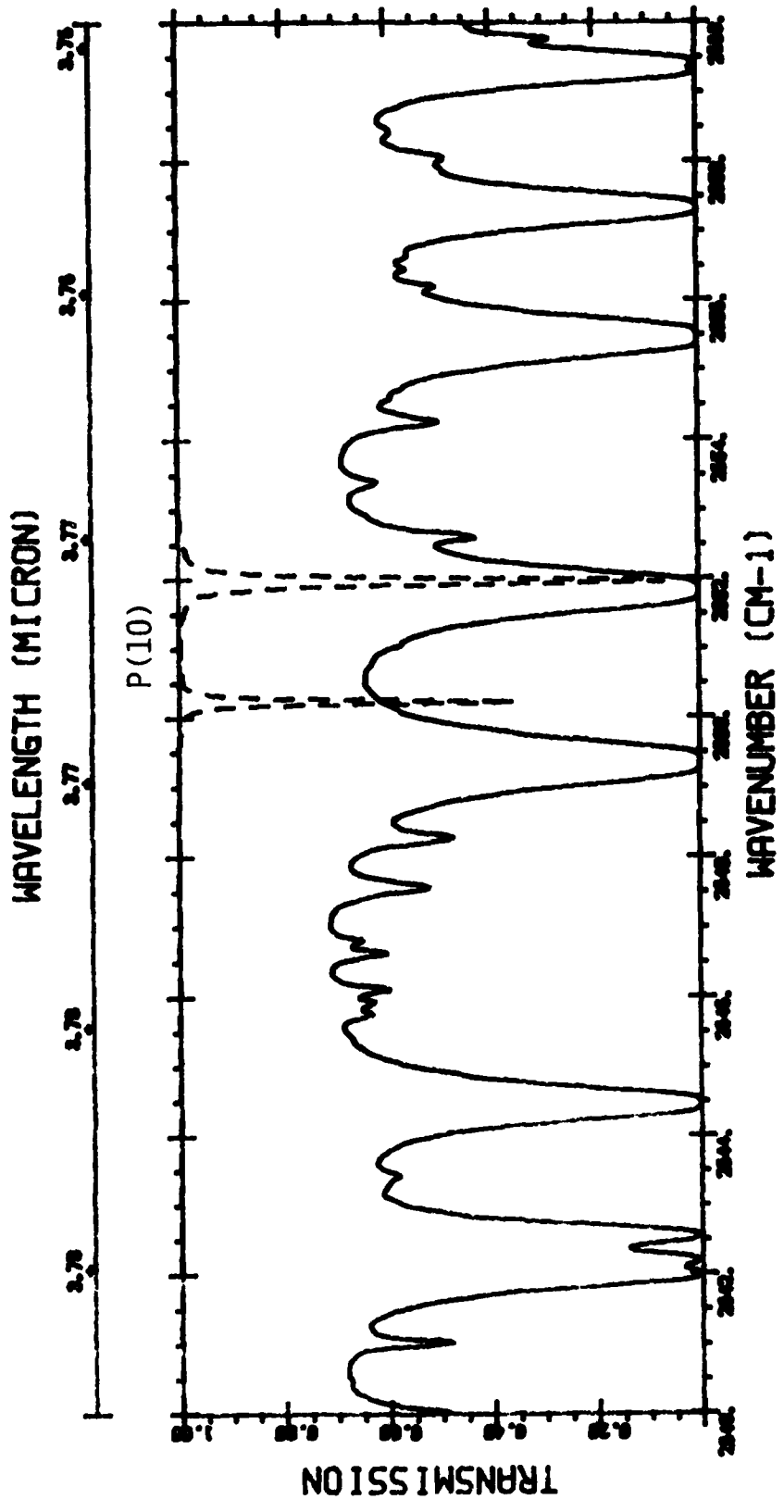
WAVELENGTH (MICRON)
WAVENUMBER (CM-1)
TRANSMISSION
P(10)

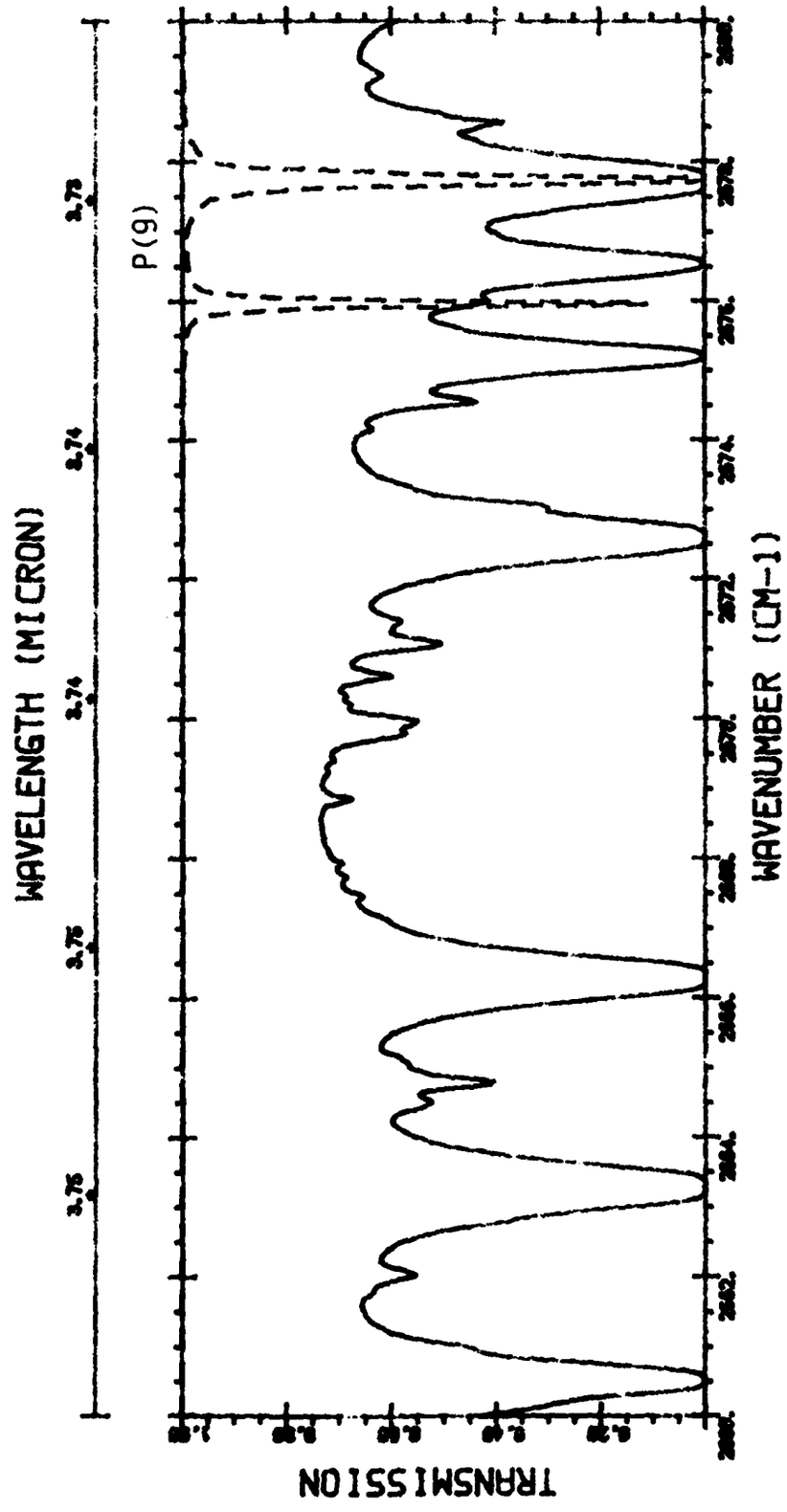
P(9)
WAVELENGTH (MICRON)
WAVENUMBER (CM-1)
TRANSMISSION

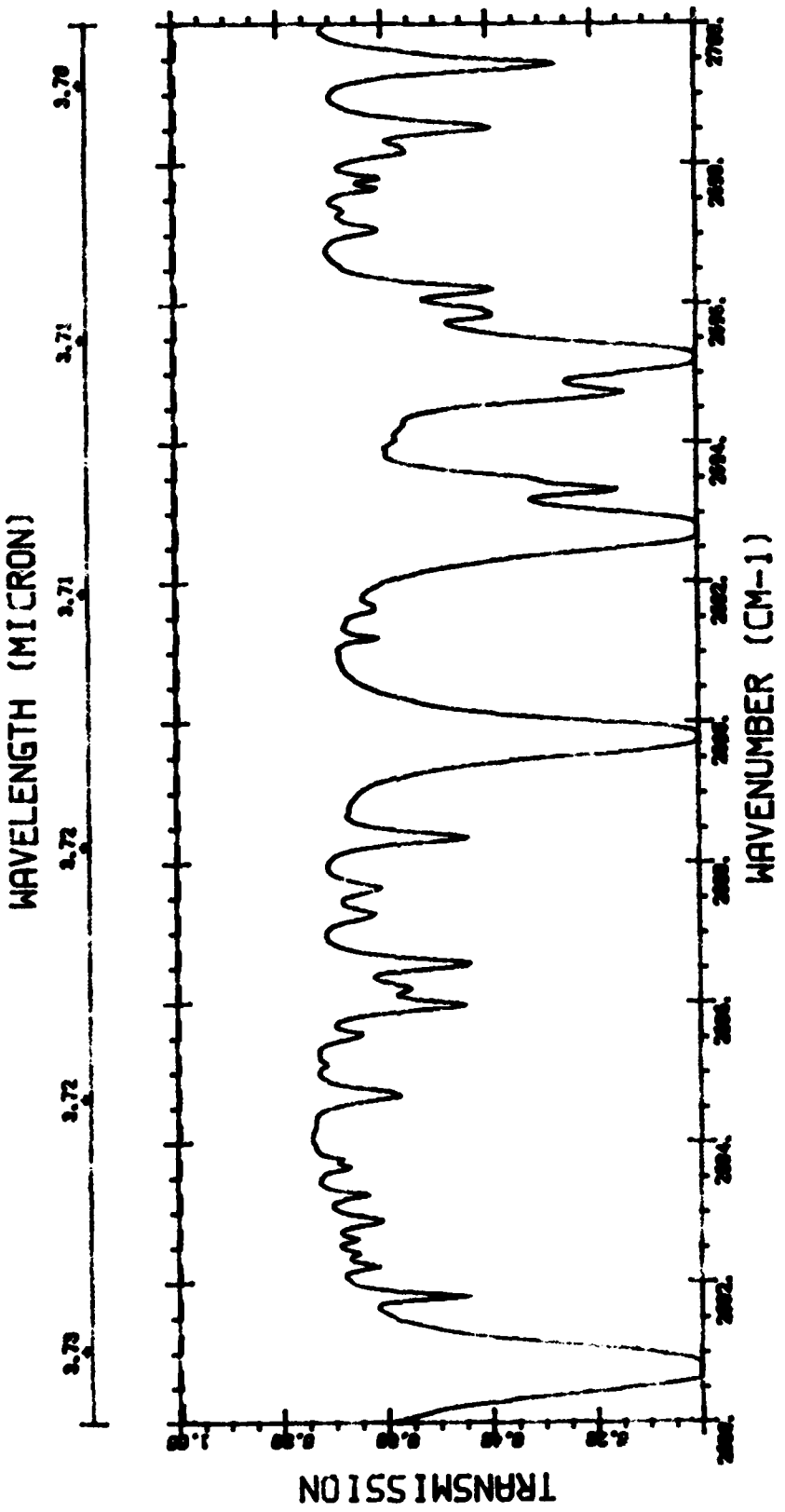
WAVELENGTH (MICRON)
3.70
3.71
3.71
3.72
3.72
3.73
WAVENUMBER (CM-1)
2700.
2698.
2696.
2694.
2692.
2690.
2688.
2686.
2684.
2682.
2680.
TRANSMISSION

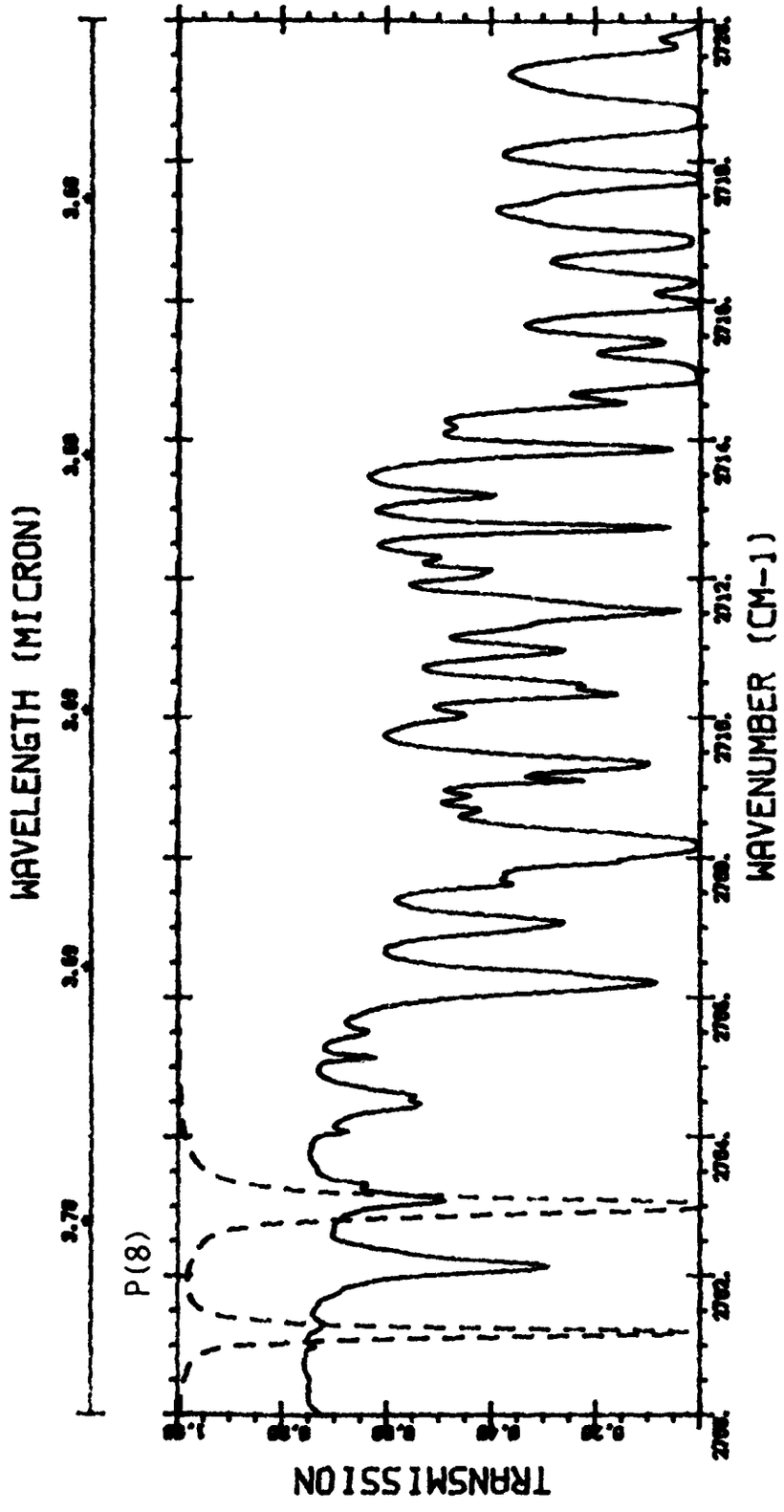
WAVELENGTH (MICRON)
WAVENUMBER (CM-1)
TRANSMISSION
P(8)

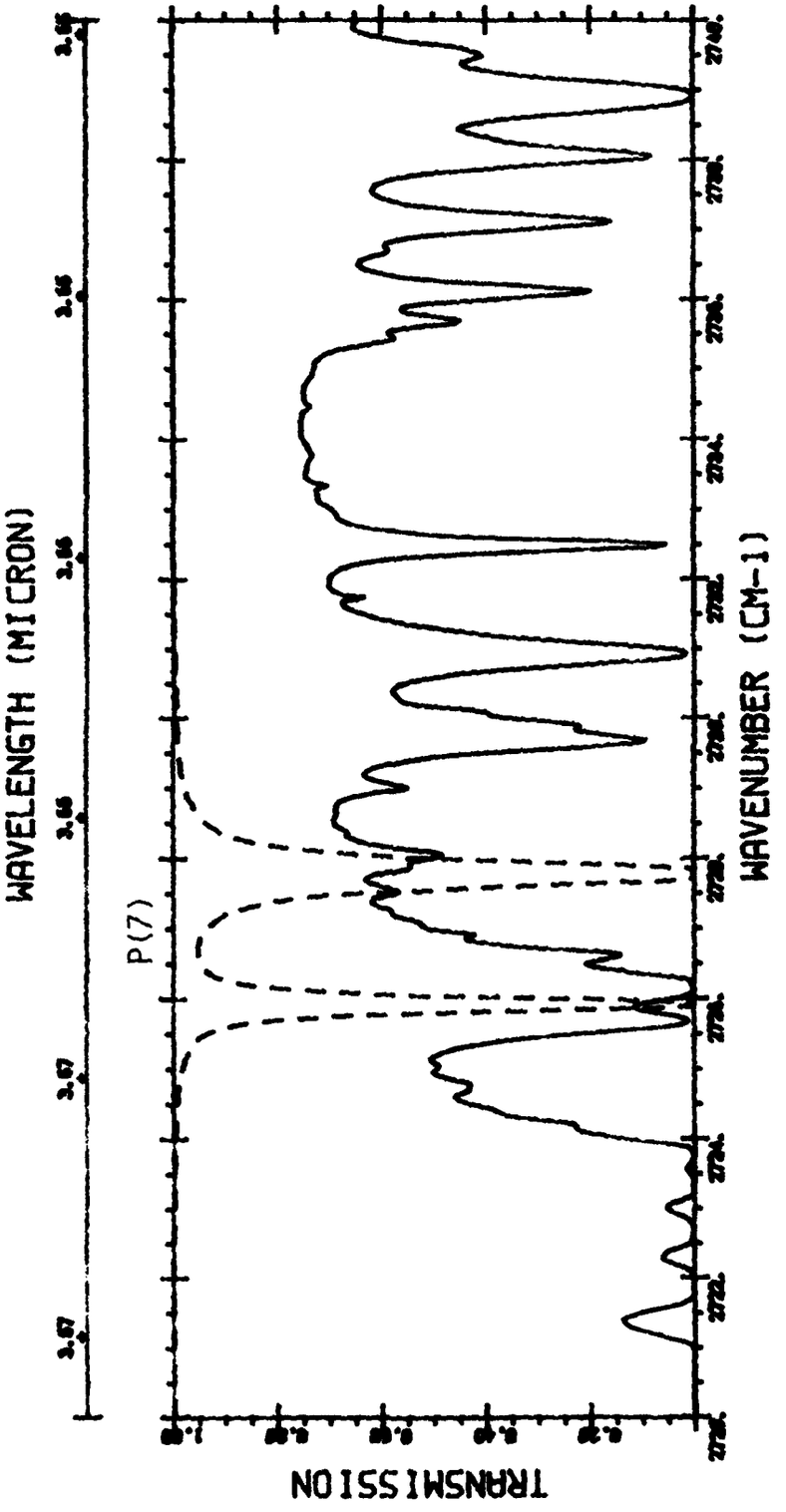
WAVELENGTH (MICRON)
WAVENUMBER (CM-1)
TRANSMISSION
P(7)

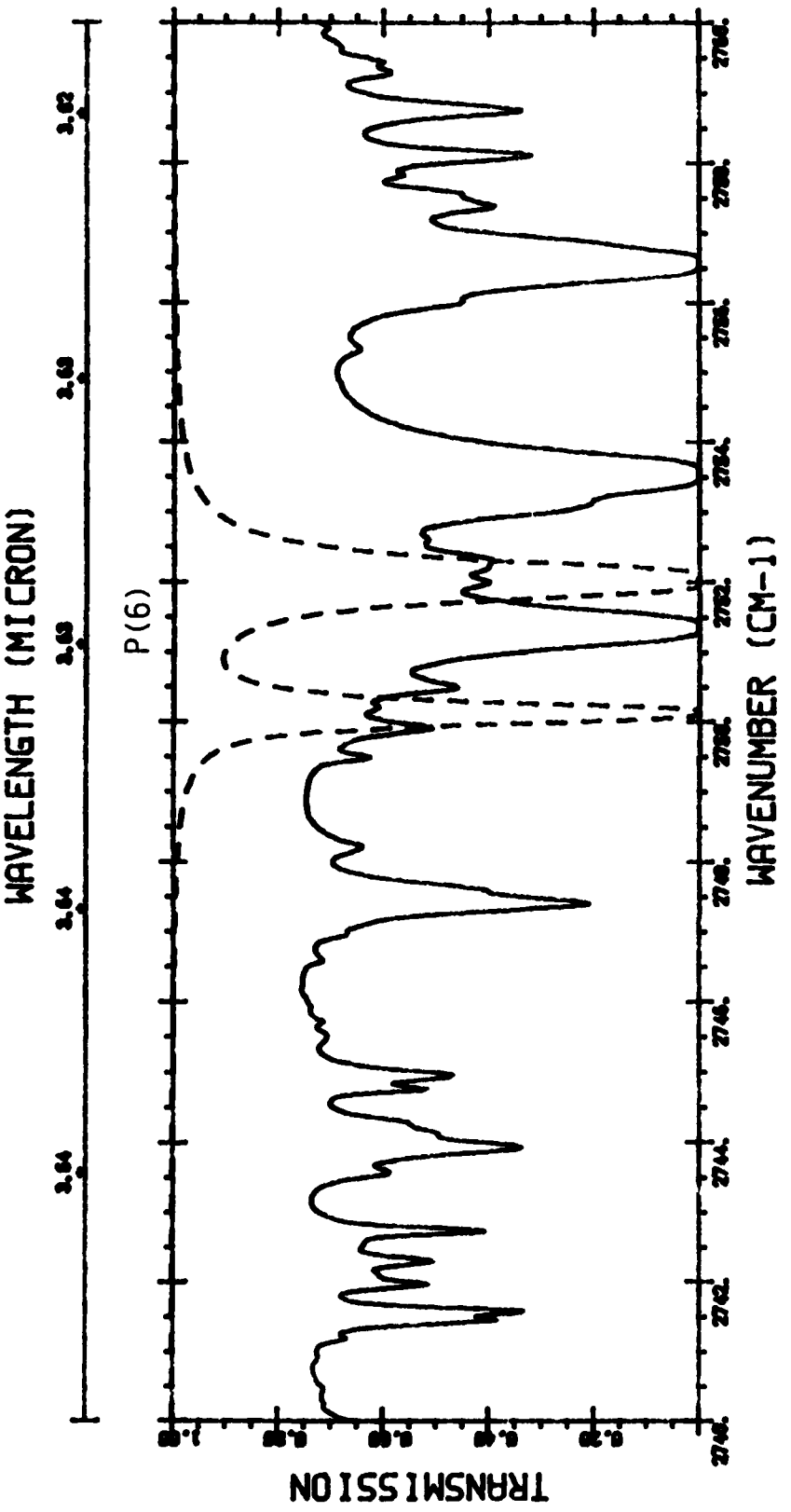
WAVELENGTH (MICRON)
P(6)
WAVENUMBER (CM-1)
TRANSMISSION

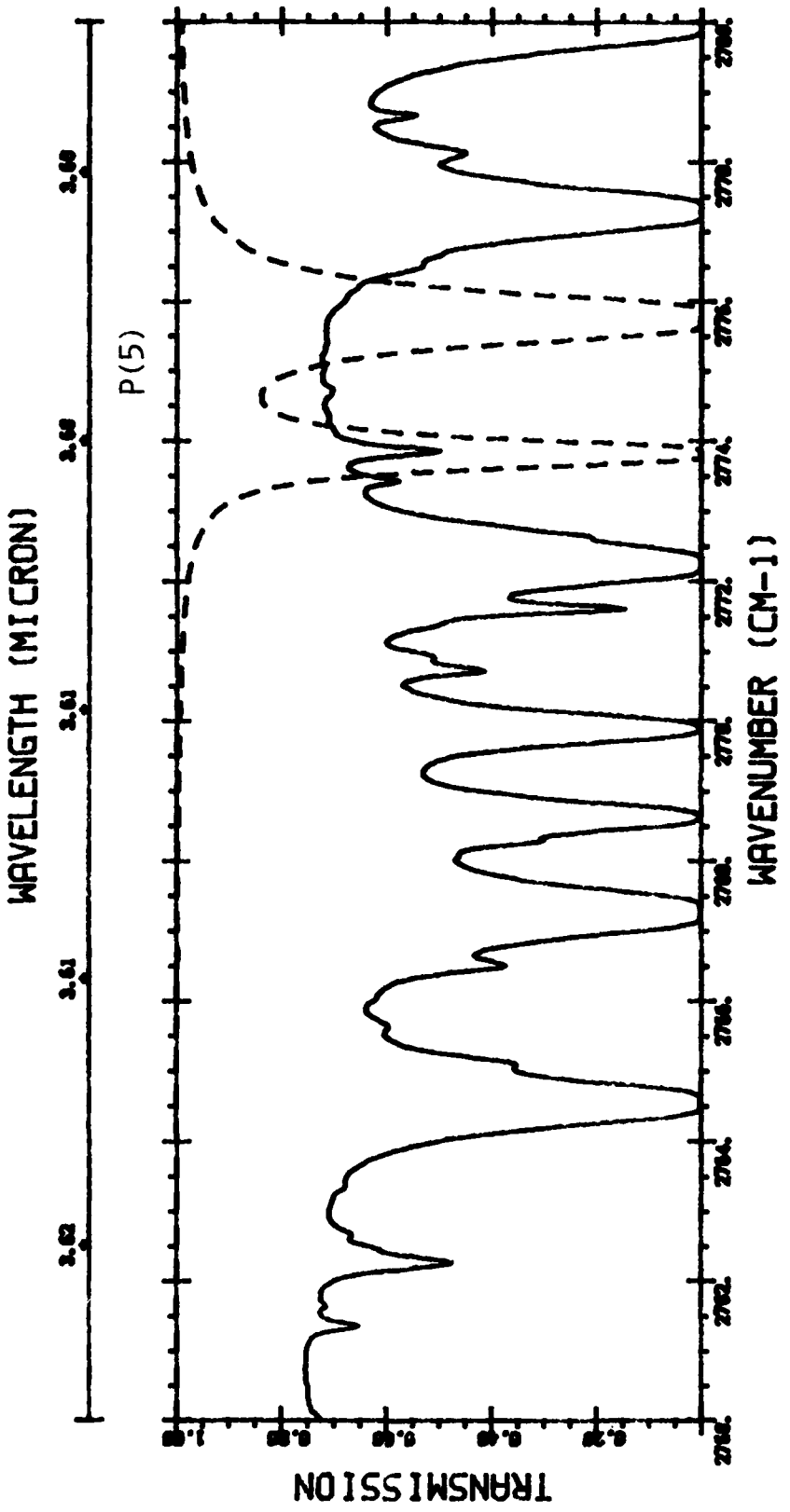
P(5)
WAVELENGTH (MICRON)
WAVENUMBER (CM-1)
TRANSMISSION

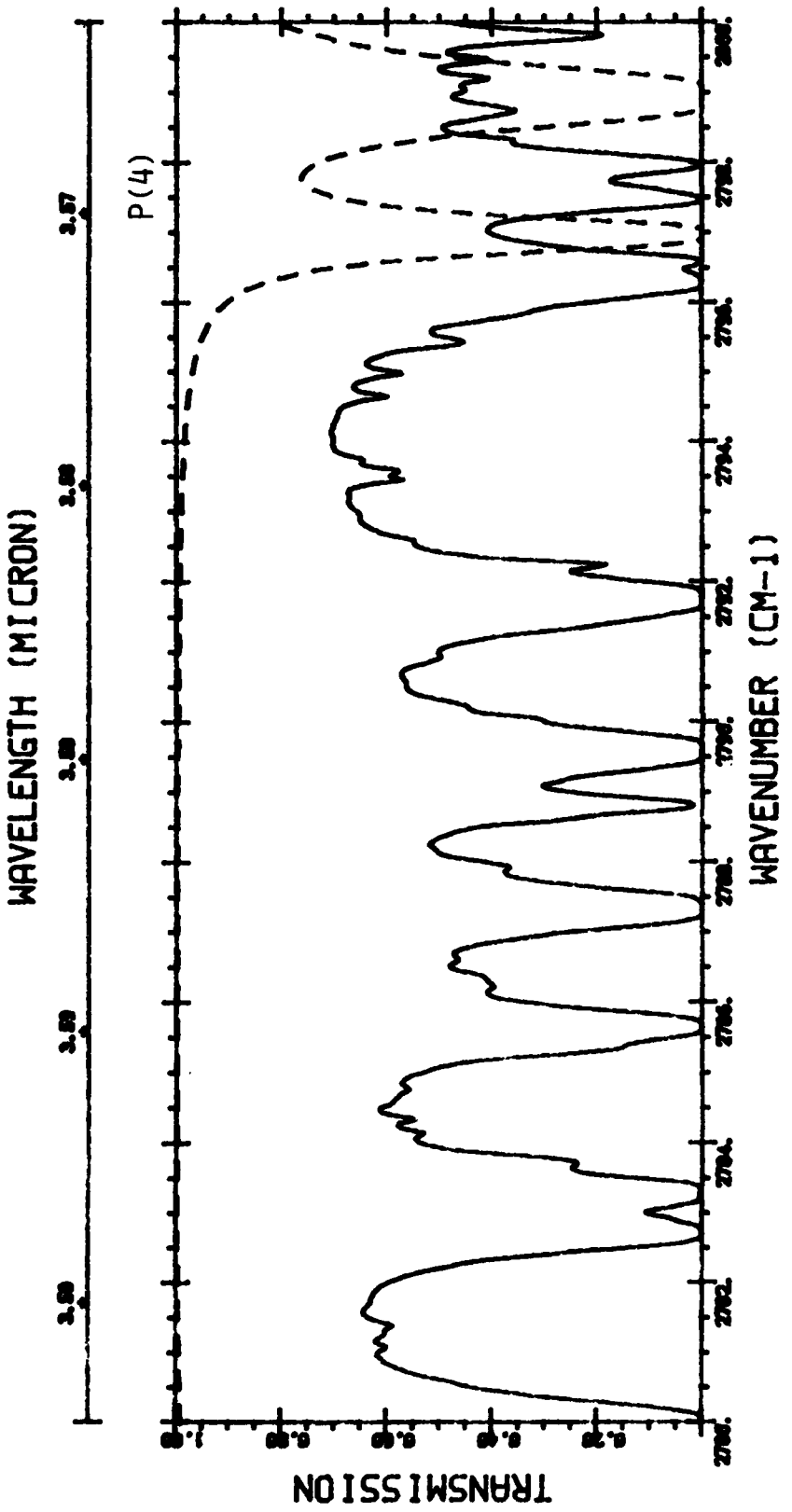
P(4)
WAVELENGTH (MICRON)
WAVENUMBER (CM-1)
TRANSMISSION

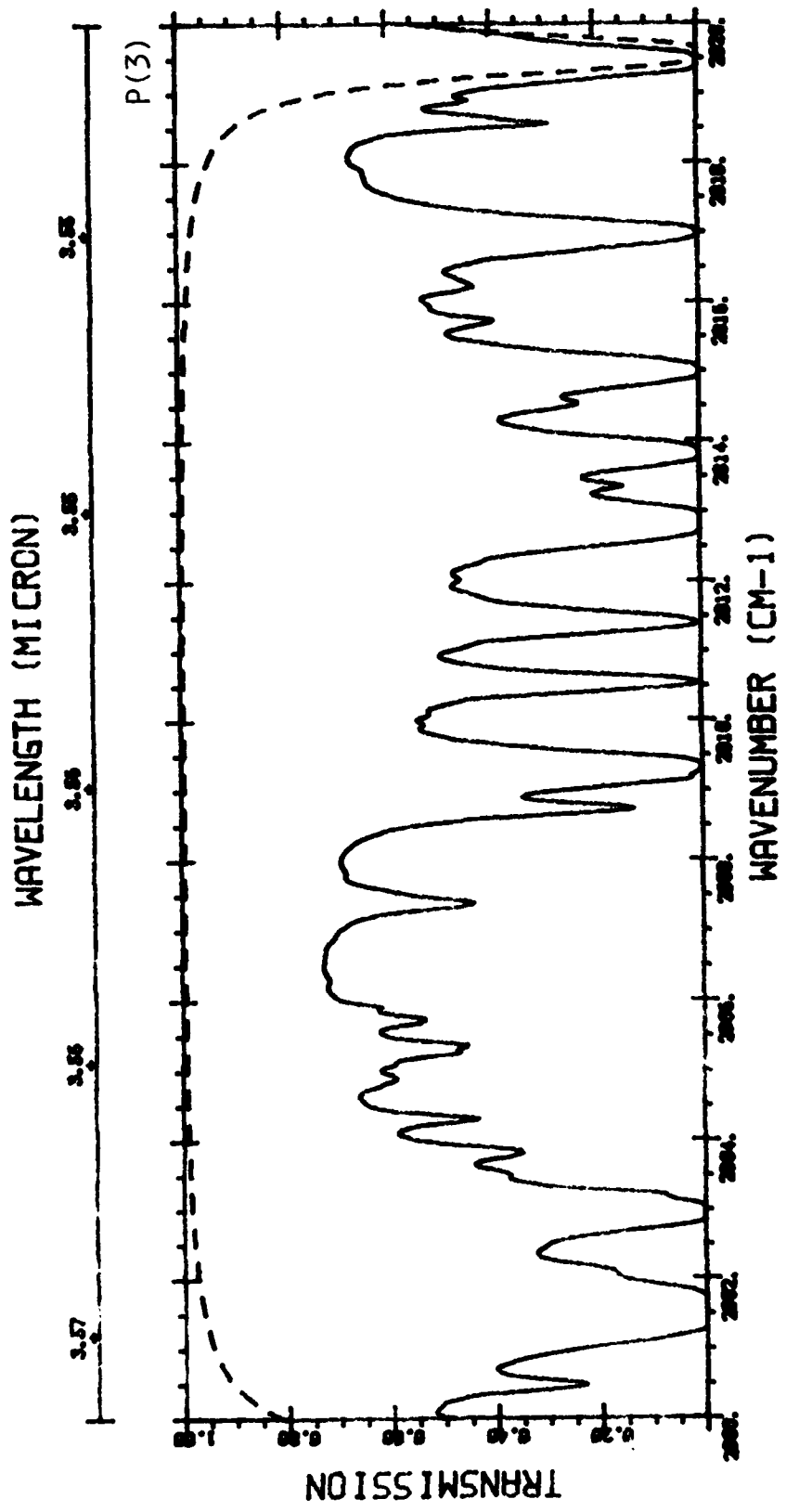
P(3)
WAVELENGTH (MICRON)
WAVENUMBER (CM-1)
TRANSMISSION

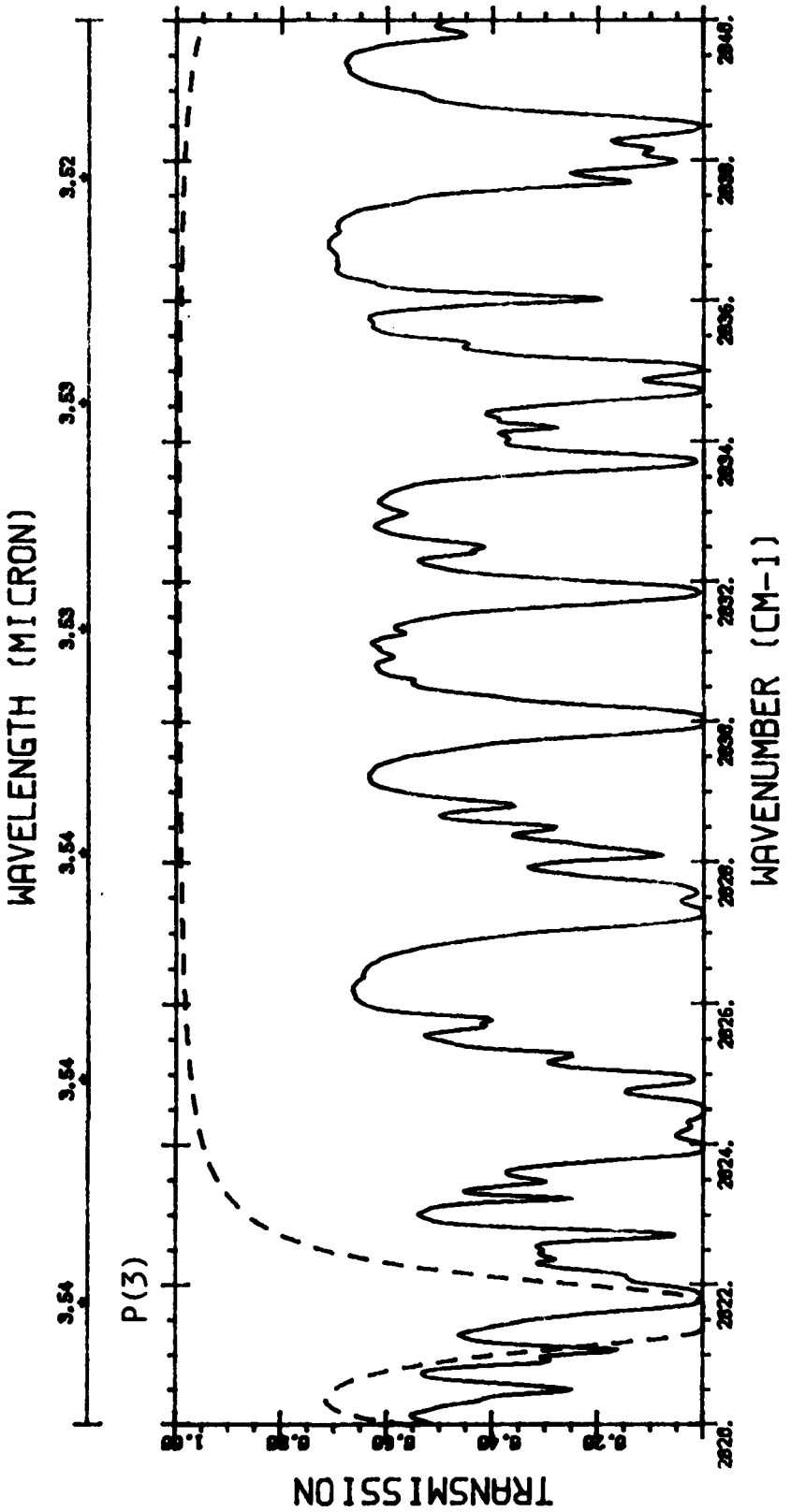
WAVELENGTH (MICRON)
3.54
3.54
3.54
3.53
3.53
3.52
P(3)
WAVENUMBER (CM-1)
2820.
2822.
2824.
2826.
2828.
2830.
2832.
2834.
2836.
2838.
2840.
TRANSMISSION

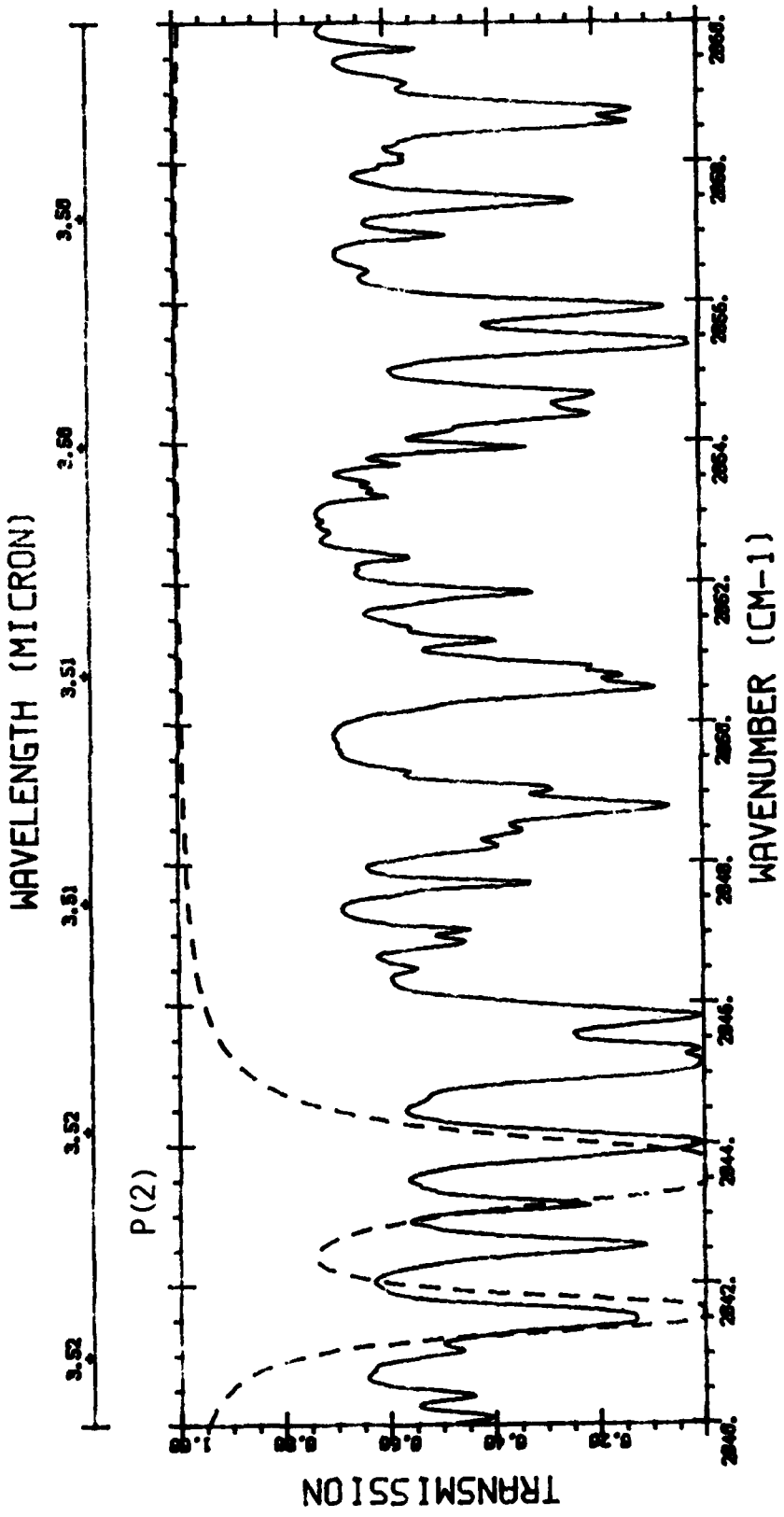
WAVELENGTH (MICRON)
3.52
3.52
3.51
3.51
3.50
3.50
P(2)
WAVENUMBER (CM-1)
2846.
2844.
2842.
2840.
2848.
2850.
2852.
2854.
2856.
2858.
2860.
TRANSMISSION

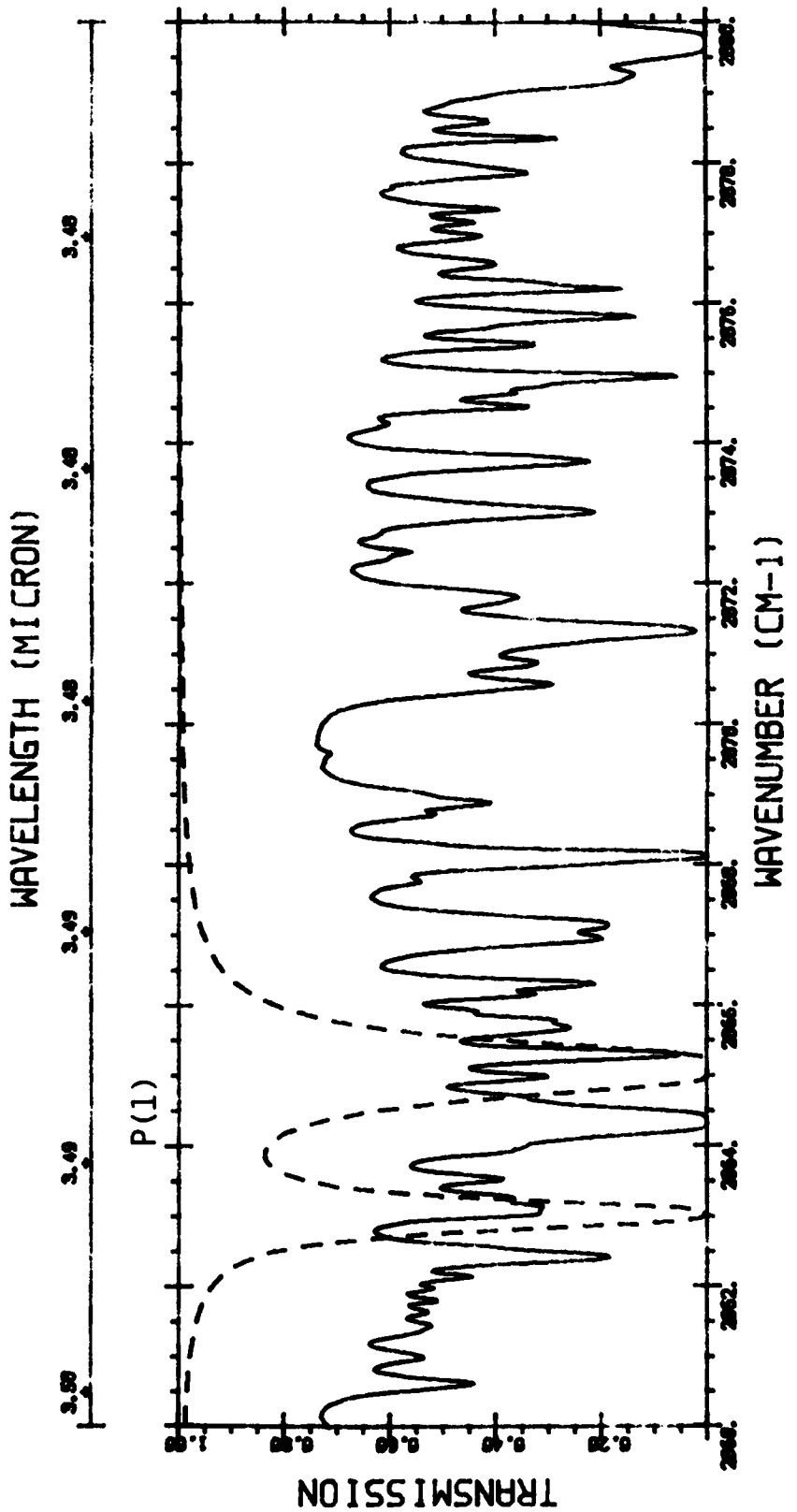
WAVELENGTH (MICRON)
3.50
3.49
3.48
3.47
3.46
P(1)
WAVENUMBER (CM-1)
2880.
2878.
2876.
2874.
2872.
2870.
2868.
2866.
2864.
2862.
2860.
TRANSMISSION

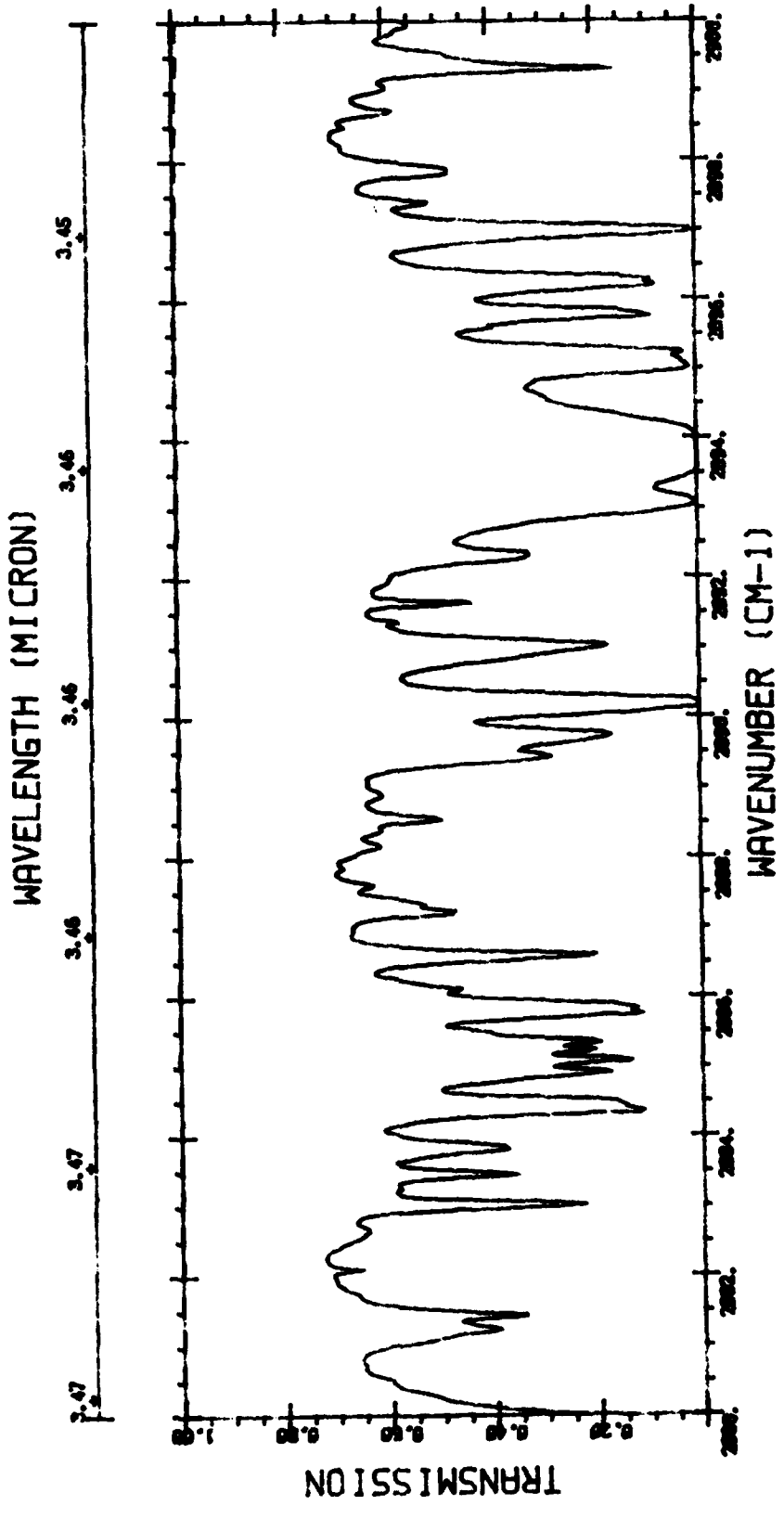
WAVELENGTH (MICRON)
3.45
3.46
3.46
3.46
3.47
3.47
WAVENUMBER (CM-1)
2900.
2898.
2896.
2894.
2892.
2890.
2888.
2886.
2884.
2882.
2880.
TRANSMISSION

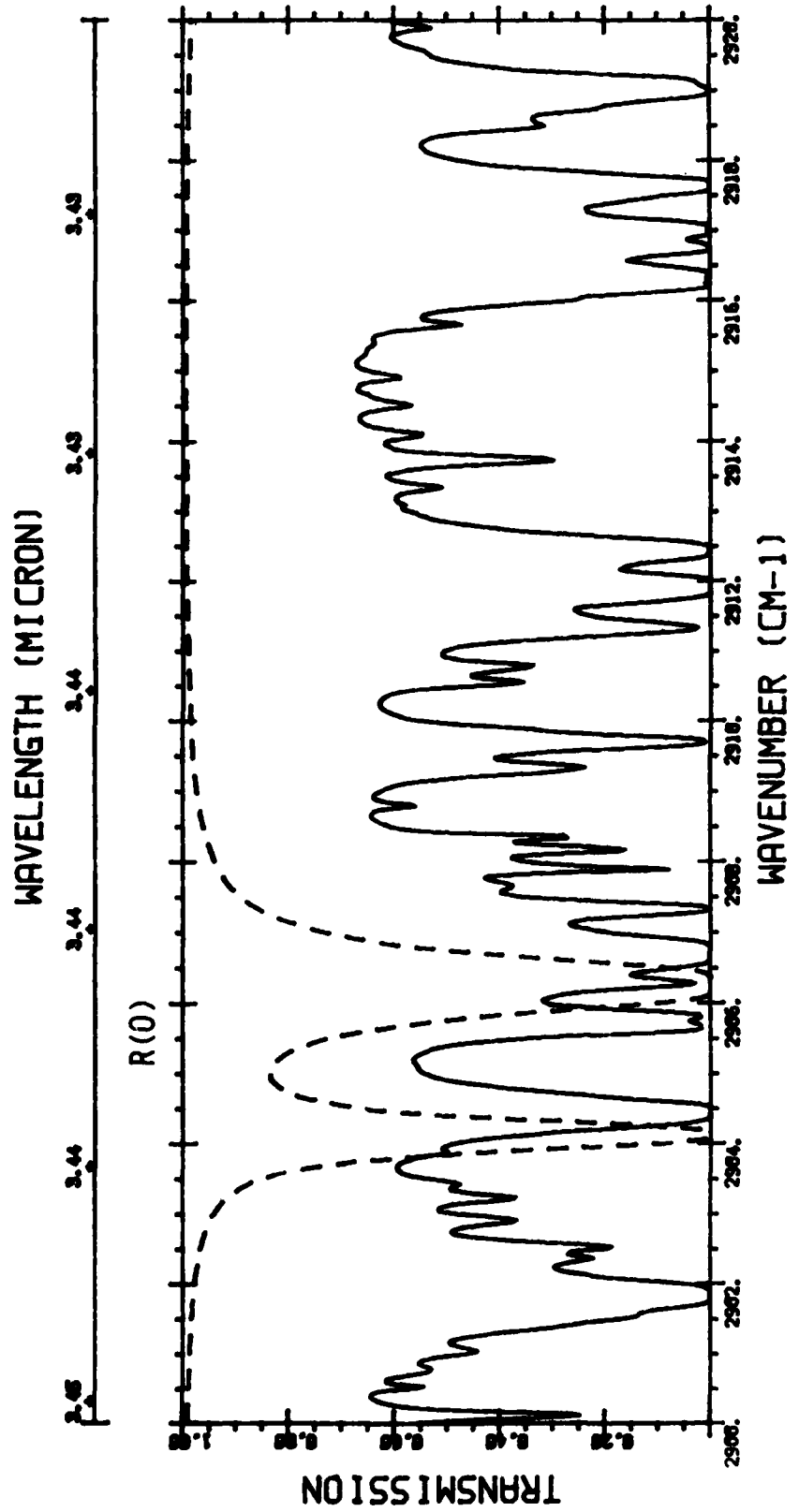
WAVELENGTH (MICRON)
3.45
3.44
3.44
3.43
3.43
R(0)
WAVENUMBER (CM-1)
2928.
2918.
2916.
2914.
2912.
2910.
2908.
2906.
2904.
2902.
2900.
TRANSMISSION

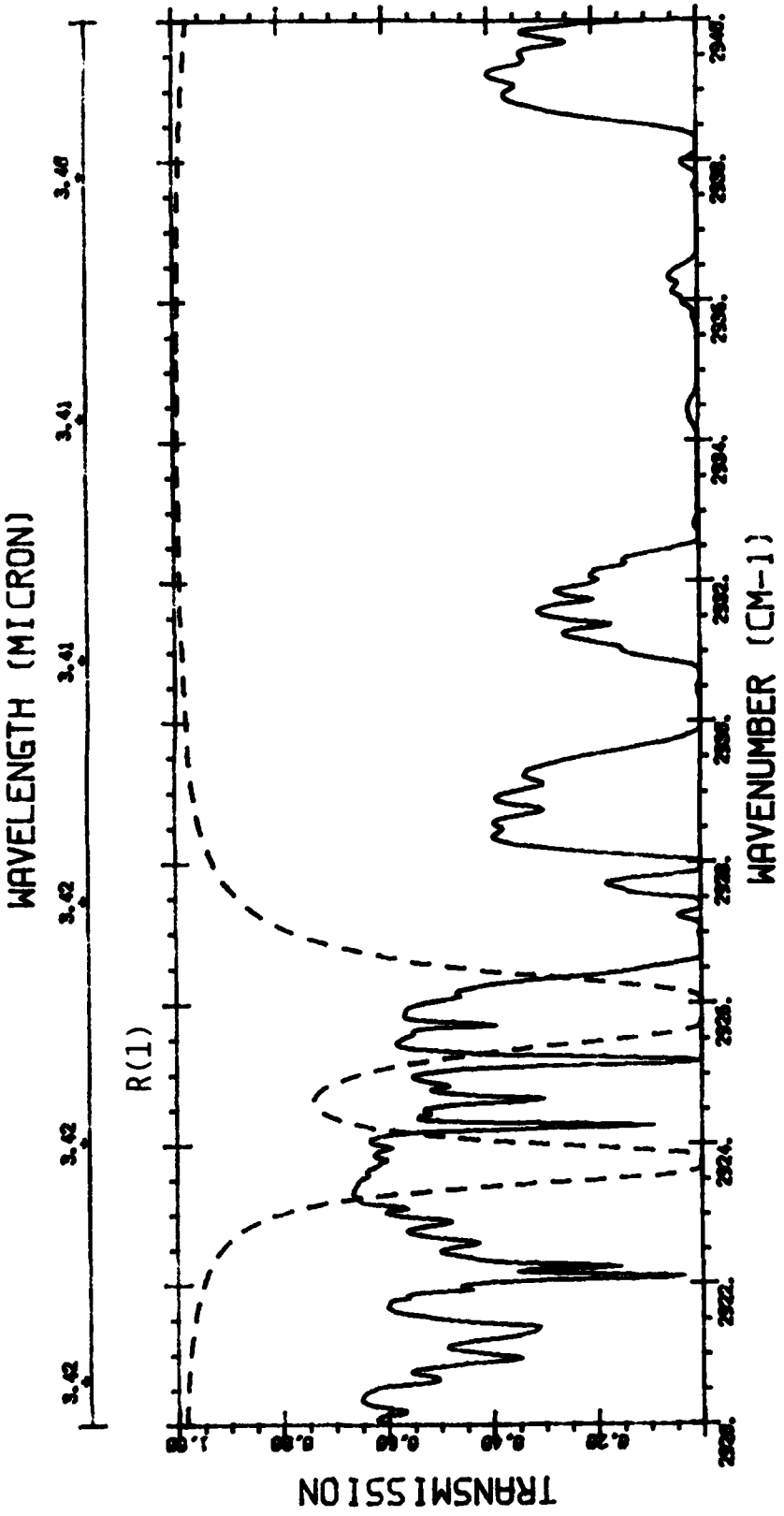
WAVELENGTH (MICRON)
3.42
3.42
3.41
3.41
3.40
R(1)
WAVENUMBER (CM-1)
2926.
2928.
2930.
2932.
2934.
2936.
2938.
2940.
TRANSMISSION

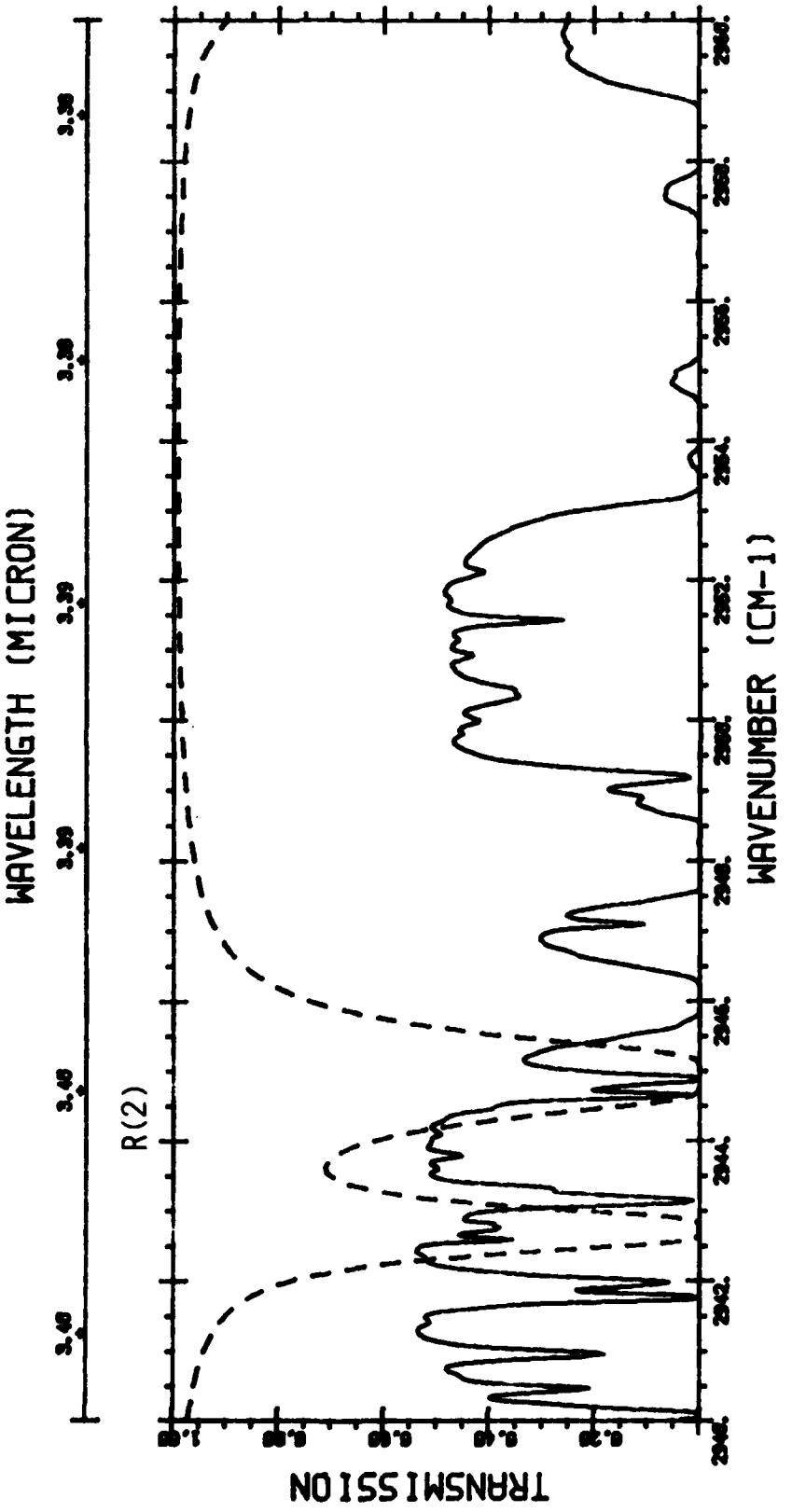
WAVELENGTH (MICRON)
WAVENUMBER (CM-1)
TRANSMISSION
R(2)

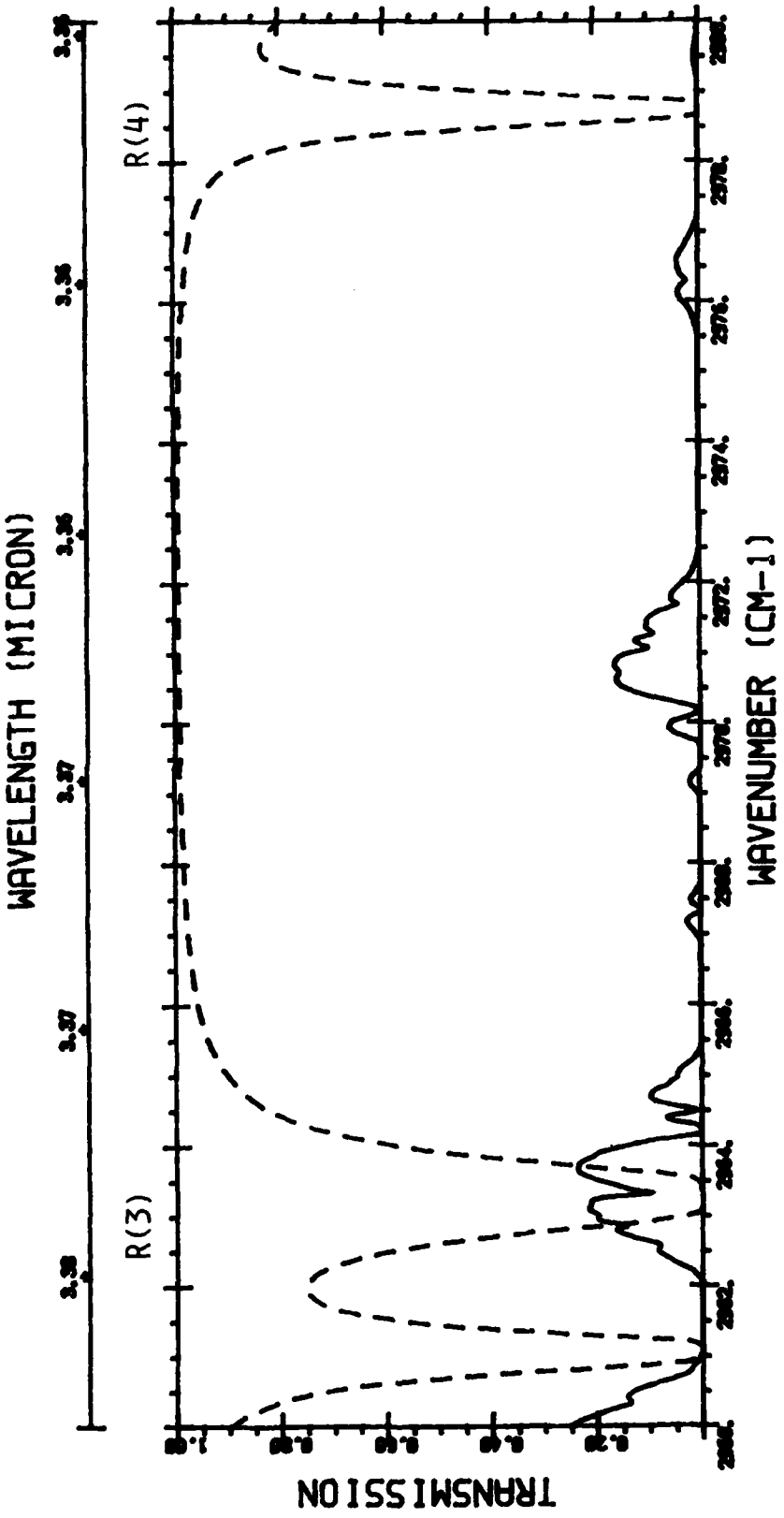
WAVELENGTH (MICRON)
WAVENUMBER (CM-1)
TRANSMISSION
R(4)
R(3)

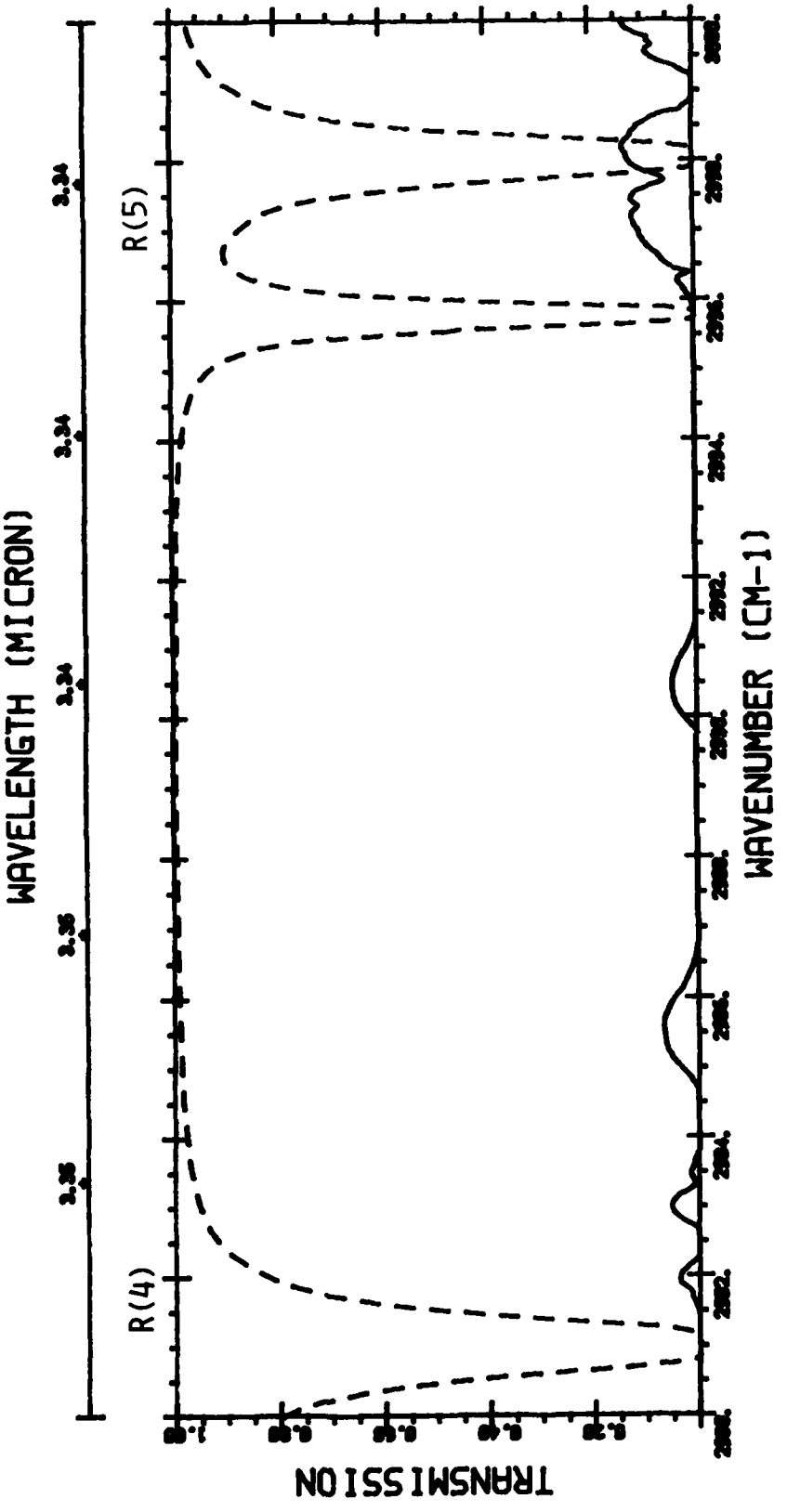
WAVELENGTH (MICRON)
WAVENUMBER (CM-1)
TRANSMISSION
R(4)
R(5)

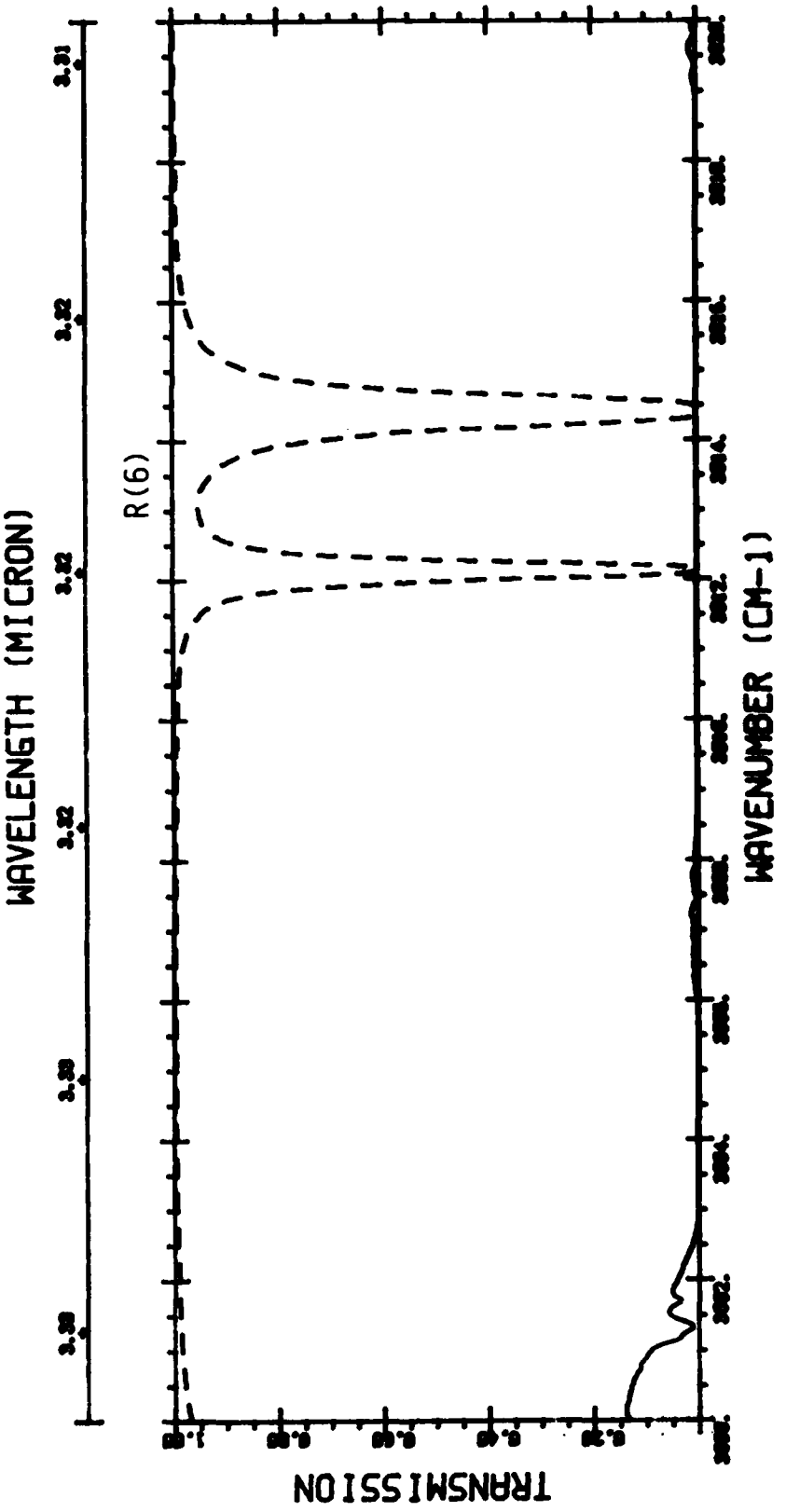
WAVELENGTH (MICRON)
R(6)
WAVENUMBER (CM-1)
TRANSMISSION

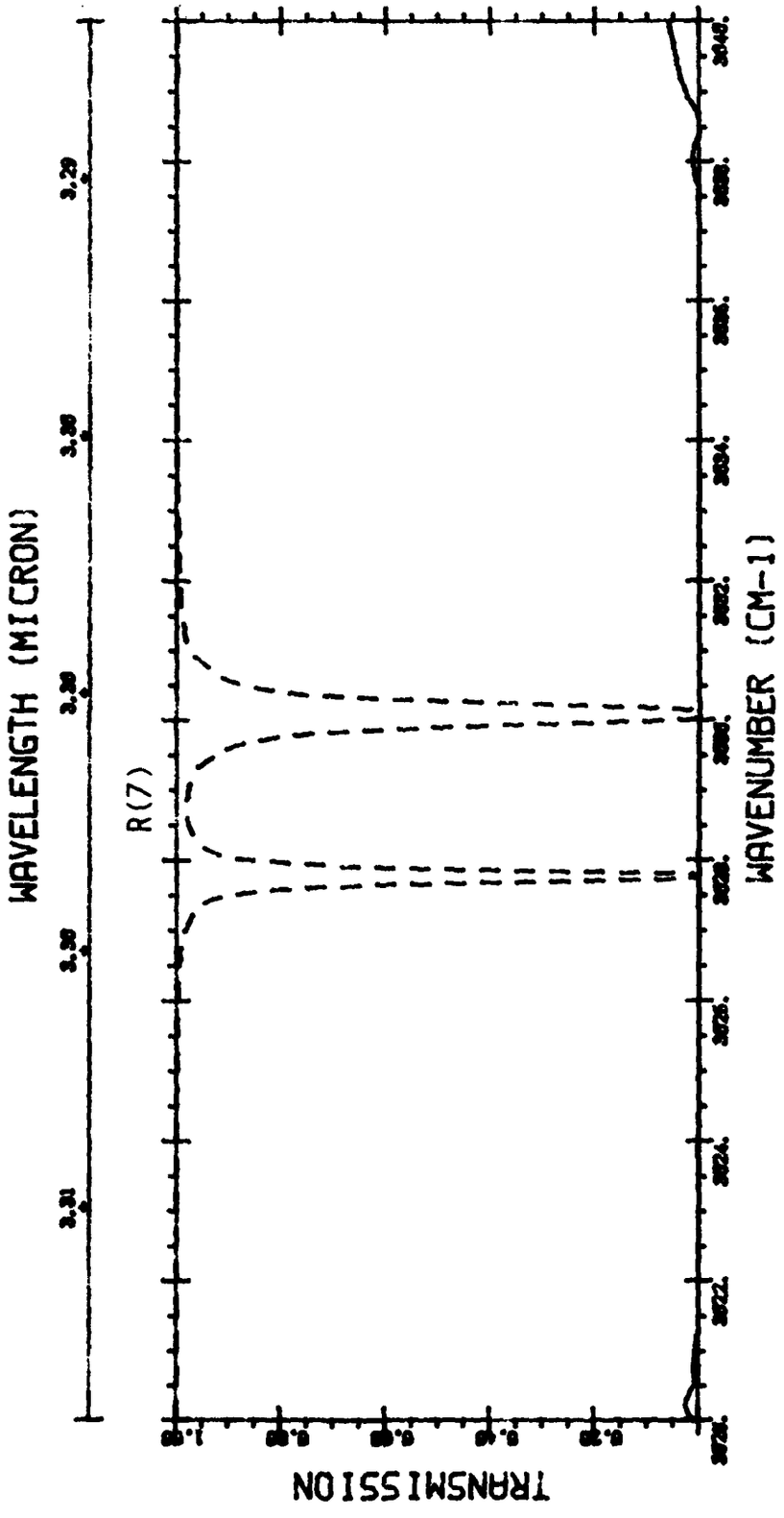
WAVELENGTH (MICRON)
WAVENUMBER (CM-1)
TRANSMISSION
R(7)

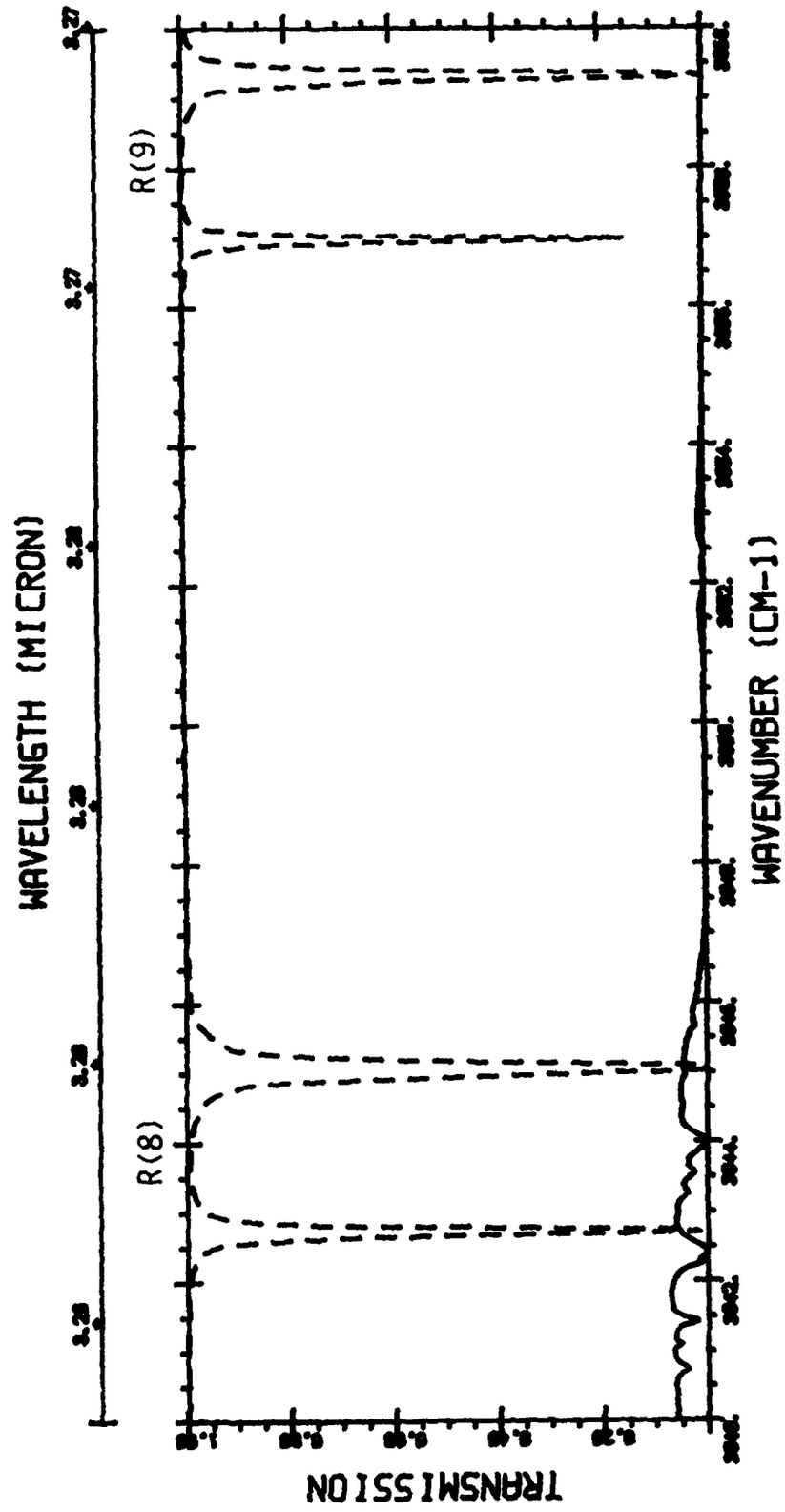
R(9)
R(8)
WAVELENGTH (MICRON)
WAVENUMBER (CM-1)
TRANSMISSION

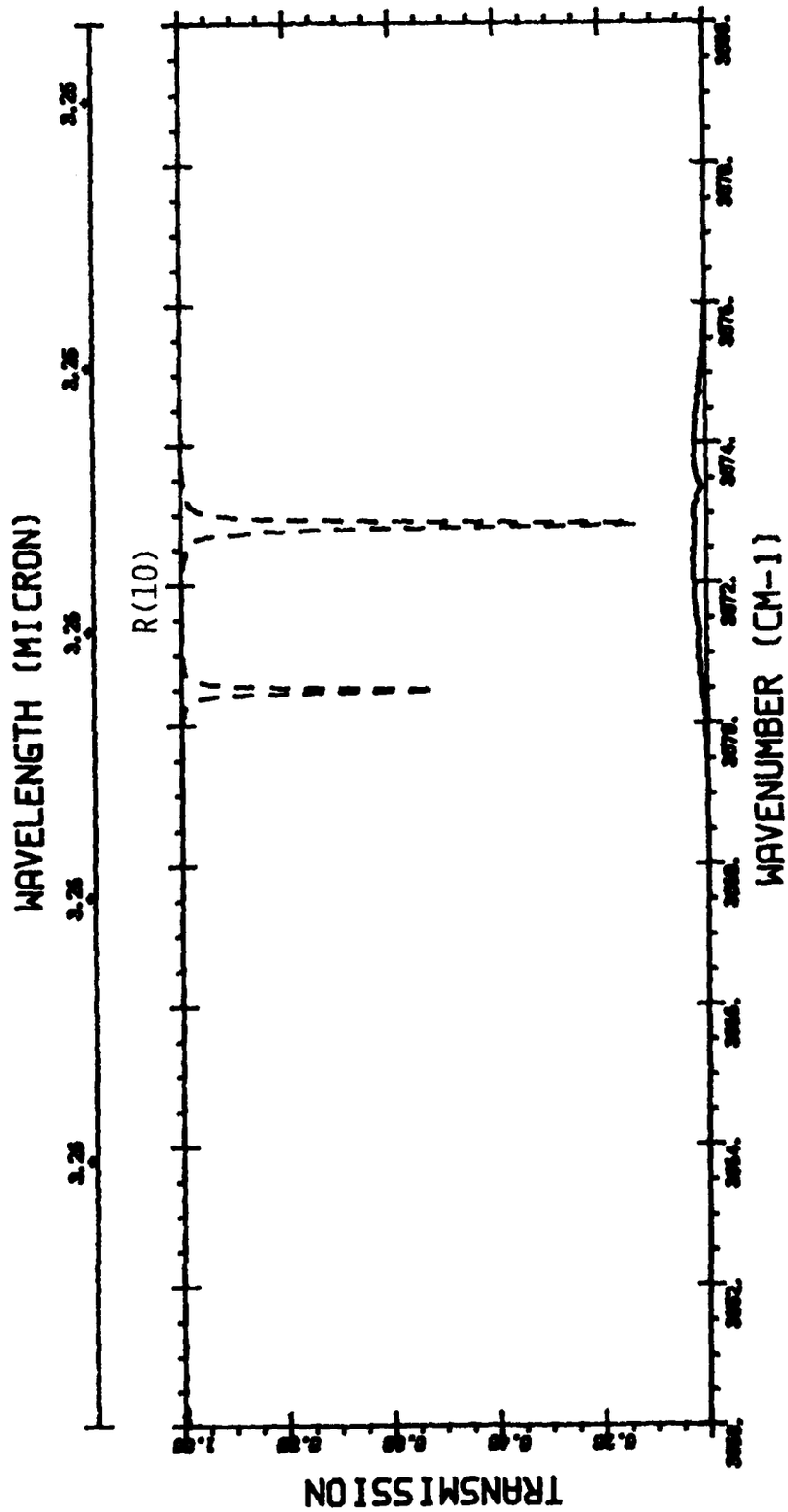
WAVELENGTH (MICRON)
WAVENUMBER (CM-1)
TRANSMISSION
R(10)

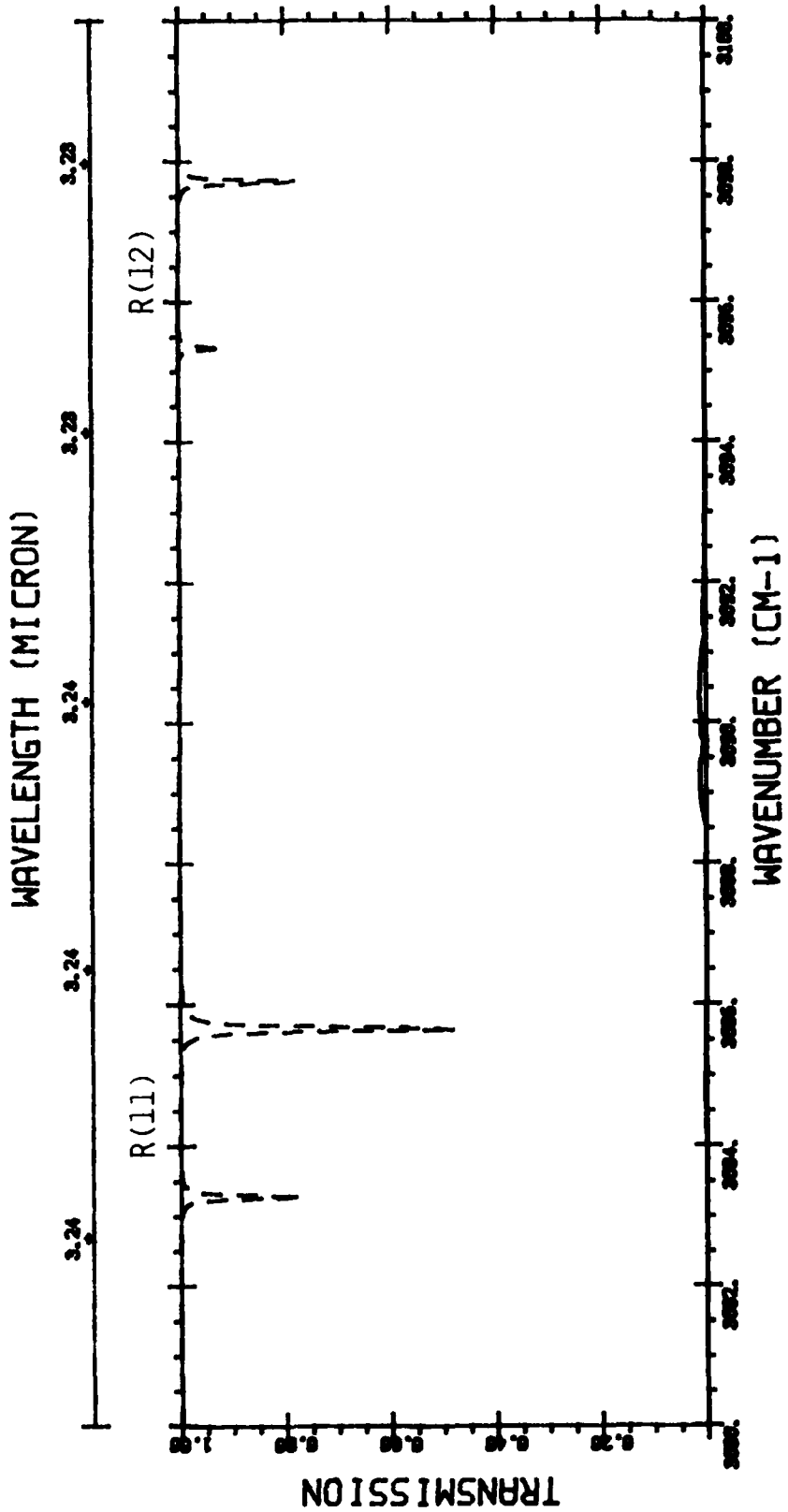
WAVELENGTH (MICRON)
WAVENUMBER (CM-1)
TRANSMISSION
R(12)
R(11)

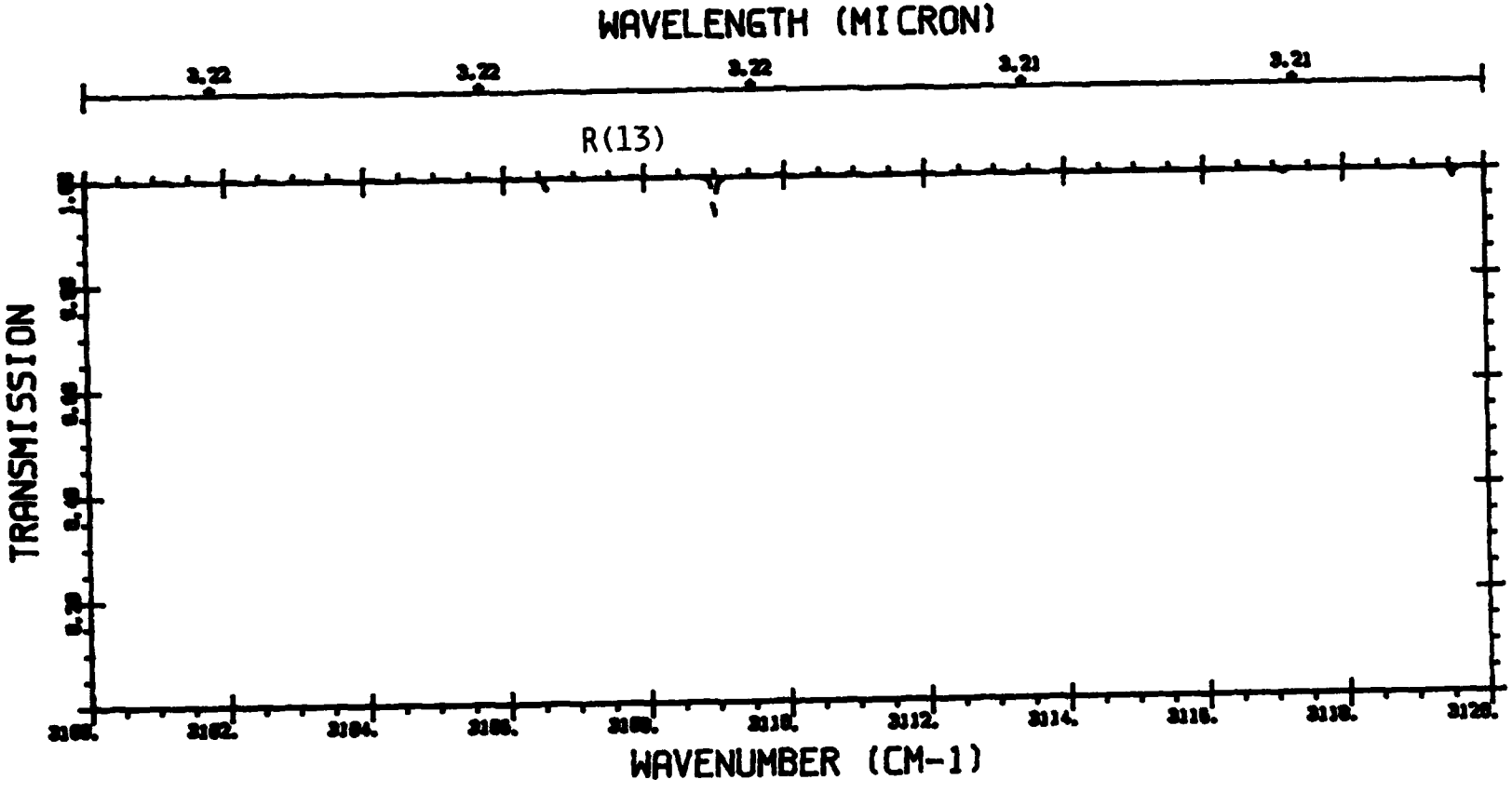
WAVELENGTH (MICRON)
3.22
3.22
3.22
3.21
3.21
R(13)
TRANSMISSION
2100.
2102.
2104.
2106.
2108.
2110.
2112.
2114.
2116.
2118.
2120.
WAVENUMBER (CM-1)

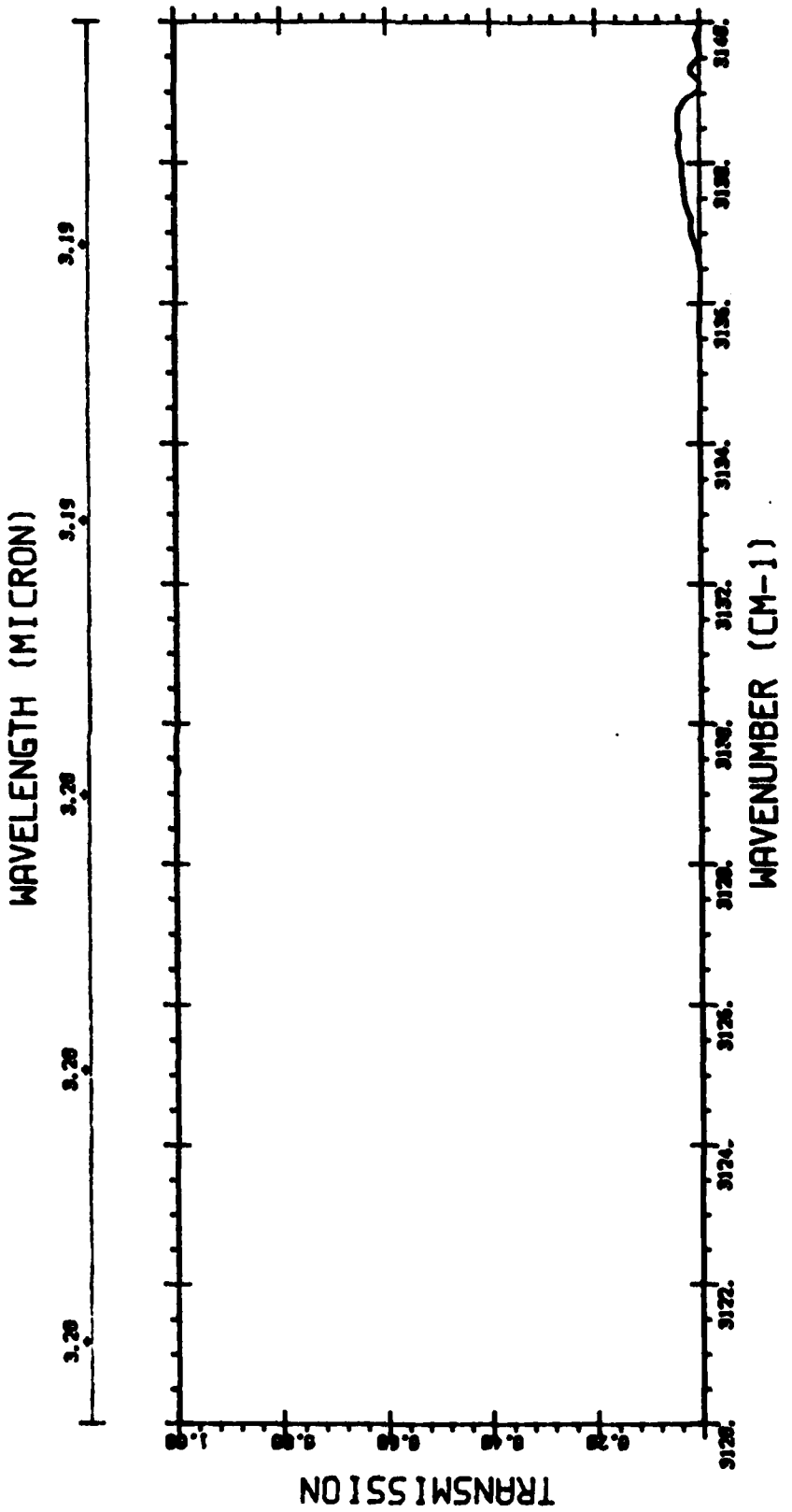
WAVELENGTH (MICRON)
3.19
3.19
3.20
3.20
WAVENUMBER (CM-1)
3168.
3136.
3134.
3132.
3130.
3128.
3126.
3124.
3122.
3120.
TRANSMISSION

END

DTIC

5-86